

Title	Controllable magnetic systems for minimally invasive surgery
Authors	Desmond, Philip
Publication date	2020-08
Original Citation	Desmond, P. 2020. Controllable magnetic systems for minimally invasive surgery. MRes Thesis, University College Cork.
Type of publication	Masters thesis (Research)
Rights	© 2020, Philip Desmond. - <a href="https://creativecommons.org/licenses/by-nc-nd/4.0/">https://creativecommons.org/licenses/by-nc-nd/4.0/</a>
Download date	2023-05-07 22:14:44
Item downloaded from	<a href="http://hdl.handle.net/10468/10906">http://hdl.handle.net/10468/10906</a>

# Controllable Magnetic Systems for Minimally Invasive Surgery

Philip Desmond

BE

114431248

**Thesis submitted for the degree of  
Master of Engineering Science**



NATIONAL UNIVERSITY OF IRELAND, CORK

SCHOOL OF ENGINEERING

DEPARTMENT OF ELECTRICAL AND ELECTRONIC ENGINEERING

August 2020

Head of Department: Dr Jorge Oliveira

Supervisors: Dr Pádraig Cantillon-Murphy  
Dr John Hayes

Research supported by SFI



# Contents

List of Figures . . . . .	iv
List of Tables . . . . .	xi
Abstract . . . . .	xiii
Acknowledgements . . . . .	xiv
<b>1 Introduction</b>	<b>1</b>
1.1 Structure of Presented Work . . . . .	3
1.2 External Influences on the Project Development . . . . .	4
<b>2 Background Theory and Literature Review</b>	<b>5</b>
2.1 Colorectal Anastomosis . . . . .	5
2.1.1 End to end anastomosis . . . . .	7
2.1.2 End to side anastomosis . . . . .	7
2.1.3 Side to side anastomosis . . . . .	7
2.1.4 Complications in colorectal anastomosis . . . . .	9
2.2 Tools for Colorectal Anastomosis . . . . .	9
2.3 Magnetics for Medical Devices . . . . .	13
2.4 Magnetism . . . . .	15
2.4.1 Permanent Magnets . . . . .	15
2.4.1.1 Permeance coefficient . . . . .	18
2.4.2 Electromagnets . . . . .	20
2.5 Mechanically Controlled Magnet Systems . . . . .	21
2.6 Electrically Controlled Magnetic Systems . . . . .	25
2.6.1 Electromagnet Systems . . . . .	25
2.6.2 Combination Magnet Systems . . . . .	25
2.6.3 Electropermanent Magnet Systems . . . . .	29
2.7 Methods of Magnet Analysis . . . . .	37
2.7.1 Analytical Analysis . . . . .	39
2.7.1.1 Magnetic equivalent circuit . . . . .	39
2.7.1.2 Magnetic charge model . . . . .	40
2.7.1.3 Magnetic current model . . . . .	42



2.7.2	Numerical Analysis . . . . .	44
<b>3</b>	<b>Preliminary Device Design</b>	<b>45</b>
3.1	Device Simulation Method . . . . .	45
3.2	Safer Magnetic Behaviour for Arrays . . . . .	51
3.3	Electropermanent Magnet Array Design . . . . .	53
3.3.1	Design Considerations . . . . .	53
3.3.2	Power Delivery Design . . . . .	56
3.4	Predicted Electropermanent Magnet Array Performance . . . . .	61
3.5	Limitations of the Electropermanent Magnet Device . . . . .	67
3.6	Final Comments . . . . .	68
<b>4</b>	<b>Simulation Methods for Device Design</b>	<b>69</b>
4.1	Safer Magnetic Behaviour . . . . .	69
4.1.1	Linear Increase in Force with Reduced Separation . . . . .	72
4.1.2	Peak Force Achieved at a Non-Zero Separation . . . . .	72
4.1.3	Zero Force Crossing Point . . . . .	74
4.2	Anastomosis Device Constraints . . . . .	75
4.3	Electromagnet Optimisation . . . . .	79
4.4	Modification of Electromagnet to Achieve Safer Magnetic Behaviour	83
4.4.1	Interface Magnets . . . . .	86
4.4.2	Embedded Magnets . . . . .	86
4.5	Advanced Control States . . . . .	90
4.5.1	Strong Coupling State . . . . .	90
4.5.2	Weak Interaction State . . . . .	91
4.6	Conclusions . . . . .	92
<b>5</b>	<b>Prototype Design Specification</b>	<b>93</b>
5.1	Prototype 1: Using Commercially Available Magnets . . . . .	93
5.2	Prototype 2: Optimised Device Design . . . . .	97
5.2.1	Custom Embedded Magnet Design . . . . .	97
5.2.2	Further Design Revisions . . . . .	101

5.3	Conclusions . . . . .	102
<b>6</b>	<b>Clinical Context</b>	<b>103</b>
6.1	Regulatory Overview . . . . .	103
6.2	Medical Device Classification . . . . .	104
6.3	Device to Market - United States . . . . .	106
6.4	Device to Market - Ireland . . . . .	108
6.5	Bio-compatibility of Device Materials . . . . .	109
6.6	Risk Analysis and Electrical Safety . . . . .	110
6.7	Patent Protection . . . . .	110
6.8	Summary . . . . .	111
<b>7</b>	<b>Future Work and Closing Comments</b>	<b>112</b>
7.1	Lessons Learned . . . . .	113
	<b>References</b>	<b>113</b>

## List of Figures

1.1	Anastomosis of ascending and descending colon following the removal of the transverse colon ( <a href="http://www.hopkinsmedicine.org">www.hopkinsmedicine.org</a> accessed August 2020). . . . .	2
2.1	Example drawing of an arteriovenous fistula surgically introduced in the forearm for hemodialysis courtesy of: National Institute of Diabetes and Digestive and Kidney Diseases, National Institutes of Health. . . . .	6
2.2	Diagram of the gastrointestinal (GI) tract with key organs labelled [3]. . . . .	6
2.3	Labelled diagram showing the different sections of the large intestine/colon [5]. . . . .	7
2.4	End-to-end anastomosis (EEA) formed using a stapling device [6].	8
2.5	Ileocolic anastomosis using an end-to-side (ESA) technique. A EEA stapling device is used to create the anastomosis [6]. . . . .	8
2.6	Side-to-side anastomosis (SSA) technique used to join the small intestines to the colon [6]. . . . .	8
2.7	Stages of producing a hand-sewn end-to-side anastomosis (ESA) in the colon [6]. . . . .	9
2.8	ECHELON CIRCULAR Powered Stapler device used for colorectal anastomosis, produced by Ethicon United States. . . . .	10
2.9	Biodegradable anastomosis ring (BAR) used for compression anastomosis [14]. . . . .	11
2.10	Nitinol compression device (CAR) produced by NiTi Medical Technologies [15]. . . . .	12
2.11	Magnetic compression anastomosis device (magnamosis) [17]. . .	12
2.12	Intraocular electromagnet device from Dutch Ophthalmic, USA used for the removal of metallic foreign bodies. . . . .	13
2.13	Conceptual drawing of a magnetically propelled capsule endoscope. A rotating external field causes the capsule to rotate which propels the device due to its external spiral shape [19]. . . . .	14
2.14	Magnetic anchoring and guidance system (MAGS) requiring only one transabdominal trocar to insert four MAGS instruments, A- deployment trocar, B- camera, C- retractors, D- cauterizer. The MAGS instruments are positioned using external magnets E. [20].	14

2.15	Magnetic domains orientated: (a) randomly , (b) aligned after application of external field. . . . .	16
2.16	The normal and intrinsic magnetic hysteresis loops for a hard ferromagnetic material with the residual flux density, $B_r$ , and coercivities, $H_{cb}$ and $H_{cj}$ , labelled. . . . .	17
2.17	Demagnetising quadrant of the hysteresis loop showing an example load line and operating point for a magnet of that material with a permeance coefficient, $P_c$ . The effect of a strong demagnetising field, $H_{ext}$ , on the operating point is shown. . . . .	19
2.18	Example demagnetisation curves and load line, adapted from K&J Magnetics (K&J Magnetics, Inc., Pipersville, United States), for a N40 disk magnet with a thickness and diameter of 10 mm. The max demagnetising field that will not result in permanent demagnetisation is marked, $H_{max} \simeq 9.25$ kOe (736 kA/m). . . . .	19
2.19	Magnetic field produced around a current carrying conductor following the right hand rule. . . . .	20
2.20	Mechanically switched magnetic holding device using a single rotatable permanent magnet to turn on and off a holding force on a work piece. (K. Yanagisawa [27]) . . . . .	22
2.21	H-type switchable permanent magnet holding device using-(a) parallel slices of switchable permanent magnets sandwiched between ferromagnetic slices [28], (b) stacked cylindrical magnets with rotation plane parallel to face of work piece [29], (c) rotating disk and concave magnets [30]. . . . .	23
2.22	Linear movement switchable magnet [32], where permanent magnet polarisation directions are indicated by the direction of the arrows. . . . .	25
2.23	Electromagnetic control of armature position with combination of permanent and electromagnets [34]. The permanent magnets are labelled 12 and 14, coils are labelled 24 and 26, and armature labelled 18 . . . . .	26
2.24	Magnetic suspension system using a combination of electromagnets and permanent magnets [36] . . . . .	28
2.25	Magnetic system for magnetic fluid finishing [37] . . . . .	28
2.26	Electropermanent magnet design proposed by Ara kniain [38] . . . . .	30

2.27	Adapted image showing a two core electropermanent magnet cycling through its "off" and "on" states, (a) to (d). The bottom permanent magnet has a higher coercivity remains polarised in the same direction across all states. The top magnet has a lower coercivity and its magnetisation direction is varied by powering the surrounding coil [39]. . . . .	31
2.28	Proposed EPM design for a climbing robot and target surface by P. Ward et al. [40]. . . . .	31
2.29	Proposed EPM wheel design with six total permanent magnet cores with just the AlNiCo permanent magnets surrounded by the coil by F. Ochoa-Cardenas et al. [42]. . . . .	32
2.30	Cylindrically symmetric EPM chuck design [44]. . . . .	34
2.31	Circular EPM lifting assembly aimed at drone picking and delivery systems [45] . . . . .	35
2.32	Valve design using ball bearing to restrict flow based on EPM state [46] . . . . .	36
2.33	Cut view of spherical magnet array, magnetised radially, analysed using the magnetic charge model [47]. . . . .	42
3.1	Simple rod magnet with the pole surface divided into small facets of area $\Delta A$ with a "magnetic charge". . . . .	46
3.2	Annular permanent magnet surface division using: (a) a tailored approach and (b) a general predefined grid. Magnet shape is approximated when using general, i.e. an area that is mostly north pole will be assumed to be all north pole. . . . .	47
3.3	Comparison of predicted forces between a tailored and general surface division approach. The approaches are further compared to results from FEMM software. Forces refer to two annular N40 permanent magnets with inner radius of 2 cm, outer radius of 4 cm, and thickness of 1 cm. . . . .	48
3.4	Surface of a cylindrical magnet where red colouring denotes magnetic north pole, blue colouring denotes magnetic south poles, and green colouring denotes free space. The original image (a) consists of 550x550 pixels. Image (b) is a fine grid approximation of the cylinder consisting of 110x110 pixels. Image (c) is a coarse 10x10 grid approximation of the cylinders top surface. . . . .	49
3.5	Interacting surface magnetisation patterns for an annular set of magnets based off the spring magnet demonstration produced by CMR Polymagnets. . . . .	50

3.6	Custom magnet vice used to hold spring polymagnet demonstration during tensile testing. . . . .	51
3.7	Net measured force between spring polymagnets using tensile testing equipment. . . . .	52
3.8	Square wire packing around bobbin. . . . .	53
3.9	Labeled top view diagram of a hexagonal electropermanent cell. The outer radius of the coil, $R$ , is the sum of the magnet radius, $r$ , and the coil thickness, $t$ . . . . .	53
3.10	Variation in winding thickness and the total number of turns required for changing wire diameter. . . . .	54
3.11	Diagram of a seven cell electropermanent array where the light red represents magnet area, dark red represents coils, and black represents the hexagonal bobbin. . . . .	55
3.12	Relation of magnet area to total device footprint for increasing core magnet sizes. A selection of coil wire diameters show the trend of smaller wire diameters leading to greater percentage area of magnets. . . . .	55
3.13	Prototype hexagonal electropermanent magnet cell using a cylindrical AlNiCo 5 magnet core and 220 turns of 0.56 mm wire. . .	56
3.14	Simplified schematic for a capacitor discharge circuit. . . . .	56
3.15	Capacitor discharge supply schematic. . . . .	58
3.16	Measured voltage and current pulse through an electropermanent magnet cell (with AlNiCo 5 core material) from the capacitor discharge circuit. Capacitors had an initial voltage of 35 V. . . . .	60
3.17	Permanent magnet simulated layouts for a seven cell electropermanent magnet array. Both magnetisation patterns shown consist of magnet cores with the same polarity, (a) with north poles at the interacting surface, (b) with south poles at the interacting surface. . . . .	62
3.18	Simulated maximum attractive force between two seven cell electropermanent magnet arrays. Magnetic patterns used for the simulation of two interacting arrays are shown in Figure 3.17. Zero force plane is shown as a translucent black plane. . . . .	62
3.19	Simulated example of a seven cell array demonstrating safe magnetic behaviour (repulsive at close separations, attractive at further separations) along certain relative rotations. Safe magnetic behaviour is unstable as arrays will rotate away from repulsion to the relative rotations that are most attractive. . . . .	63
3.20	Simulated energy of the unstable safe magnetic response for a seven cell array. . . . .	64

3.21	EPM cell array prototype side (a) and top (b) views. Points of measurement for separation distance and relative rotation between the two cell arrays are shown. The magnet core of the central cell in each array has been replaced by a bar and bearing to restrict separation but allow for relative rotation. . . . .	64
3.22	Diagram of the larger electropermanent array consisting of nineteen cells. The light red represents magnet area, dark red represents coils, and black represents the hexagonal bobbin. . . . .	65
3.23	Simulated nineteen cell array demonstrating stable safe magnetic behaviour. The zero force plane assists in highlighting where the force transitions from repulse to attractive as the separation increases. . . . .	66
3.24	Permeance coefficient and load lines for different AlNiCo 5 magnet geometries, courtesy of Eclipse Magnetics (Eclipse Magnetics Ltd, Sheffield, UK). . . . .	67
3.25	Measured flux density at points on the surface of the north pole of a single prototype magnet. Measured values are in mT and were obtained using the GM08 Gaussmeter from Hirst Magnetic Instruments. . . . .	68
4.1	Sample force-separation plot for two different sets of N40 magnets from K&J Magnetics. Sample disk magnets have a diameter and thickness of 10 mm. Sample ring magnets have an outer diameter of 15 mm, inner diameter of 10 mm, and thickness of 10 mm. . .	70
4.2	Modified image of magnetic anchoring system from a report by G. Domingues et al. [53] showing the Imanlap system. External magnets pull on smaller internal magnets, which are tethered to an organ. . . . .	71
4.3	A safer linear force response compared to a force response from typical magnets. . . . .	72
4.4	Force response from typical magnets compared to a safer magnetic behaviour where the peak force is achieved at a non-zero separation.	73
4.5	Force response from typical magnets compared to a safer magnetic behaviour where the force between magnets changes from attractive to repulsive. A zero force crossing point is introduced due to this behaviour. . . . .	73
4.6	Set of Polymagnets by Correlated Magnetics used to demonstrate magnetic spring behaviour where north poles are coloured red and south poles coloured blue. . . . .	74

4.7	Annotated render of the proposed electromagnet anastomosis device, where $r_{dm}$ is the radius of the daughter magnet, $r_{core}$ is the radius of the iron core, and $r_{device}$ is the radius of the full electromagnet device. . . . .	75
4.8	Process flow diagram for the design of an electromagnet colorectal anastomosis compression device. . . . .	76
4.9	Amp-turns achievable given temperature and sizing/packing constraints (assuming packing factor from "Principles of Power Electronics" by J.G. Kassakian, et al. [55]) . . . . .	78
4.10	Simulated force on a iron disk (10 mm thick, 30 mm wide) due to an electromagnet of fixed outer dimensions for varying iron core sizes. . . . .	78
4.11	Simulated force on a N40 disk (10 mm thick, 30 mm wide) due to an electromagnet for varying iron core sizes with the coil operating in both directions (at the current limit) and the net force control range. . . . .	79
4.12	Simulated force on a N40 ring magnet (10 mm thick, 30 mm outer diameter) of differing inner diameters due to an iron core electromagnet. . . . .	80
4.13	Simulated pressure on a N40 ring magnet (10 mm thick, 30 mm outer diameter) of differing inner diameters due to an iron core electromagnet. . . . .	81
4.14	Simulated force on a N40 disk magnet (10 mm thick) of differing outer diameters due to an iron core electromagnet. . . . .	81
4.15	Simulated pressure on a N40 disk magnet (10 mm thick) of differing outer diameters due to an iron core electromagnet. . . . .	82
4.16	Simulated force-separation plot between a N52 disk daughter magnet (OD=12 mm) and the basic iron cored electromagnet design. Steady state limits of control are shown with the coil operating in both directions. A custom control current between the limits shows a possible controlled response. . . . .	82
4.17	Required force contribution shape from added magnets to achieve safer magnetic force response from electromagnet design. . . . .	84
4.18	2-D Planar cut of device design with possible additional magnets (Interface and Embedded) for tuning of force response shape. Shaded regions mark device permanent magnets. . . . .	85
4.19	Simulated force-separation plot for device with embedded disk magnets of varied dimensions. . . . .	87
4.20	Embedded disk magnet diameter effect on the simulated force control magnitude of the device. . . . .	88



4.21	Simulated force response variations with height for the promising embedded ring magnet, inner radius 4 mm, outer radius 6 mm and force control range. . . . .	89
4.22	Simulated force control magnitude for embedded ring magnet, inner radius 4 mm, outer radius 6 mm for two different heights. . .	89
4.23	Simulated comparison of the original electromagnet device performance to an embedded magnet design with a custom current tuned force response . . . . .	90
4.24	Simulated performance of device in the strong coupling state for different powers. The device is observed to exclusively undergo repulsion at higher powers. . . . .	91
4.25	Simulated performance of device in the weak interaction state for different powers. . . . .	92
5.1	Predicted force separation plots for the two different embedded magnets used for first prototypes. N38 ring has an inner diameter of 8 mm compared to 9 mm for the N45 ring. . . . .	94
5.2	Stack of N38 disk magnets to produce a daughter magnet of diameter 12 mm and height 12 mm. . . . .	95
5.3	Electromagnet iron core with embedded N38 ring magnet. . . .	95
5.4	A sample force-separation plot for a safe magnetic compression device with key grading features marked. . . . .	97
5.5	Design sequence for selecting the best colorectal anastomosis device given constraints. . . . .	99
5.6	Simulated response of a device configuration that produces a strong working point force and a linear response. Daughter magnet material is N48H, Embedded magnet material is N42H with $R_i = 4.9$ mm and $R_o = 5.9$ mm. . . . .	100
5.7	Simulated response of a device configuration that produces a strong peak force at a non-zero separation distance. Daughter magnet material is N48H, Embedded magnet material is N42H with $R_i = 4$ mm and $R_o = 6$ mm. . . . .	100
5.8	Demonstration of how the zero-power force response of the first prototype can be increased by increasing the diameter of the iron core. . . . .	101
5.9	Range of force control reducing as the size of the iron core in the first prototype is increased (i.e. reduction in number of turns). . .	102

## List of Tables

3.1	Summarised results for a force simulation between two cylindrical N40 magnets with a diameter and height of 36.6 mm at a separation distance of 10 mm. The force between the magnets was measured as they were rotated relative to one another at a constant separation distance. . . . .	50
3.2	Voltage values for power schematic. . . . .	59
3.3	Voltage regulator used for power schematic. . . . .	59
3.4	Resistance values for power schematic. . . . .	59
3.5	Capacitance values for power schematic. . . . .	59
3.6	Inductance values for power schematic. . . . .	59
3.7	MOSFETs used for power schematic. . . . .	59
4.1	Colorectal anastomosis device constraints. . . . .	77
4.2	Electromagnet parameters given size and temperature constraints. . . . .	77
4.3	Characteristics of the additional magnet types to improve device performance. . . . .	84
4.4	Device power consumption for different rates of temperature increase. . . . .	91
5.1	Prototype 1 magnet BOM . . . . .	94
5.2	Effect of daughter magnet casing on the forces required to produce suitable anastomosis pressures . . . . .	96
6.1	Devices used for colorectal anastomosis approved for market by FDA. . . . .	107

I, Philip Desmond, certify that this thesis is my own work and has not been submitted for another degree at University College Cork or elsewhere.

---

*Philip Desmond*

## Abstract

This thesis covers the design and development of a controllable electromagnetic compression medical device that addresses the need for control of magnetic attraction in the clinical setting. This work outlines the design of a magnetic medical device to be used for anchoring or compression, namely by shaping the attraction profile between two coupled magnets. The designed device, which consists of both electromagnetic and permanent magnetic components, may be used for colorectal anastomosis.

The thesis includes a review of the existing devices and methods used for colorectal anastomosis. The different methods for which the magnetic strength of a device can be varied are investigated along with how these methods have been previously incorporated into different device designs. A review of the different methods of analysing magnetic systems is also included. These reviews facilitate the choice of a suitable technology for this new design and guide certain device constraints. The advantages of controllability of magnetic attraction and compression are introduced. The incremental simulation-based design stages of the device are presented. Modifications to the starting electromagnet device design are investigated to better achieve safer magnetic behaviour. Additional control states of the device are analysed for how they might ease the installation and removal of the device. A prototype was developed and produced making use of off-the-shelf magnets to be used mainly as a proof of concept. Unfortunately, due to the COVID-19 pandemic, facilities and equipment necessary for experimental testing were inaccessible during crucial stages of the project leading to an absence of some experimental results. However, more extensive simulations were used to develop new prototype designs capable of achieving safer and stronger compression forces using custom magnet designs. Finally, the regulatory landscape for medical devices in key markets is examined and the pathway to market for the proposed device is laid out.

## Acknowledgements

First and foremost, I would like to express my deepest thanks to my project supervisor Dr. Pádraig Cantillon-Murphy, without which this project would not have been possible. His wealth of knowledge and committed guidance was hugely helpful to the progression of the thesis. I could not have asked for a better person to have as a mentor during this time.

I would also like to thank both the Chief and Senior Technical officers of the Mechanical Workshop, Michael O'Shea and Timothy Power. Their expertise in mechanical design and insanely quick turnover times were invaluable for prototyping. They have also guided my mechanical knowledge and helped me learn skills I will carry far beyond this project.

I extend my thanks to all of my fellow postgraduates and labmates for keeping moods and moral high. Thank you also for your friendship, contributions to brainstorming, and listening to my wandering thoughts.

Finally, to my parents Patricia and Philip Desmond, extended family, and friends, thank you for your support. Not only during the course of this thesis, but for all of the help and assistance you have all provided to get me to where I am now.

# Chapter 1

## Introduction

Within healthcare, many factors contribute to better overall patient care. Naturally, the effectiveness of treatments is of key importance but so too are time and cost efficiencies, allowing practitioners to help more patients given finite resources. Growing populations, as well as evolving requirements and expectations, place an ever-growing demand on the healthcare system, driving the need for innovation in medical technology. Within the context of surgical treatments, the development of innovative medical devices and equipment are crucial to addressing this demand. Continued development of medical devices facilitates better treatment outcomes whilst also often reducing operating and recovery times. Medical devices can achieve this by providing new or improved functionality, or by undertaking portions of surgical work, leaving a reduced number of tasks for surgical staff to carry out.

This thesis looks at some of the current limitations of medical devices used for anchoring and compression with regards to their safety and performance. The particular application of focus is a colorectal anastomosis, which involves joining sections of the colon together following the removal of a section, see Figure 1.1. The most dreaded complication of this procedure is an anastomotic leak which is reported to occur in 6% - 30% of cases [1],[2]. Reoperation may be required due to this complication and, if not suitably addressed, an anastomotic leak can be fatal. The different methods of producing the anastomosis are by suturing, stapling, and compression. As further discussed in section 2.2, the method chosen can impact the likelihood of an anastomotic leak, with each method having distinct advantages and disadvantages. Compared to the other methods, compression is of particular interest due to its more uniform compression forces.

## 1. INTRODUCTION

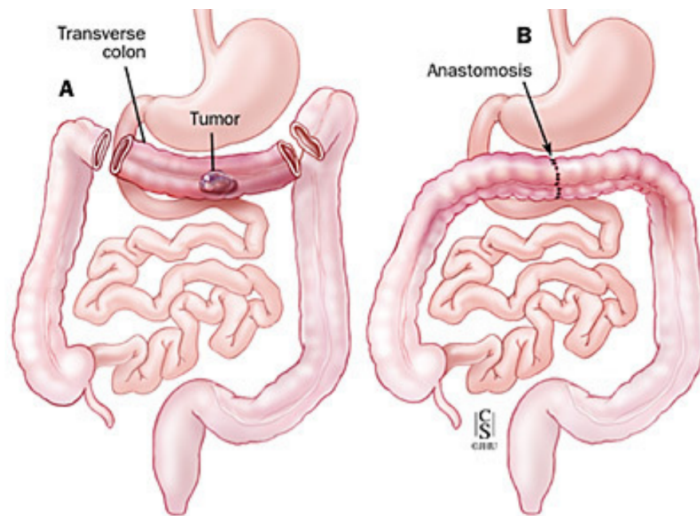


Figure 1.1: Anastomosis of ascending and descending colon following the removal of the transverse colon ([www.hopkinsmedicine.org](http://www.hopkinsmedicine.org) accessed August 2020).

Compression, using magnetic devices, has an added benefit in not introducing any foreign bodies into the healing site. However, the uptake of current magnetic compression devices has been slow mainly due to the longer time needed to produce an anastomosis. Furthermore, existing magnetic compression devices don't offer a degree of control to address different biological conditions (i.e. the thickness and condition of the colon walls can vary significantly between different patients and also along the length of the colon for an individual patient).

Engineering design solutions to address the need for control of device performance must be developed, with a focus on safety and effectiveness. In order to achieve the required degree of control, methods of producing devices with a variable magnetism should be investigated and their suitability assessed. Additionally, to address limitations of existing magnetic compression devices, methods of improving magnetic coupling must also be developed such that the time taken to create an anastomosis is reduced. Further design steps should be taken to ensure that the solutions are robust. For example, a powered solution should ideally operate safely even if power is interrupted temporarily.

The goal of this thesis is to investigate, develop, and implement the design considerations above into an electromagnetic device for colorectal anastomosis. The designed device will address the limitations of existing devices with regards to control and performance. This work will also provide a design method for similar devices to be used in compression and anchoring applications (e.g. gastrojejunostomy which is an anastomosis between the stomach and a section of the small intestines).

## 1.1 Structure of Presented Work

This thesis covers the design and development of a novel controllable magnetic medical device to be used for colorectal anastomosis and other anchoring applications in minimally invasive surgery. The presented structure of the work is as follows:

- Background medical information of importance is presented (see Chapter 2)
- A breakdown of different magnetic technologies is given (see Chapter 2)
- The methods by which magnetic systems can be analysed are reviewed (see Chapter 2)
- Preliminary work is presented on an alternative approach for the design of a controllable magnet device to achieve safer coupling in surgical applications (see Chapter 3)
- The design goals and constraints are outlined (see Chapter 4)
- The simulation methods used for the design of the device are explained (see Chapter 4)
- The simulated operational states of the device are presented (see Chapter 4)
- A prototype is designed and constructed using commercially available magnets (see Chapter 5)
- Device performance is optimised by making use of custom designed magnets (see Chapter 5)
- The regulatory environments which apply to the medical device are examined (see Chapter 6)
- Device design is reviewed for its conformity to applicable standards (see Chapter 6)
- The pathway for bringing the medical device to key markets is planned (see Chapter 6)
- The next steps to develop the device and final conclusions are given (see Chapter 7)



## 1.2 External Influences on the Project Development

During the course of this project there was a global outbreak of the Coronavirus. Measures introduced to limit the effects the COVID-19 pandemic included amongst other things, the closure of Universities and Institutions. Lab equipment and facilities crucial for obtaining experimental results were not accessible during this period, greatly limiting the experimental work which could be achieved. Much of the future work is therefore related to the experimental work which must be completed. Whilst not a substitute for experimental results, greater confidence in the simulated results was obtained by optimising and testing the sensitivity of the device behaviour to various design parameters.

## Chapter 2

# Background Theory and Literature Review

### 2.1 Colorectal Anastomosis

Anastomosis is the connection between two structures or passages that were previously separate/diverging. In a medical context, this usually refers to a connection that has been established between parts of the colon or blood vessels. There are different categories of anastomosis in the body. When occurring between hollow tubes, abnormal anastomoses are often called fistulas. There are several examples of anastomosis occurring naturally in the body (i.e. biological connections) such as in the circulatory system where many veins and arteries connect together as part of the normal body structure. They may also occur due to injuries or illnesses (pathological). An arteriovenous fistula can be caused by trauma and refers to a connection between an artery and a vein. An anastomosis may also be introduced through surgical intervention. The previously mentioned arteriovenous fistula is again one such example where it can be created surgically for some patients undergoing longer-term hemodialysis (filtering of the blood outside of the body), see Figure 2.1.

For transplantations, surgical anastomosis is required to connect the blood supply between the donor organ and recipient. The use of surgical anastomosis extends far beyond just circulatory systems example given thus far. As a result of blockages or damage, an anastomosis might be made between the bladder and urethra or along the gastrointestinal tract. A significant number of surgically produced anastomoses occur in the colon.

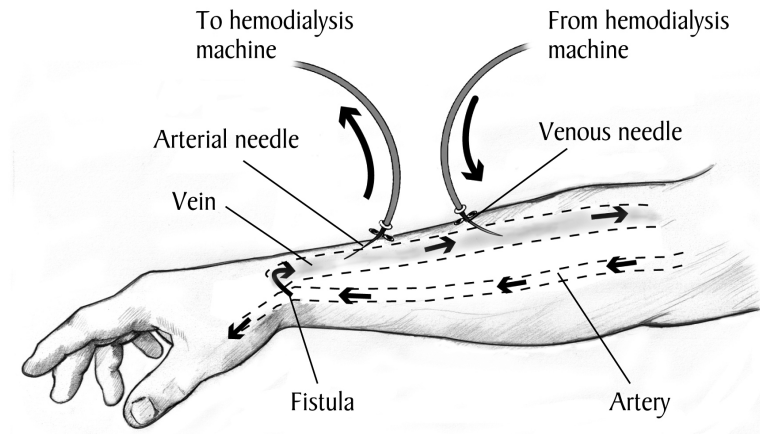


Figure 2.1: Example drawing of an arteriovenous fistula surgically introduced in the forearm for hemodialysis courtesy of: National Institute of Diabetes and Digestive and Kidney Diseases, National Institutes of Health.

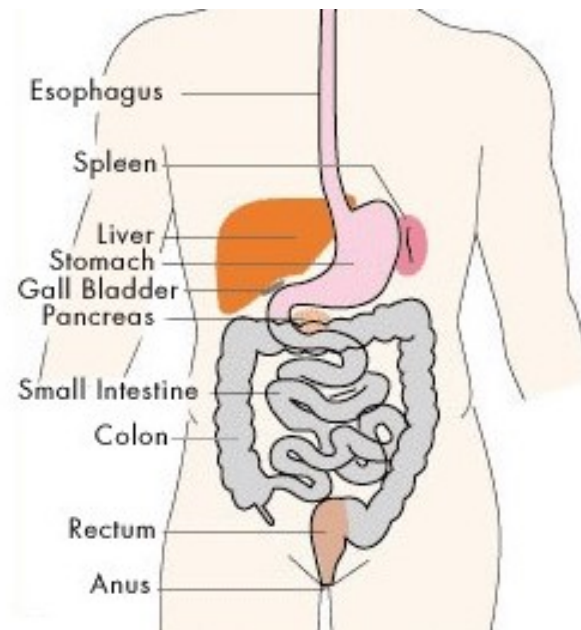


Figure 2.2: Diagram of the gastrointestinal (GI) tract with key organs labelled [3].

The intestines are a long hollow tube nearing the end of the gastrointestinal tract after the stomach, see Figure 2.2. In the intestines, nutrients and water are absorbed from digested food. The two main sections are the small intestines and the large intestines (composed of the colon, rectum, and anus), see Figure 2.3. The small intestines are roughly four times the length of the colon but have a smaller diameter and focuses on absorbing the nutrients of digested food. The colon is about one and a half metres long and adsorbs the water from waste.

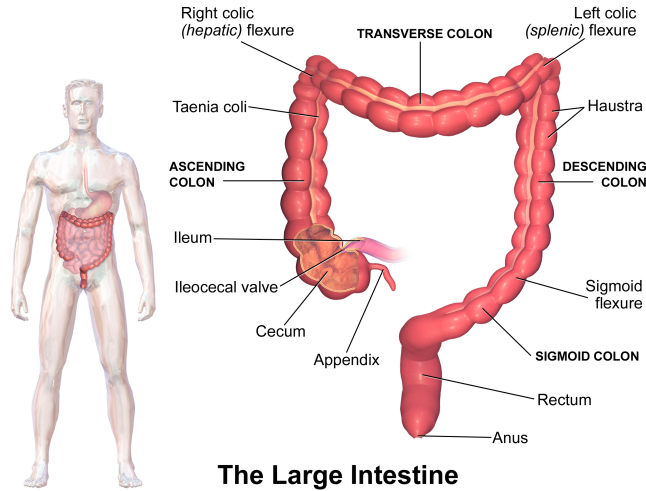


Figure 2.3: Labelled diagram showing the different sections of the large intestine/colon [5].

Colorectal cancer, Crohn's disease, and severe intestinal ulcers are some of the possible conditions leading to a need for bowel resection. In Ireland alone, there were over 18,500 people living with colorectal cancer in 2015 and just under 3000 new cases in 2018 alone [4]. Depending on the sections of the colon to be connected together there are different types of anastomosis that can be carried out, usually done using laparoscopy ("keyhole surgery").

### 2.1.1 End to end anastomosis

An end to end anastomosis (EEA) is a common form of anastomosis used to join two open ends of the colon after a section of the colon has been removed. Figure 2.4 shows the stages of an EEA using a colorectal stapling device.

### 2.1.2 End to side anastomosis

When joining a smaller section of the intestines to a larger section of the colon an end to side anastomosis technique can be used. This is demonstrated in Figure 2.5 for a ileocolic anastomosis (i.e. between the small intestines and the start of the colon).

### 2.1.3 Side to side anastomosis

Side to side anastomosis (SSA) involves connecting two sides of different sections of the colon together along their length, see Figure 2.6.

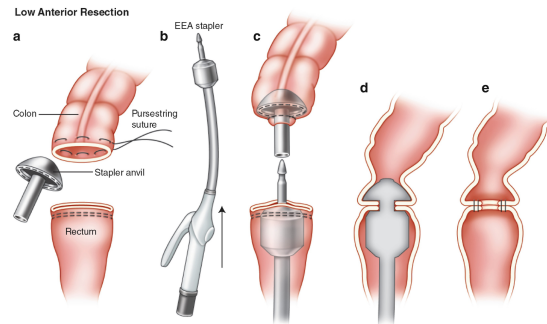


Figure 2.4: End-to-end anastomosis (EEA) formed using a stapling device [6].

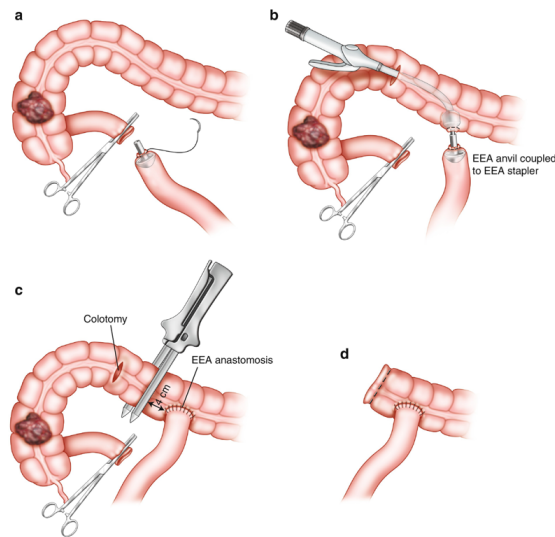


Figure 2.5: Ileocolic anastomosis using an end-to-side (ESA) technique. A EEA stapling device is used to create the anastomosis [6].

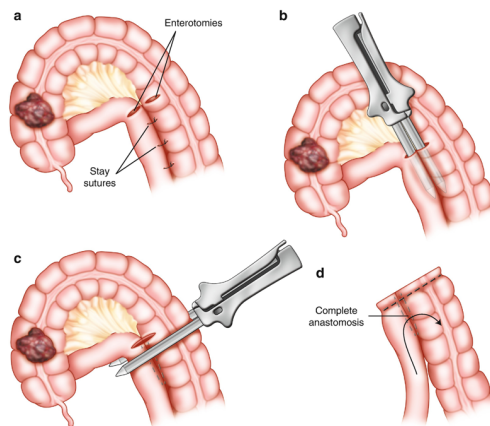


Figure 2.6: Side-to-side anastomosis (SSA) technique used to join the small intestines to the colon [6].

### 2.1.4 Complications in colorectal anastomosis

A major concern following surgical colorectal anastomoses is that a leak may occur. Several publications look at strategies for reducing the rate of anastomosis leakages, such as M. S. Thomas and D. A. Margolin [1] who reported the rate of leakage can be anywhere between 6% - 30%. Whilst they focus on definitions of leakages and risk factors like malnutrition and diabetes, it is important to note that the method or device used to carry out the anastomosis also has an effect on the leakage rate. G. Branagan et al. [2] looked at prognosis following anastomotic leakage in colorectal surgery patients. Part of their study looked at rectal anastomosis patients where it was observed that 6.3 % experienced leakage. There was a significantly higher 30 day mortality for the patients who experienced an anastomotic leakage, 10% compared to 2% for the patients who had no leakage. The exact biological process of how anastomotic leakages develop is still not well understood and, J. Bosmans et al. [7] make the point that the healing process must be better understood to allow for the development of methods to reduce leak rates.

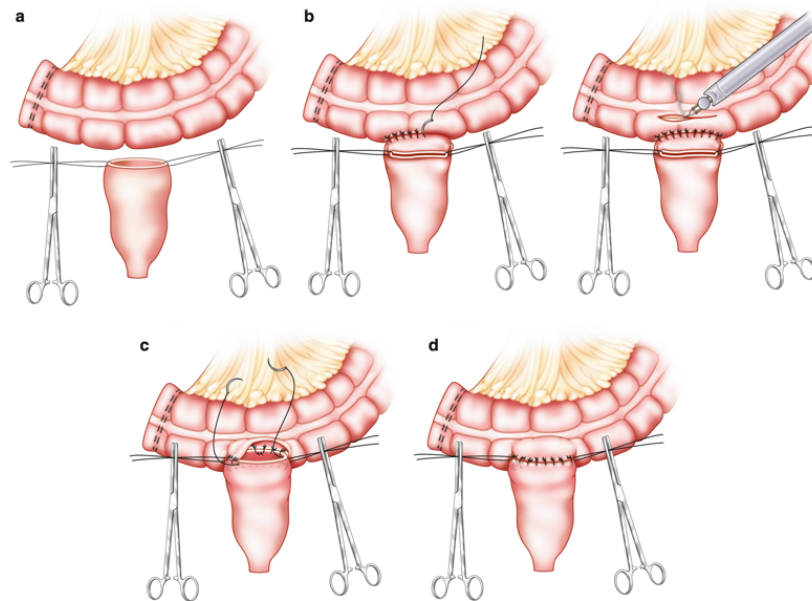


Figure 2.7: Stages of producing a hand-sewn end-to-side anastomosis (ESA) in the colon [6].

## 2.2 Tools for Colorectal Anastomosis

Given the large number of cases requiring colorectal anastomosis and dangerous possible complications, several methods and tools have been developed to carry

out colorectal anastomosis. Listed below are the main categories for which the existing approaches fall under.

- Suturing/Sewing
- Stapling
- Compression

Suturing is the original method for creating an anastomosis in the colon. Figure 2.7 shows the stages of producing a hand-sewn colorectal anastomosis. Originally, suturing materials such as nylon, silk, and linen were commonly used. Polydioxanone sutures are now the predominant material of choice for anastomoses along the GI tract. Studies have looked at the finer implementations of hand-sewn anastomoses such as, whether they are single or double layer, and if a interrupted or continuous suture is superior, but in both cases there is little to no difference in the rates of leakages [8] [9].

The most popular alternative to suturing for colorectal anastomoses is stapling. Figure 2.8 shows a commercially available stapling device from Ethicon (Ethicon, Inc., New Jersey, United States) that can be used for anastomosis in the colon. Sizes of 21 mm - 33 mm are common for anastomoses diameters using these devices. There have been many studies which look to compare stapled and hand-sewn techniques. However, the findings are often contradictory, with many surgeons using both techniques. For example two recent studies show contradicting results for the rate of leakage in ileocolic anastomosis for hand-sewn versus stapled techniques [10], [11]. What is agreed upon between the two techniques is that, the time taken to perform hand-sewn anastomosis is longer but the rate of stricture is greater for stapling [12].



Figure 2.8: ECHELON CIRCULAR Powered Stapler device used for colorectal anastomosis, produced by Ethicon United States.

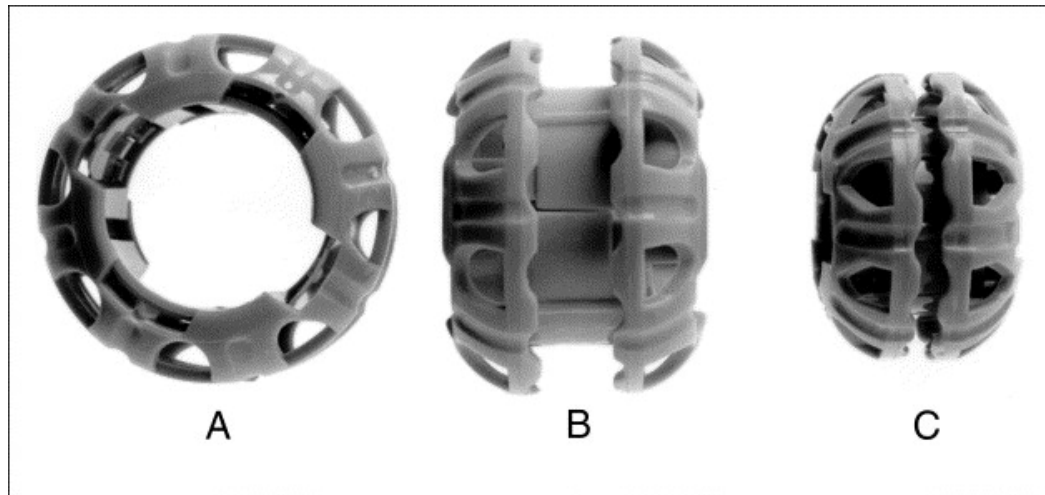


Figure 2.9: Biodegradable anastomosis ring (BAR) used for compression anastomosis [14].

Compression anastomosis in the colon was first described as early as the 1800s however it has not yet become a widely adopted method. Despite this, this method continues to be a popular topic of research. Unlike staple approaches, in compression anastomosis there are no foreign bodies in the anastomosis site. The "Murphy button" was an early mechanical anastomosis device designed for use in the intestines in 1892 [13]. The biodegradable anastomosis ring (BAR) proposed by TG Hardy was one of the most promising compression devices. Shown in Figure 2.9, the device is made of absorbable polyglycolic acid and appeared to operate safely and effectively [14]. However, supposed issues during operations contributed to the device's sidelining. NiTi Medical Technologies (NiTi Medical Technologies Ltd., Missouri, United States) produce a nitinol (nickel-titanium) compression anastomosis ring which is capable of producing end-to-end and end-to-side anastomoses. The device, shown in Figure 2.10, was studied in a clinical trial and found to have similar performance to conventional stapling technologies [15]. A magnetic compression anastomosis device (magnamosis), shown in Figure 2.11, was used to perform side-to-side anastomosis successfully in the small bowel in five patients according to C. E. Graves et al. [16]. The magnetic device consists of two magnetic rings which self align and produce a non-uniform compression in order to form an anastomosis. In compression anastomosis, there is an outer ring of compression where the anastomosis will occur. Inside this ring, the tissue undergoes necrosis as the blood supply is cut off, creating the opening.



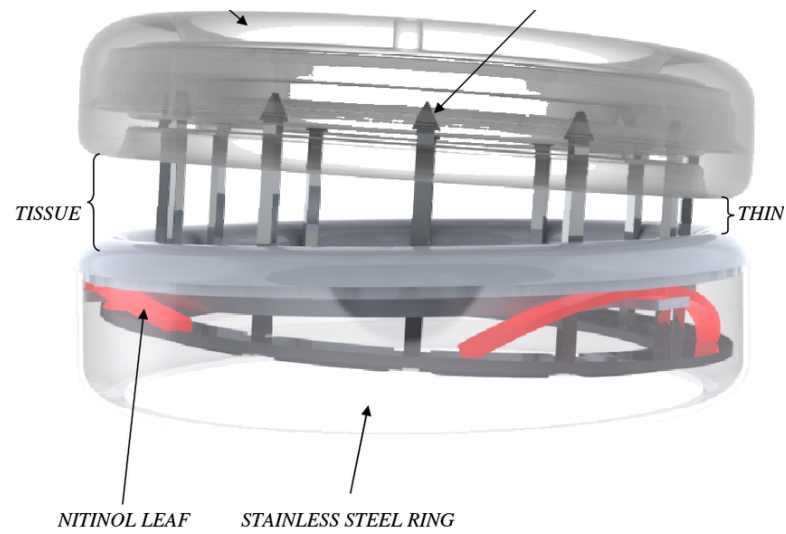


Figure 2.10: Nitinol compression device (CAR) produced by NiTi Medical Technologies [15].

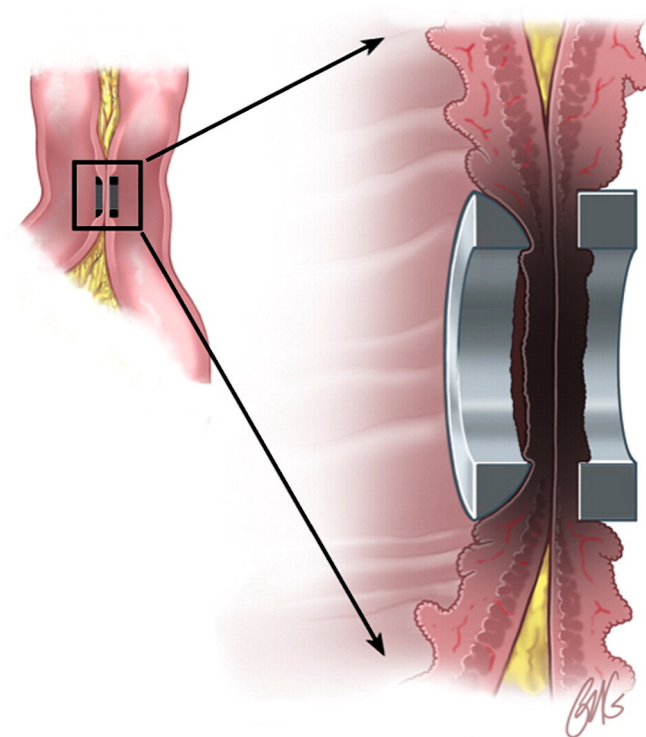


Figure 2.11: Magnetic compression anastomosis device (magnamosis) [17].

## 2.3 Magnetics for Medical Devices

Magnets are now commonplace in medical settings. The best known application is likely magnetic resonance imaging (MRI) machines, which are a crucial piece of equipment for internal imaging and diagnostics. Most MRI machines make use of super-cooled electromagnets, but machines that use permanent magnets and non-supercooled electromagnets can also be found. Magnets have been used for many years to remove metallic splinters from the body. D. Jackson Coleman et al. [18] found magnetic extraction minimized the surgical trauma on a patient with a retained intraocular foreign body injury by providing good control of the foreign body during extraction. A commercially available intraocular electromagnet is shown in Figure 2.12 produced by Dutch Ophthalmic, USA. The electromagnet in the device, controlled by a foot pedal, allows the surgeon to enable and disable the magnetic field.



Figure 2.12: Intraocular electromagnet device from Dutch Ophthalmic, USA used for the removal of metallic foreign bodies.

An endoscopy is a medical procedure to visually examine the body internally. The endoscope is inserted into the organ to be examined and returns images to the operator. Magnetically controlled capsule endoscopes were developed to reduce the trauma and suffering of the patient. M. Sendoh et al. [19] designed one such magnetically propelled capsule endoscope as shown in Figure 2.13. The capsule is wirelessly driven by a rotating external field which generates a torque on the magnet in the capsule, propelling the capsule due to its external spiraled shape. The direction of the propulsion can be changed by altering the external rotational magnetic field.

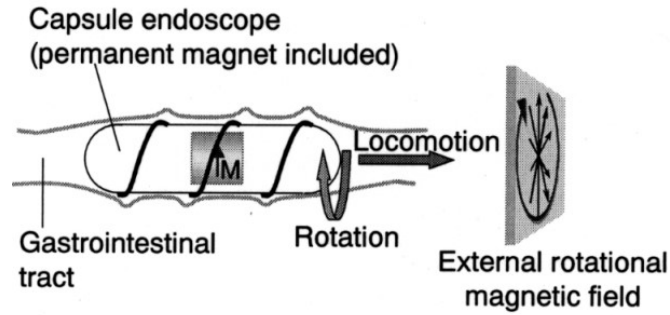


Figure 2.13: Conceptual drawing of a magnetically propelled capsule endoscope. A rotating external field causes the capsule to rotate which propels the device due to its external spiral shape [19].

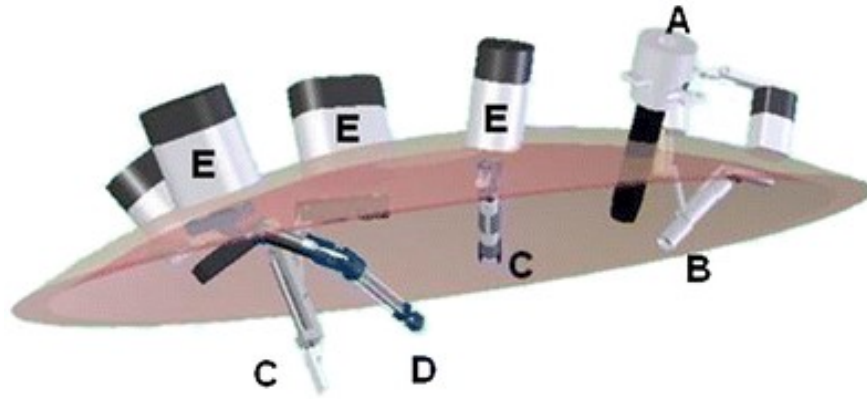


Figure 2.14: Magnetic anchoring and guidance system (MAGS) requiring only one transabdominal trocar to insert four MAGS instruments, A- deployment trocar, B- camera, C- retractors, D- cauterizer. The MAGS instruments are positioned using external magnets E. [20].

The transabdominal magnetic anchoring and guidance system (MAGS), discussed in [20], made use of a single incision to deploy four MAGS instruments, see Figure 2.14. The system was used to carry out two nonsurvival porcine nephrectomies. A single transabdominal trocar was required to insert the MAGS instruments which are coupled to external magnets for positioning and control.

The examples of electromagnetics in medical devices above is far from an exhaustive list but rather, demonstrates the wide range of applications and working principles.

## 2.4 Magnetism

For over two thousand years people have been aware of the phenomenon of magnetism. Magnetite, commonly referred to as lodestone, is the first magnetised material that was discovered. Lodestone's discovery was reported in *Historiae Naturalis XXXVII* by Pliny the Elder, a Roman naturalist, where it says that a shepherd was the first to come across the material. Whilst walking in the mountains the shepherd Magnes noticed his shoes, namely the iron parts, were attracted towards the ground. Following a bit of digging he unearthed the magnetised material, lodestone [21]. The origins of the name lodestone relate to its earliest use as a compass. Much like the lodestar which can lead one to the geographical north, the lodestone, when in the form of a small needle, could lead one to the magnetic north pole. For hundreds of years following its discovery magnets and magnetism were surrounded by superstition and suspicion. Sailors believed that missing ships may have been pulled in and dissolved by magnetic islands pulling on the nails of the ship [22]. Lodestone was also said to have a plethora of healing and health benefiting properties. Cleopatra supposedly slept with magnetic material on her head and wore magnetic jewellery in an effort to counter the effects of aging on her appearance.

There exist many forms of magnetism such as: Diamagnetism, Paramagnetism, Antiferromagnetism, Metamagnetism, Ferrimagnetism, Ferromagnetism [23]. The orbital motion and the spin of electrons give rise to the magnetisation of a material. Although not discussed in any more detail in this thesis, an interested reader may refer to [23] and [24] for more information on magnetism. Lodestone is classed as a Ferrimagnetic material meaning it has magnetised regions that are strongly linked to each other in anti-parallel directions. The anti-parallel regions are of different strengths leading to a net magnetisation of the material. In the last two centuries there have been significant developments in producing stronger, more compact, and more persistent magnets which make use of the ferromagnetic materials such as iron, cobalt, and nickel (discussed in section 2.4.1).

### 2.4.1 Permanent Magnets

Permanent magnets are largely made with ferromagnetic materials. In a ferromagnetic material, the magnetic moments interact strongly, orientating themselves parallel to one another. The materials are physically made up of a large number of magnetic domains. The alignment of the magnetic moments leads to a net magnetism of each magnetic domain even in the absence of an external

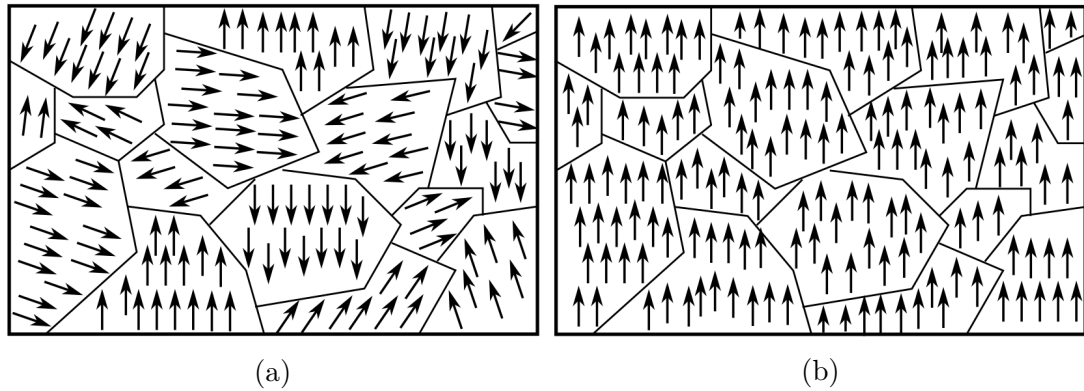


Figure 2.15: Magnetic domains orientated: (a) randomly , (b) aligned after application of external field.

magnetic field. Nevertheless, ferromagnetic materials are often found to have no net magnetism due to their magnetic domains being randomly orientated, Figure 2.15a. The magnetic domains of the material can be aligned, as in Figure 2.15b, by applying an external magnetic field. A portion of the now magnetised material remains magnetised even after the external magnetic field is removed. The residual flux density,  $B_r$ , is the term describing the flux density that remains when an external field, that was strongly saturating the material, is removed. The material can be demagnetised if an external field of suitable strength is applied in the opposite direction of the materials magnetisation. The minimum value of this demagnetising field is the ‘coercivity’ of the material,  $H_c$ . Ferromagnetic materials with large coercivities are considered ‘hard’ whereas materials with small coercivities are considered to be ‘soft’. A hysteresis loop is produced when the flux density,  $\mathbf{B}$ , is plotted against the field strength,  $\mathbf{H}$ , for a ferromagnetic material. The full magnetic hysteresis loops of a typical ferromagnetic material to an external field is shown in Figure 2.16. The normal loop includes the both the external field and field of the material whereas the intrinsic loop is just the contribution from the material. The magnetic polarisation,  $\mathbf{J}_p$ , is used for representing the field flux density from only the material. The normal and intrinsic loops can cross the H axis at different points which are marked as  $H_{cb}$  and  $H_{cj}$  respectively. The recoil permeability is measured off of the normal loop as shown in Figure 2.16.

Magnetised materials may also be demagnetised by heating them to a suitably high temperature. Each material will have its own temperature at which it demagnetises, called the Curie point. Above the Curie point, the magnetic domains are thermally excited to the point where they break down. The domains, consisting

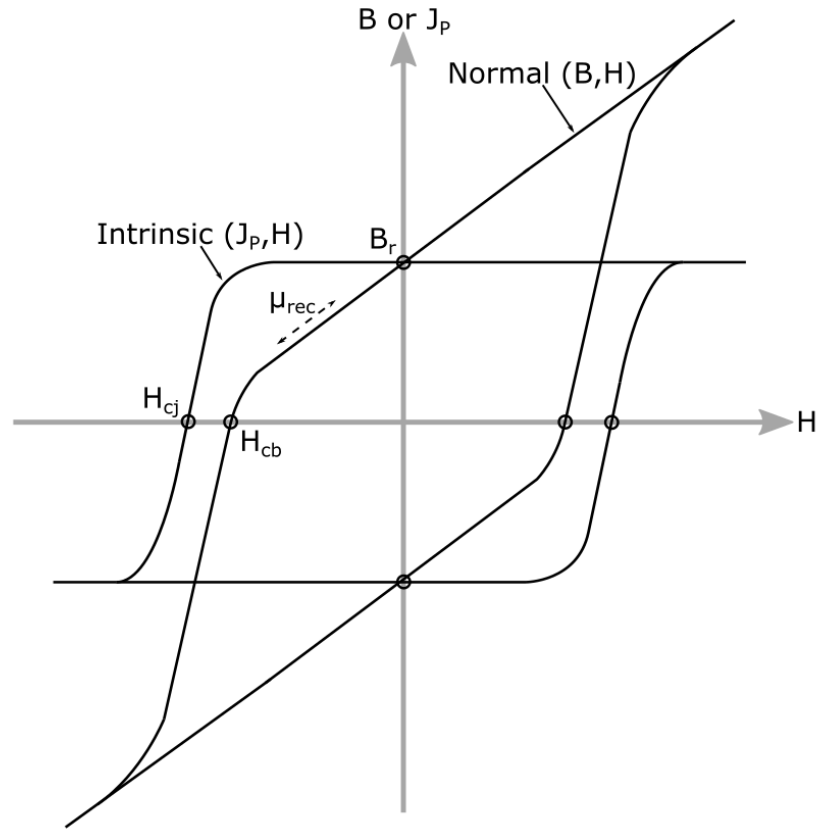


Figure 2.16: The normal and intrinsic magnetic hysteresis loops for a hard ferromagnetic material with the residual flux density,  $B_r$ , and coercivities,  $H_{cb}$  and  $H_{cj}$ , labelled.

of areas where the spins are aligned, are broken down as the thermal perturbations overcome the interactions that previously caused the spins to align. The spins are then randomly orientated with respect to each other, providing no net magnetism [23].

During the 20th century, major advances were made in magnet materials with the maximum energy product doubling every twelve years [25]. Since the 1980s, advances in alloys of ferromagnetic materials and rare earth materials, particularly Neodymium, have led to magnets that are stronger, much more compact, and more resistant to demagnetisation. The advances in magnetic materials have greatly increasing the prospective applications. There is now an abundance of common items which make use of permanent magnets, with everything from refrigerator magnets to motors and generators to old televisions to jewellery clasps taking advantage of magnetic phenomenon.

### 2.4.1.1 Permeance coefficient

There are many factors that dictate where on the hysteresis loop a permanent magnet will operate. When designing a device with that will make use of hard magnet materials, it is important to consider the conditions the magnet will be exposed to, such as temperature and external field strengths. A permanent magnet will largely operate in the upper left quadrant of the loop from Figure 2.16, this is known as the second quadrant or demagnetising quadrant. Figure 2.17 describes the operation of a permanent magnet under the effects of a strong demagnetising field,  $H_{ext}$ . The slope of the load line is dependant on the physical shape of the magnet and is often referenced as the permeance of the magnet,  $P_c$ , which is related to the slope by Equation 2.1.

$$P_c\mu_0 = \frac{B_d}{H_d} = \text{Load line slope} \quad (2.1)$$

Once magnetised, the magnet will operate at the point where the load line intersects with the normal hysteresis loop, with a flux density,  $B_d$ , and field strength,  $H_d$ . A strong demagnetising field can permanently reduce the field produced by a magnet, as is the case with,  $H_{ext}$ , in Figure 2.17. When exposed to the strong external field, the load line shifts along the H axis, now intercepting the hysteresis loop at point  $p_2$ . As  $p_2$  is after the knee of the curve, even after the removal of the external field, the magnet does not return to its original operating point but instead returns along the slope  $\mu_{rec}$  to point  $p_3$ . At point  $p_3$  the external field produced by the magnet has been reduced. Therefore, in order to avoid undesired demagnetisation, the expected demagnetising fields should be estimated and taken into account for the choice of permanent magnet material and physical shape. For simple magnet geometries such as bar magnets and cylinder magnets the permeance coefficient,  $P_c$ , can be calculated by hand. Simulations can be used for more complicated magnet systems to determine magnet performance.

As an example, a disk magnet with a diameter of 10 mm and thickness of 10 mm has a permeance coefficient of around 3.46. From Figure 2.18, the maximum demagnetising field this magnet can be exposed to,  $H_{max}$ , can be estimated by shifting the load line until its intersection point with the normal hysteresis loop is no longer along the linear portion of the loop. For a N40 magnet operating at 20°C,  $H_{max} \simeq 9.25$  kOe (736 kA/m). If the external field remains less than  $H_{max}$  then the disk magnet will return to its original operating point when the external field is removed.

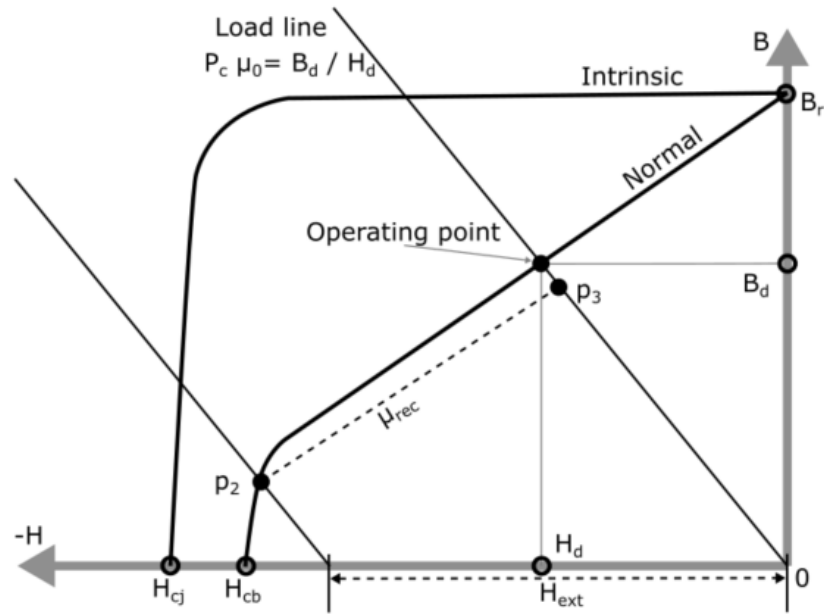


Figure 2.17: Demagnetising quadrant of the hysteresis loop showing an example load line and operating point for a magnet of that material with a permeance coefficient,  $P_c$ . The effect of a strong demagnetising field,  $H_{ext}$ , on the operating point is shown.

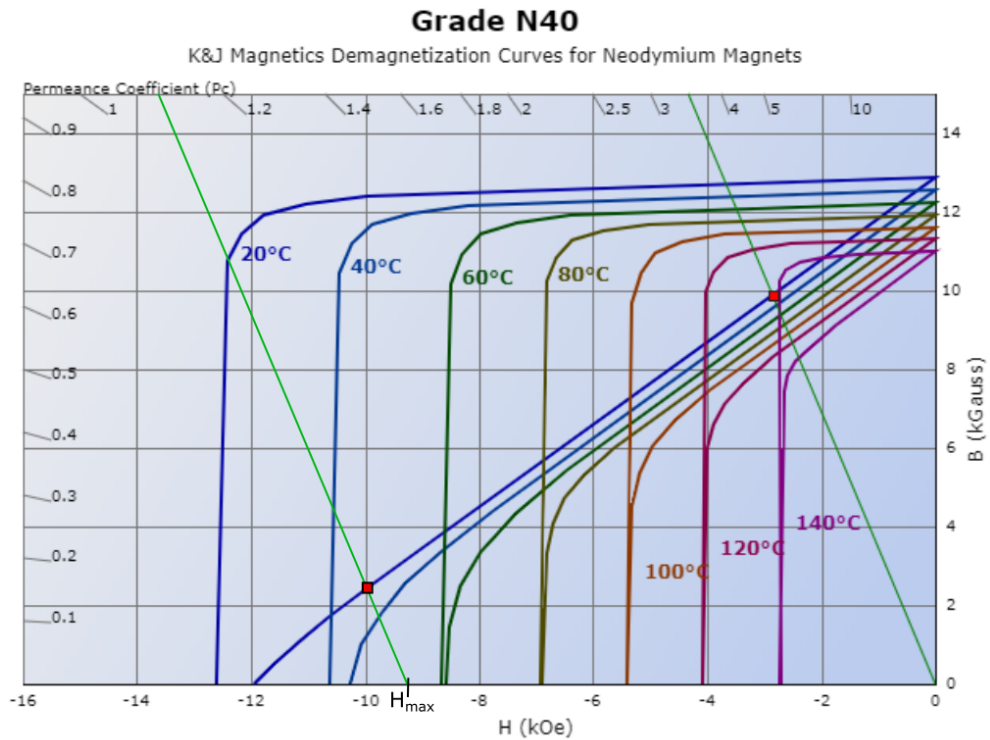


Figure 2.18: Example demagnetisation curves and load line, adapted from K&J Magnetics (K&J Magnetics, Inc., Pipersville, United States), for a N40 disk magnet with a thickness and diameter of 10 mm. The max demagnetising field that will not result in permanent demagnetisation is marked,  $H_{max} \simeq 9.25$  kOe (736 kA/m).



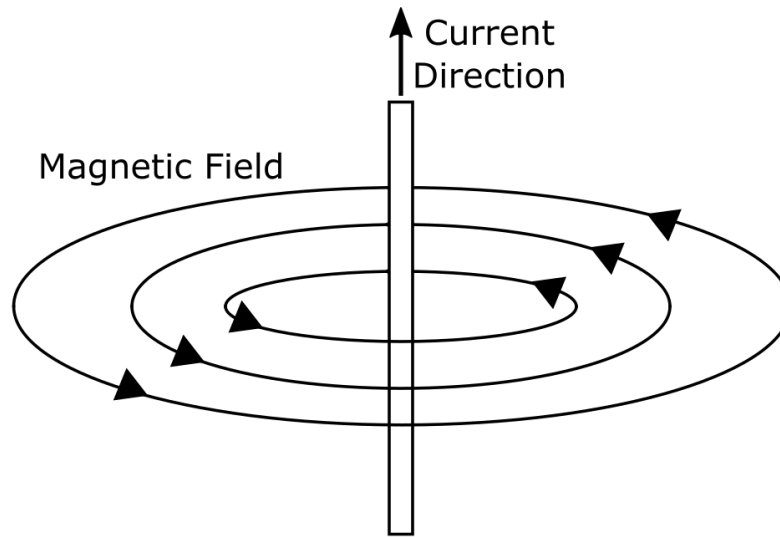


Figure 2.19: Magnetic field produced around a current carrying conductor following the right hand rule.

### 2.4.2 Electromagnets

A current carrying conductor generates a magnetic field according to Ampère's law (introduced as one of Maxwell's equations in section 2.7). The direction of a magnetic field around a conductor is given by the right hand rule where, if the current travels in the direction of the thumb then the magnetic field circulates around the conductor in the direction of the fingers, see Figure 2.19. When a current carrying conductor is formed into multiple successive turns, forming a solenoid or coil, a strong magnetic field is generated at the coils centre. This is called an electromagnet.

Controlling the current through the conductor controls the magnetic field of the electromagnet. The ability to vary the magnetic field by current leads to a diverse range of applications. Electromagnets are used in electric motors, in lifting cars in scrapyards, for writing data to a hard disk drive, in transformers for power transmission, and are crucial to the operation of MRI machines.

To improve the performance of an electromagnet, a soft ferromagnetic core made of iron or steel is often placed inside the coil. The core itself does not act like a magnet until it is placed in an external magnetic field. When the external field is applied, some of the magnetic domains of the material align giving the material a net magnetism which adds to that produced by the coil of the electromagnet. Following the removal of the external field, the core material will retain a portion of the net magnetisation as the magnetic domains aligned with the external field grew and domains in other alignments shrunk.

## 2.5 Mechanically Controlled Magnet Systems

Applications demanding control of magnetic strength have lead to the development of variable and switching magnetic systems. There exists two main types of systems: those varied by mechanical control, and those that are electrically controlled.

Mechanically varying magnetic systems are designed such that their overall magnetisation state ("on", "off", variable) is altered by changing the spatial arrangement of the system in some manner. Generally, this involves physically turning or displacing a part of the system such that the preferred path of the magnetic field is changed. In this section, when the system is said to be turned "on" or turned "off" this refers to how it appears externally, i.e. if the system is "off" there is still the same amount of magnetic flux as in its "on" state but that flux is now contained within the system and therefore the system appears to be turned "off" externally.

Such mechanically controlled magnetic holding devices are demonstrated by G. N. Levesque [26] and K. Yanagisawa et al. [27] whereby a magnetic system can be turned "on" and "off" through the rotation of a single cylindrical permanent magnet within two keepers, see Figure 2.20. In the design of Yanagisawa et al., there are two permanent magnet orientations of interest: (1) when the magnets magnetisation is aligned horizontally, and (2) when its magnetisation is aligned vertically. In case 1, ignoring any air gaps, the magnetic field from the north pole of the magnet links directly with only one of the keepers, then into the base material, before it links back through the second keeper and into the south pole of the magnet as shown by the dotted field lines of Figure 2.20. In this situation the magnetic system is in its "on" state supplying a force to pull the magnet and base together. In case 2, when the magnet has been rotated such that its magnetisation is vertically aligned, the field from the north pole of the magnet does not link solely into either keeper but instead is shared equally into both. On its return path the field links along the keepers and into the south pole of the magnet as shown by the solid field lines of Figure 2.20. In case 1, there will exist an air gap between the keepers and the base. The majority of the energy is stored in these air gaps. In an effort to minimise the system energy, the field generates a force to draw the keepers and base together, thereby reducing the air gap size. In the second case the magnetic field is fully contained within the PM and its keepers, never linking into the base and hence no force is generated to pull the two together. Such a design is well suited for strong holding devices. In

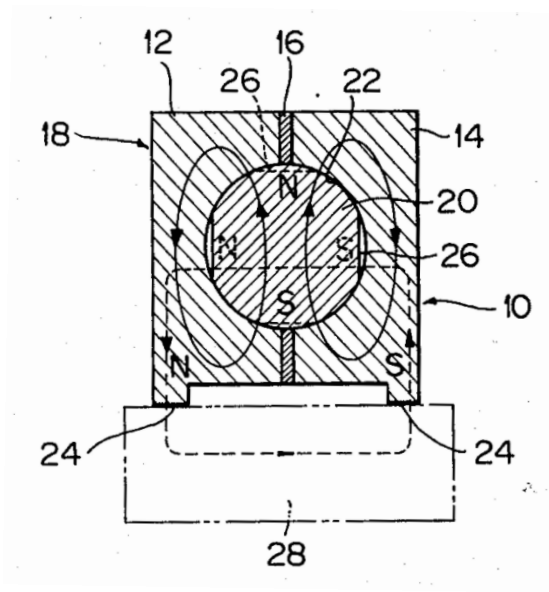


Figure 2.20: Mechanically switched magnetic holding device using a single rotatable permanent magnet to turn on and off a holding force on a work piece. (K. Yanagisawa [27])

its "on" state the permanent magnet can produce a large holding force but, when holding is no longer required, the force necessary to separate the holding device is only that required to rotate the magnet (for which mechanical advantage can be used) and not that to directly oppose the magnetic holding force.

There have been several other designs for switching magnetic systems that make use of two permanent magnets one of which may rotate. Figure 2.21a shows the design of a magnetic holding device as proposed by M. Baermann [28]. The device is composed of alternate layers of, (1) a square permanent magnet with a circular cut-out in which a circular magnet fits, (2) a ferromagnetic material with a partition of non-magnetically conductive material which splits the layer in half.

The magnets are polarised in the direction normal to the layer contact face. The first state of the device occurs when the magnetisation direction of the inner circular magnet matches that of the outer square magnet such that each half of the ferromagnetic layer sees a singular magnetic polarity from the magnetic layer. As each layer of magnets is polarised in an opposite direction, they provide the same magnetic polarity into the ferromagnetic layer giving it a net magnetisation. This is the "on" state of the device and it can hold a work piece to any of its sides. In the alternative case, the inner circular magnet is rotated so that each ferromagnetic layer has both north and south poles in contact with a singular half. In this configuration, the field is fully contained within the magnets and

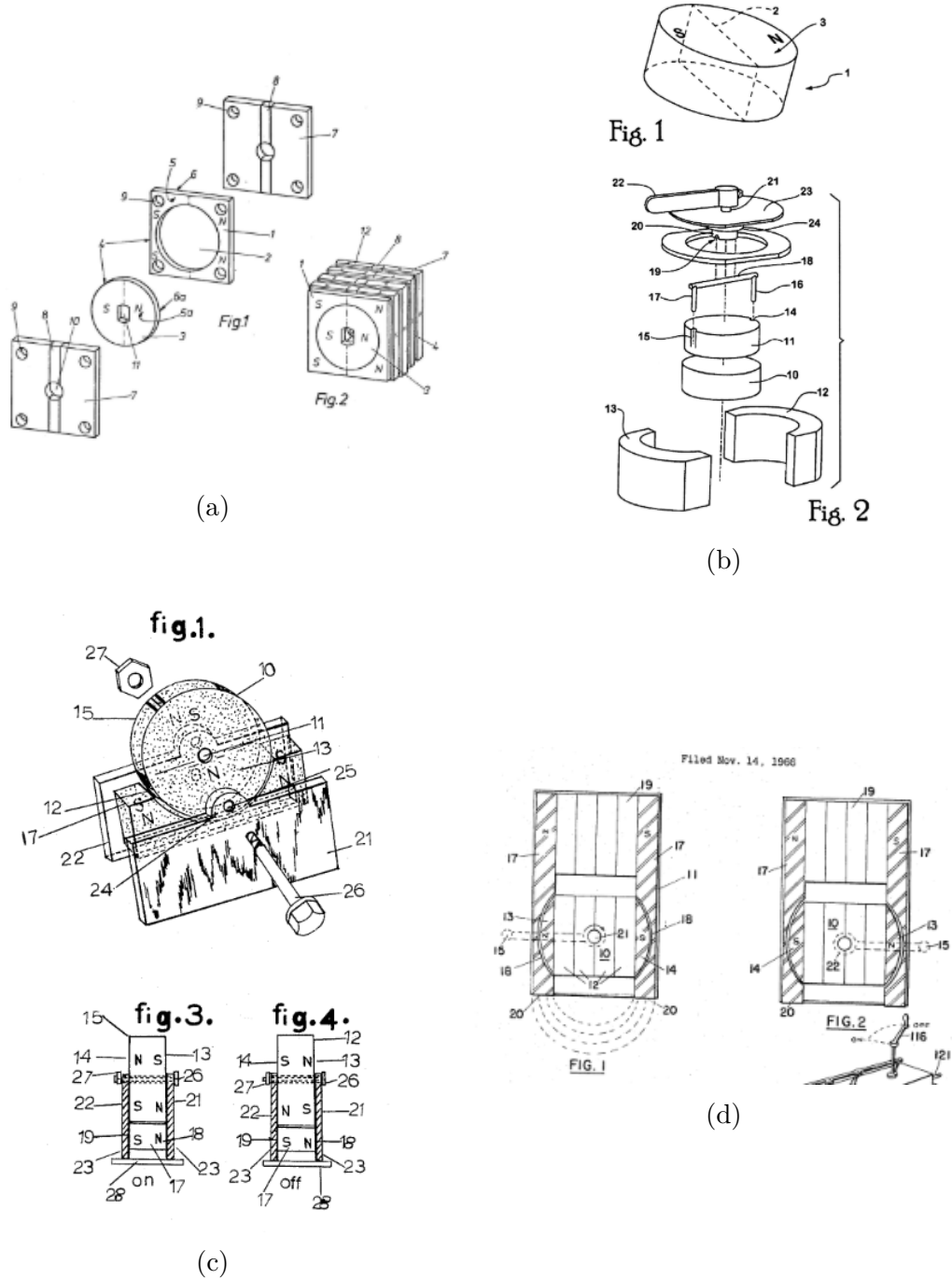


Figure 2.21: H-type switchable permanent magnet holding device using-(a) parallel slices of switchable permanent magnets sandwiched between ferromagnetic slices [28], (b) stacked cylindrical magnets with rotation plane parallel to face of work piece [29], (c) rotating disk and concave magnets [30].

ferromagnetic layer. The device is in its "off" state. This design has the form of a H-type switchable magnet device. A H-type switchable magnet consists of two permanent magnets placed in parallel between two pieces of magnetically conductive material. Typically, one of the permanent magnets can rotate so as to change its direction of magnetisation. Other H-type switching magnets are presented in Figures 2.21b to 2.21d. A. K. Bey [31], Figure 2.21c is the earliest of these designs. Despite having the simplest construction, the bulky design limited its commercial implementation. More robust designs are presented by P. J. Underwood [29], in Figure 2.21b, and A. F. Israelson [30], in Figure 2.21d, where the rotating magnet turns in a plane parallel and perpendicular to the surface of the work piece respectively. In their "on" state, the magnetisation of the two magnets aligned in the same direction, magnetising one ferromagnetic keeper piece as a magnetic north pole and the other as a magnetic south. In their "off" state, one magnet is rotated such that opposite poles are in contact with the same ferromagnetic material, thus the field is fully contained and there is no net linking flux external to the device.

An alternative to rotational actuation for the mechanically switched magnet devices is linear actuation. This approach is far less common with very limited coverage in literature. Figure 2.22 shows an example of such a system described in J.M.D. Coey's "Permanent magnet applications" [32]. This design involves two layers with spaced blocks of iron on the bottom layer and spaced magnet blocks on the top layer. The top layer slides in order to join or separate the magnets with the blocks of iron. When the top layer is shifted such that the iron and magnets are connected, the field from the magnets is directed through the iron and into the work piece. As the magnets are magnetised in alternate directions, the field travels into the work piece from one block and returns back to a magnetic pole through the neighbouring blocks. This is the "on" state of the device. Shifting the top layer so that the magnets are not in contact with the iron blocks breaks the holding force of the device on the work piece.

M. Tavakoli et al. [33] demonstrated the versatility of these mechanically switched magnetic systems for robotics applications. By attaching a servo motor to a design like that proposed in [29], they were able to implement these permanent magnet devices in a mobile climbing robot. Despite the larger spontaneous power requirement, they found this implementation of magnetic anchoring to be more energy efficient than an equivalent electromagnetic system.

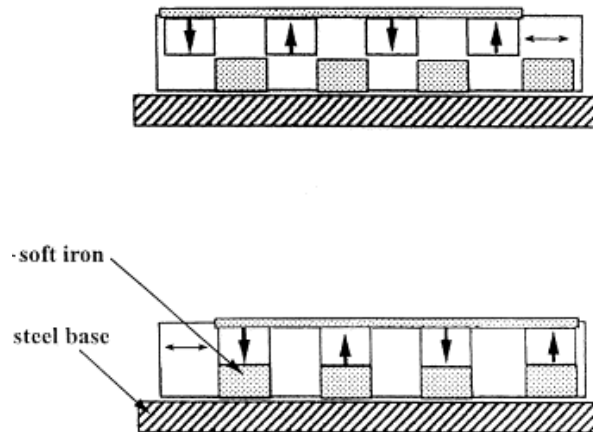


Figure 2.22: Linear movement switchable magnet [32], where permanent magnet polarisation directions are indicated by the direction of the arrows.

## 2.6 Electrically Controlled Magnetic Systems

### 2.6.1 Electromagnet Systems

There exists a great variety in magnetically controlled systems that use electricity to change their state. Electromagnets are themselves a form of electrically switched magnet. As discussed earlier in section 2.4.2, a current carrying coil generates a magnetic field, while controlling the current allows for the electromagnet to be turned "on" and "off". The main issue with electromagnets is the heat generated by a long duration "on" state. In order to maintain its magnetic field, an electromagnet requires constant current which in turn generates Joule heating. To compensate for heating during operation, cooling systems may have been implemented. However, they are often large and introduce more cost and complexity to the overall design. In the case of a disruption in power, the system will move to its "off" state, posing potential reliability risks. This issue may be lessened through the addition of an uninterruptible power supply (UPS) to the design which again adds to the complexity and cost of electromagnet solutions.

### 2.6.2 Combination Magnet Systems

Electromagnets are not suited to extended "on" applications due to their constant current dissipation in the "on" state. Some designers have made use of a combination of electromagnets and permanent magnets to achieve a normally "on" system that can be temporarily turned "off" with magnetic flux cancellation. Such a device is detailed by T. Ito et al. for electromagnetic control of armature position [34]. As shown in Figure 2.23, the design is composed of two permanent magnets

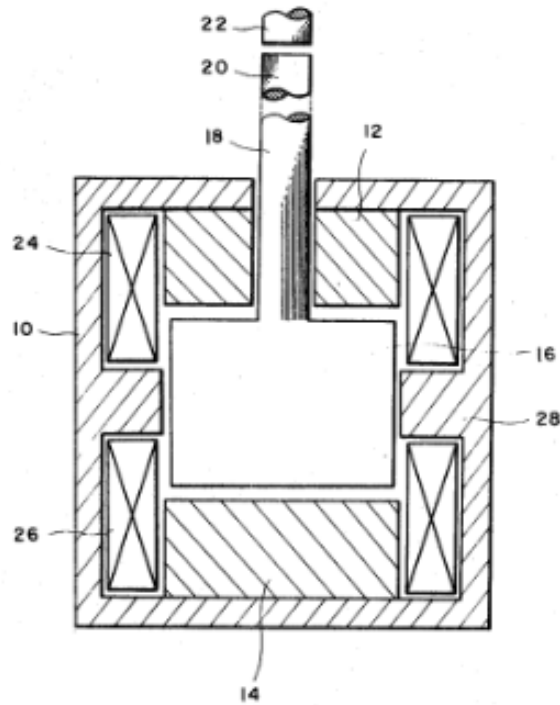


Figure 2.23: Electromagnetic control of armature position with combination of permanent and electromagnets [34]. The permanent magnets are labelled 12 and 14, coils are labelled 24 and 26, and armature labelled 18

surrounded by coils between which an armature was positioned. The strength of either permanent magnet is sufficient to hold the adjacent armature without the need for the accompanying electromagnets to be powered. The electromagnets are designed such that, when powered, their magnetic field essentially cancels the magnetic field of the surrounded permanent magnet, allowing for the armature to be released from its current position and be attracted to the position of the other permanent magnet. The benefit of such a design is that, during normal operation, the magnetic field required to hold the armature in position is produced solely by the permanent magnet, requiring no power, yet the magnetic system may still be turned "off" when a change in armature position is required. As with purely electromagnet solutions, a combination of electromagnets and permanent magnets in such a topology has its limitations and downsides. It too requires a constant current to achieve one of its states (be it the "on" or "off" state for a particular design) and therefore can carry the same drawbacks mentioned for electromagnets.

Implementations of combined electromagnets and permanent magnets are not only restricted to "on"/"off" systems but can be designed to produce varying degrees of magnetic coupling strength. Such systems have allowed for advancements in magnetic suspension where they offer more energy efficient solutions than purely electromagnets and superior control compared to purely permanent magnet systems. The magnet suspension conveyor proposed by H. J. Shin et al. [35] and the device for large air-gap suspension proposed by N. A. Shirazee and A. Basak [36] both demonstrate how the combination of different types of magnets may be used in magnetic suspension systems. The two systems have similar working principles where permanent magnets are used to provide a large base magnetic flux which then can then be varied slightly by driving current thorough the electromagnets. In the case of the Maglev system considered in [35], the permanent magnets are used to provide the main field strength required for suspension of the load and the electromagnets are then used to slightly adjust the air-gap. Figure 2.24 shows the magnetic system implemented by N. A. Shirazee and A. Basak. Their system is composed of NdFeB permanent magnets on top and bottom of a mild steel core. Surrounding the core are coil windings making up the electromagnetic component of the system. A final NdFeB permanent magnet was mounted on the top of the load. As with the Maglev system, the vast majority of suspension forces are generated by the permanent magnets and the electromagnet is used for maintaining the load at the suspended position. Due to its limited contribution to the suspension force, the electromagnet current may be kept small, alleviating the need for a large cooling system. For a current of only 173 mA the authors achieved the suspension of a 491 gram load at 61 mm.

Beyond their use in magnetic suspension systems, combinations of electromagnets and permanent magnets have been used to create controlled magnetic systems for other innovative applications. I. El-Amri et al. use the combinational magnet design for magnetic fluid finishing [37]. Their implemented magnetic system is shown in Figure 2.25. Of note in their design is the bolt base for the electromagnet which the authors claim, provides field concentration, increasing the magnetic field strength over their area of interest. Like the magnetic suspension systems, the electromagnets are used to vary the magnetic field produced by the permanent magnets. Two of these magnetic systems at different locations with phase shifted AC currents in the coils cause a magnetic fluid to slosh back and forth between the magnets. By choosing an abrasive fluid, the authors achieve material finishing of awkwardly shaped workpieces.



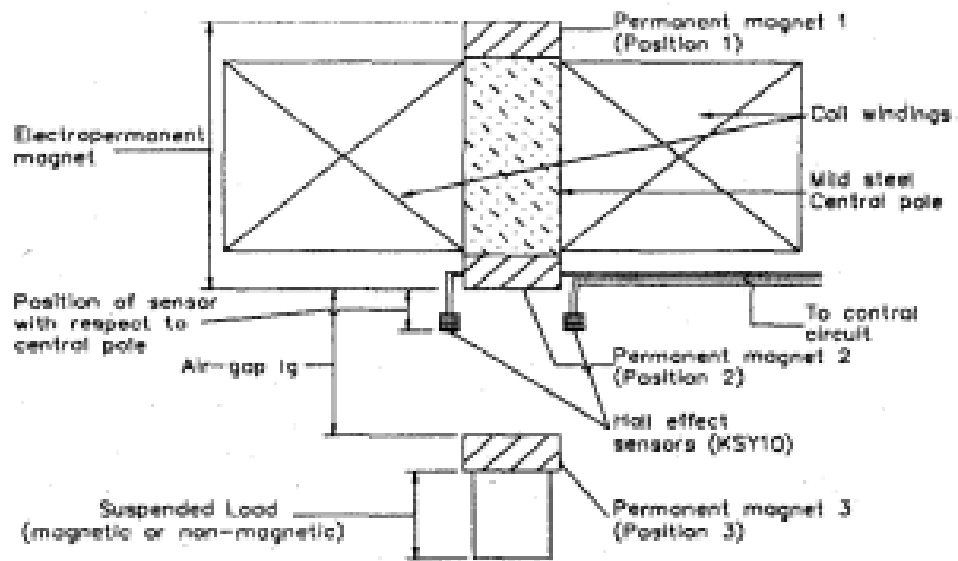


Figure 2.24: Magnetic suspension system using a combination of electromagnets and permanent magnets [36]

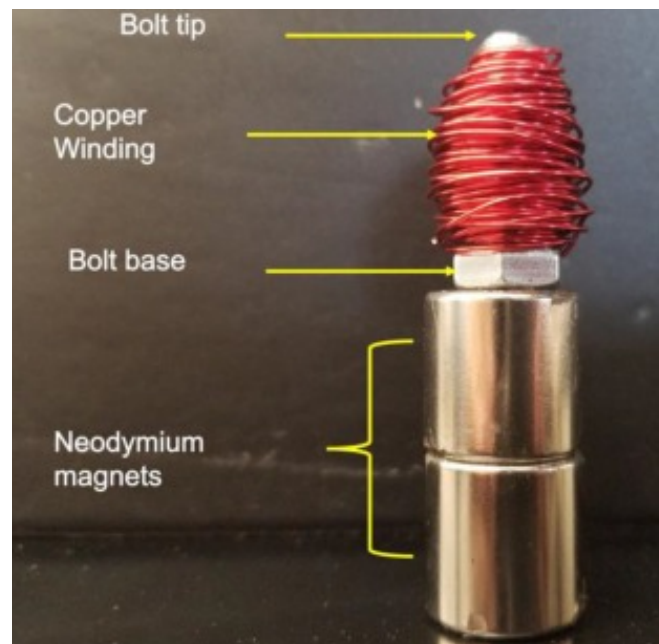


Figure 2.25: Magnetic system for magnetic fluid finishing [37]

### 2.6.3 Electropermanent Magnet Systems

An electropermanent magnet (EPM) is essentially a programmable magnet. The term EPM has a short history, first appearing less than 50 years ago, but has gathered a few different meanings with some assigning it to the combination magnet systems described in section 2.6.2. The definition followed in this thesis is that popularised by the PhD thesis of Ara Knaian [38] whereby an EPM is a solid state device whose external magnetism may be set or changed between "on" and "off" with short pulses of current. An EPM can be thought of as combining the main strengths of both electro- and permanent magnets, allowing for the magnetisation state to be varied but consuming zero steady state power to hold that magnetisation state. For zero continuous current, all of the electrically controlled magnetic systems viewed thus far have only one magnetisation state; either "off" for electromagnets or the "on" strength of the permanent magnets in the combined systems. As such, none of these designs are optimal for applications that require maintaining an arbitrary magnetisation state for an extended period. These applications are where the benefits of EPM systems are most clearly observed.

EPM systems are of two main forms. The less common form is made up of only semi-hard permanent magnets whose magnetisation is varied by a surrounding magnetising coil. Far more common is the form consisting of two types of permanent magnets of largely differing coercivities, a coil for the magnetisation/demagnetisation of the softer permanent magnet, and high permeability keepers to provide low reluctance return paths for the magnetic field. Figure 2.26 shows a popular EPM topology proposed in [38]. Here, a hard permanent magnet, e.g. NdFeB, is placed in parallel with a softer permanent magnet, e.g. AlNiCo. A coil is wrapped around the two magnets and a ferromagnetic material such as iron is used to connect the poles of the different magnets together. The direction of magnetisation of the softer permanent magnet is reversed in order to change the state of the external magnetic field. The EPM is in its "off" state when the magnetic flux of the permanent magnets is fully contained within the device, i.e. there exists no external magnetic field. In this state, the magnets are magnetised anti-parallel to each other and the keepers provide a low reluctance path from the north pole of one magnet to the south pole of the other magnet, as per Figure 2.27a. To switch the EPM to its "on" state the magnetisation of the softer permanent magnet must be reversed. The reversal of the magnetisation direction is accomplished by subjecting the soft magnet to a strong magnetic field,

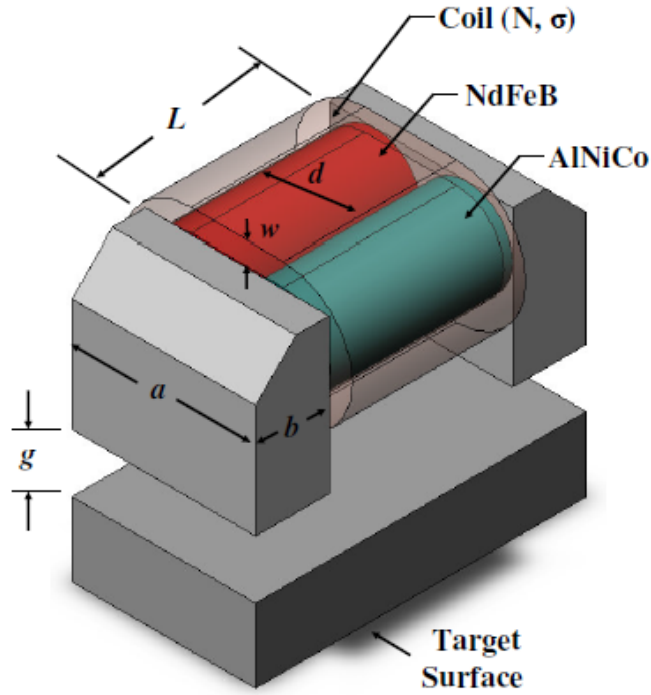


Figure 2.26: Electropermanent magnet design proposed by Ara kniain [38]

generated by driving a large current through the surrounding coil as shown in Figure 2.27b. Only a short pulse of current is required to reverse the direction of magnetisation, after which there is no longer a need for the magnetic field from the coil and the current can be turned off. Both magnets are now magnetised in the same direction and the device is considered to be in its "on" state. Alike poles are connected to the same keeper which forces the magnetic field to link outside of the device as in Figure 2.27c. Finally, to turn the device "off" again, the magnetisation direction of the soft magnet must be reversed such that the two permanent magnets are anti-parallel. As with the switching on stage, this is accomplished by subjecting the soft magnet to a strong enough field generated from the surrounding coil, as indicated in Figure 2.27d. During the switching stages both permanent magnets in the EPM are within the coil generated field. While this field is capable of reversing the magnetisation of the softer magnet, it is not strong enough to change the direction of magnetisation of the harder magnet. This is due to the difference in coercivity between the two magnets. Two common EPM magnets choices are NdFeB and AlNiCo as the coercivity of NdFeB is nearly 19 times that of AlNiCo. The strength of the field required to reverse the magnetisation direction of AlNiCo moves through the linear region of the NdFeB demagnetisation curve allowing it to return to its original magnetisation when the field is removed.

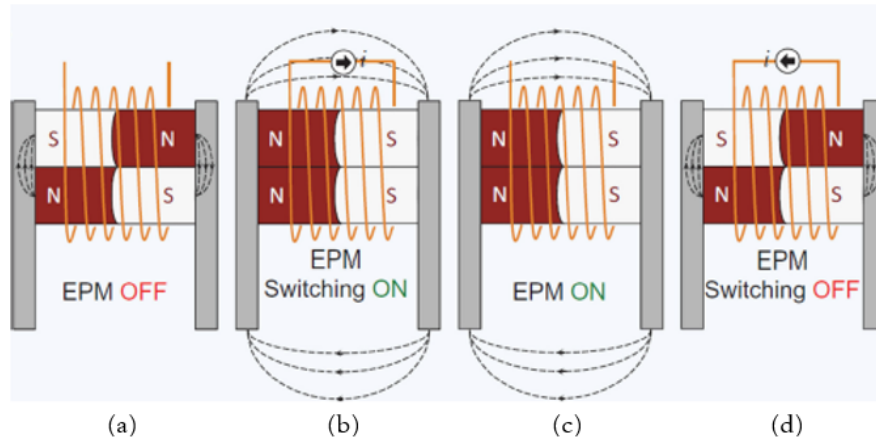


Figure 2.27: Adapted image showing a two core electropermanent magnet cycling through its "off" and "on" states, (a) to (d). The bottom permanent magnet has a higher coercivity remains polarised in the same direction across all states. The top magnet has a lower coercivity and its magnetisation direction is varied by powering the surrounding coil [39].

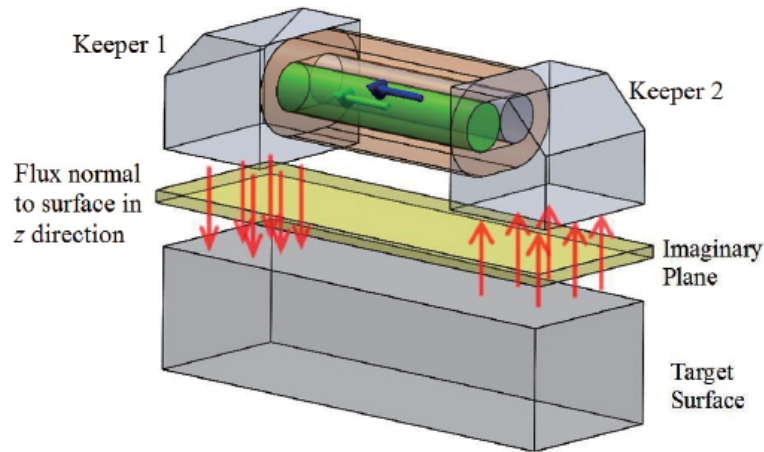


Figure 2.28: Proposed EPM design for a climbing robot and target surface by P. Ward et al. [40].

Some systems, designed originally to make use of electro- or permanent magnets, have seen improvements in reliability and power usage by replacing these more conventional magnet types with EPMs. Climbing robots used for inspection are a primary example of systems that have benefited by replacing their magnetic systems with EPMs. Due to the popularity of ferromagnetic materials such as steel for construction, there have been several proposed designs for climbing inspection robots that use magnetic anchoring. P. Kriengkamol et al. [41] present such a system that they called Asterisk. Asterisk is a six-legged robot whose design was inspired by insects. It is designed for the inspection of steel structures using switching magnetic systems in the robots legs to provide anchoring to the

structures. Prior to the use of EPMS, the group had made use of electromagnets. Despite the increased difficulty of controlling EPMS the authors the decision to change was motivated by safety concerns in the case of power loss [41]. In the case that Asterisk is anchored upside down and power is interrupted or depleted, electromagnets would lose all magnetic anchoring ability, causing the robot to fall. By changing to EPMS this limitation is addressed. The key benefit of the EPM is that it only requires power during its switching, holding its magnetisation state without power draw. Therefore, in the case of power loss, Asterisk will remain anchored to the structure. P. Ward et al. [40] and F. Ochoa-Cardenas et al. [42] both present analysis and experimentation of electropermanent magnets with a focus on magnetic adhesion for climbing robots. Ward et al. [40] identify and compare various adhesion methods, preferring EPM to mechanically switched permanent magnet devices due to their higher switching speed and solid state construction. For the design of their EPM they use single cores of semi-hard AlNiCo and hard NdFeB magnets encased in 116 turns of 24 AWG insulated copper wire. Figure 2.28 shows the design of their device, the total dimensions of which is 25 mm x 50 mm x 14 mm. For a magnetising pulse of 4 ms, at 27 V, a peak current of 43 A was generated and the resulting EPM state achieved a maximum holding force of 82.2 N. The repeatability of the design was tested and it was found that over 5 tests there was a standard deviation of .5 N for an average holding force of 74.7 N. As previously mentioned, one of the main benefits of EPMS for climbing robots is the degree of safety they provide in the case of power failure. The ability of the presented design to support a 5 kg weight was

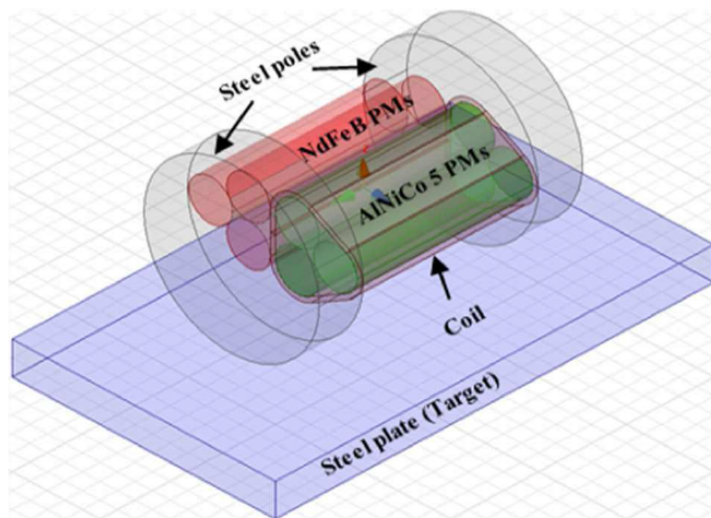


Figure 2.29: Proposed EPM wheel design with six total permanent magnet cores with just the AlNiCo permanent magnets surrounded by the coil by F. Ochoa-Cardenas et al. [42].

successfully demonstrated for two weeks before the test was stopped. However, when not attached to a target surface, the EPM was observed to drop from 74 N to 42 N over the course of a 5 hour period. F. Ochoa-Cardenas et al. [42] present a slightly different EPM design shown in Figure 2.29 and pay particular interest to the ability to not only set the state of the EPM as "on" or "off" but to also set it at some value in between. This group also used NdFeB and AlNiCo for their hard and semi-hard magnets but have included three cores of each per device. Unlike the previous design, the authors have only wrapped the semi-hard AlNiCo in a coil of 250 turns of 32 AWG insulated copper wire and have used disk shaped keepers to produce a wheel-like EPM design as shown in Figure 2.29. For device dimensions of 30 mm x 20 mm x 20 mm, a force of just under 4 N was recorded at an air gap of 1 mm. It was also found that for magnetising voltages greater or equal to 19 V, the same holding force was generated by the EPM due to the saturation of the AlNiCo.

Section 2.5 covered the design of mechanical varying magnetic devices, many of which were designed to act as holding devices. In the age of electronics and automation, EPMS have emerged as an alternative to such devices, offering the control of an electromagnet without the power and heat constraints. Thyssenkrupp magnettechnik (Branch of thyssenkrupp Schulte GmbH, Johanniskirchstrasse, Essen, Germany) and Armstrong Magnetics(Armstrong Magnetics, Inc., Bellingham, Washington, United States) both provide industry with capable EPM lifting systems. As presented in a report from Thyssenkrupp magnettechnik [43], there are many advantages to the use of EPMS for load lifting in modern logistics networks. Beyond the inherent safety advantages in the case of power loss, the report details many cost and time saving benefits of such systems. Dunnage (for the purpose of separating a ships cargo such that chains could be installed for lifting) is no longer required for EPM systems. Not only is this more environmentally friendly and reduces cost but it also allows for more dense packing so that more product may be shipped. In comparison to electromagnet systems, the report also quantifies energy savings with EPMS consuming only about one tenth of the energy. When used for machining purposes, these EPM holding devices are often called magnetic chucks. J. Bydžovský et al. [44] proposes and tested a new design for an EPM chuck. In addition to its simpler construction, the cylindrically symmetric EPM design, shown in Figure 2.30, allowed for a less intensive 2D simulation of the system. As with most EPM designs, this design incorporated NdFeB for the hard magnet and AlNiCo for the semi-hard magnet. A coil of 228 turns surrounded both magnets. However, the AlNiCo has been positioned

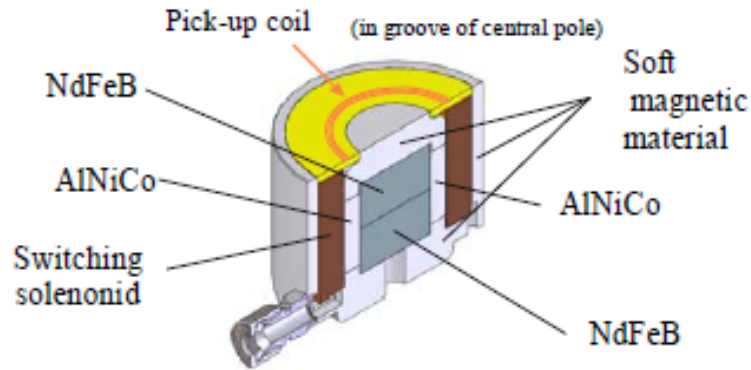


Figure 2.30: Cylindrically symmetric EPM chuck design [44].

next to the coil such that a lower current is required to produce the necessary switching field. Even in the 2D magneto-static case it was found that the design of the device can be optimised. EPM chucks for work holding are widely commercially available from companies such as Braillon Magnetiques ( Braillon Magnetiques, Alpespace, Montmelian, France) and Tecnomagnete (Tecnomagnete S.p.A., Via Nerviano, Lainate, Italy). The power fail-safe capabilities is an important characteristic of these EPM designs. Another characteristic of these designs is that the magnetic flux remains close to the surface leading to their suitability for working with sheet metals or thin work pieces. However, for applications where the work piece is uneven or particularly rough this may result in poor holding forces due to the field rapidly dropping off over air gaps.

EPMs have not only replaced conventional magnets in certain devices but have also been used to new applications for magnetic control systems. A. Gawel et al. [45] developed a drone magnetic picking and delivery system making use of EPMs. Of vital importance for such a mechanism is low weight, strong holding force, and low power consumption. Figure 2.31 shows the designed magnetic lifting assembly. The EPMs were arranged in a circular pattern which produces an equally distributed lifting force. Previously magnetic solutions have been hampered by their lack of versatility or higher power consumption over long flights. The EPM solution directly addresses these problems requiring only a pulse of power during its switching. The full system proposed by the authors was effective in picking and delivering under the many disturbances that can occur such as wind, an angled load, and even a moving load. Another novel implementation of EPMs is proposed by J. I. Padovani et al. [39] for magnetic actuation in droplet ferro-microfluidics. Purely permanent magnet solutions have been used in passive systems. However, these lack the controllability of active systems. Electromag-



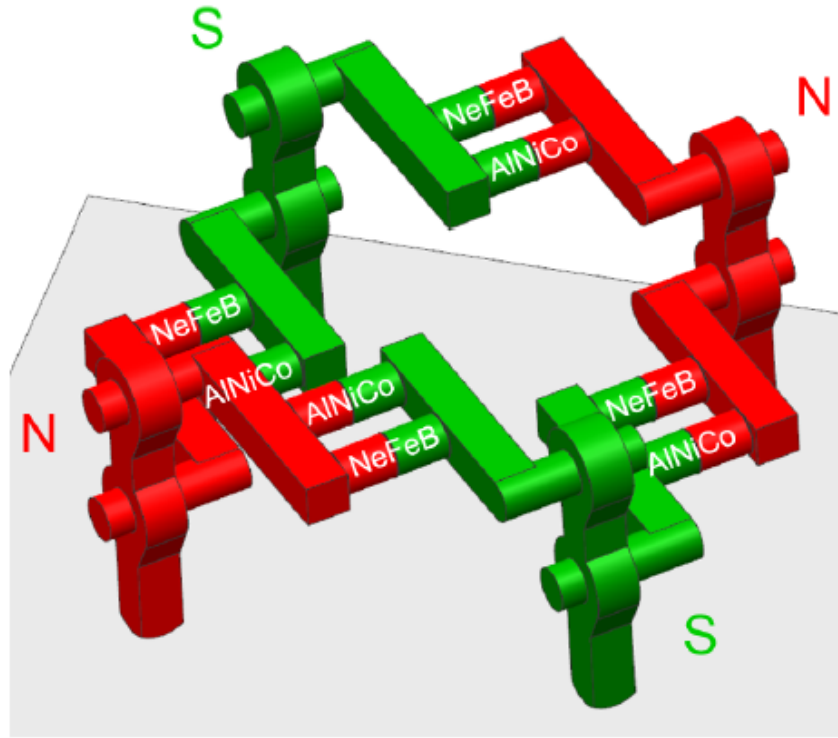


Figure 2.31: Circular EPM lifting assembly aimed at drone picking and delivery systems [45]

nets have a switching ability, however at small scales the thin wires required to produce such magnets produce a large amount of undesirable Joule heating. As an alternative, EPMs may be switched quickly "on" and "off" without the need for constant power. A side benefit of EPM is the high field gradient close to the pole which is desirable for many applications. The implemented EPMs separated droplets with forces up to 70 nN on 80  $\mu\text{m}$  water-in-ferrofluid droplets. At such sizes the performance of the EPM is seen to scale well, needing only a 50  $\mu\text{s}$  pulse of current to switch state.

The scalability of EPM down to very small sizes has made it an attractive technology for millimetre-scale actuators. A. D. Marchese et al. [46] present an EPM valve design for use in soft robots. The novel design, shown in Figure 2.32, operates by releasing a soft ferrous ball to plug an opening or by pulling the ball away from the opening. The valve is open when the magnetic field links through the fluid channel attracting the ball away from the opening. To close the valve, the magnetism through the fluid channel is turned off and the flow causes the ball to plug the opening. The magnetism is turned on or off through the channel by an EPM consisting of AlNiCo 5 and NdFeB N40 with a ferrous core material to route the magnetic field through the fluid channel. To switch the state of the EPM, a



short 5 ms pulse current is required. Soft fluidic actuators are then driven with these valves at their inlet and outlet causing pressure changes which result in deformation of the elastomer fluidic actuators. Using such actuators, the authors produced a rolling robot. Although valve design is said to not be optimised for this particular application, the final valve weighed just 5 g and could theoretically allow for peak flows of 5 litres per minute.

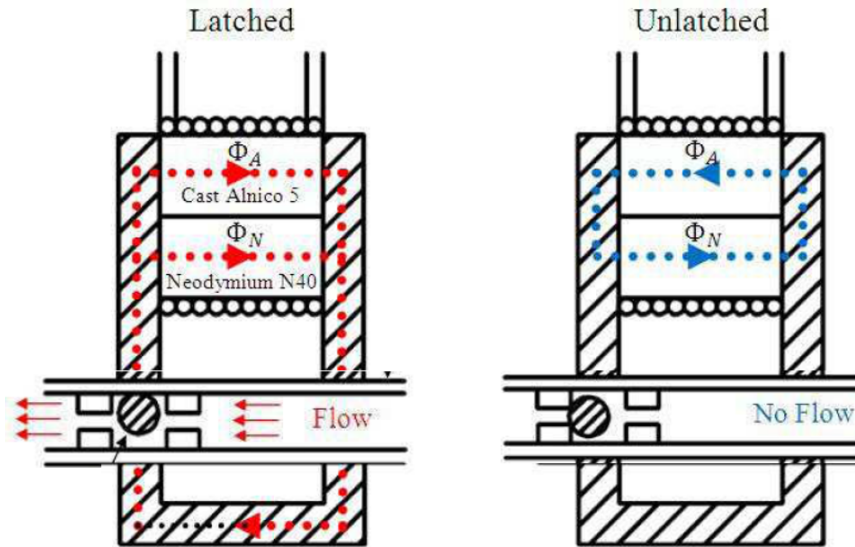


Figure 2.32: Valve design using ball bearing to restrict flow based on EPM state [46]

## 2.7 Methods of Magnet Analysis

Classical methods used to analyse magnetic systems make use of Maxwell's equations. Below are the four equations in both differential and integral form, Equations 1.2 to 1.5:

<u>Equation name:</u>	<u>Differential form:</u>	<u>Integral form:</u>
Ampere-Maxwell law	$\nabla \times \mathbf{H} = \mathbf{J} + \frac{\partial \mathbf{D}}{\partial t}$	$\oint_c \mathbf{H} \cdot d\mathbf{l} = \int_s \left( \mathbf{J} + \frac{\partial \mathbf{D}}{\partial t} \right) \cdot d\mathbf{s}$

(2.2)

Gauss' law for magnetism	$\nabla \cdot \mathbf{B} = 0$	$\oint_s \mathbf{B} \cdot d\mathbf{s} = 0$
-----------------------------	-------------------------------	--

(2.3)

Faraday's law of induction	$\nabla \times \mathbf{E} = -\frac{\partial \mathbf{B}}{\partial t}$	$\oint_c \mathbf{E} \cdot d\mathbf{l} = -\int_s \frac{\partial \mathbf{B}}{\partial t} \cdot d\mathbf{s}$
-------------------------------	--	---

(2.4)

Gauss' law	$\nabla \cdot \mathbf{D} = \rho$	$\oint_s \mathbf{D} \cdot d\mathbf{s} = \int_v \rho \cdot d\mathbf{s}$
------------	----------------------------------	--

(2.5)

Where:

- $\mathbf{H}$  Magnetic field strength (A/m)
- $\mathbf{B}$  Magnetic flux density (T)
- $\mathbf{E}$  Electric field (V/m)
- $\mathbf{D}$  Electric displacement (C/m<sup>2</sup>)
- $\mathbf{J}$  Current density (A/m<sup>2</sup>)
- $\rho$  Free electric charge density (C/m<sup>3</sup>)

Relation:  
Electric flux density & field  
intensity

Equation:

$$\mathbf{D} = \epsilon \mathbf{E} = \epsilon_0 \mathbf{E} + \mathbf{P} \quad (2.6)$$

Magnetic flux density & field  
strength

$$\mathbf{B} = \mu \mathbf{H} = \mu_0 (\mathbf{H} + \mathbf{M}) \quad (2.7)$$

Where:  
 $\mathbf{P}$  Polarisation (C/m<sup>2</sup>)  
 $\mathbf{M}$  Magnetisation (A/m)  
 $\epsilon$  Permittivity (F/m)  
 $\mu$  Permeability (H/m)

In addition to the Maxwell's equations, relations between  $\mathbf{B}$  &  $\mathbf{H}$  and  $\mathbf{D}$  &  $\mathbf{E}$  are required to fully represent the fields, see Equations 2.6 and 2.7. When the dynamics of a system to be analysed are very slow or static, the time derivatives can be ignored and set to zero values. The equations for these static cases now form two sets of independent equations for magnetostatics and electrostatics. The magnetostatic equations are given as follows:

<u>Equation name:</u>	<u>Differential form:</u>	<u>Integral form:</u>	
Ampere-Maxwell law	$\nabla \times \mathbf{H} = \mathbf{J}$	$\oint_c \mathbf{H} \cdot d\mathbf{l} = \int_s \mathbf{J} \cdot d\mathbf{s}$	(2.8)

Gauss' law for magnetism	$\nabla \cdot \mathbf{B} = 0$	$\oint_s \mathbf{B} \cdot d\mathbf{s} = 0$	(2.9)
-----------------------------	-------------------------------	--	-------

Many dynamic magnetic systems can be analysed as a set of static states. Electropermanent magnet operation can be modelled using the static equations by looking at the magnet in either its "on" or "off" state.

Unfortunately, for many systems a closed form solution may be too tedious or even impossible to obtain. For this reason, other methods of analysing magnetic systems, both analytical and numerical, have been developed.

## 2.7.1 Analytical Analysis

### 2.7.1.1 Magnetic equivalent circuit

The magnetic equivalent circuit model involves converting magnetic systems into a magnetic circuit closely resembling an electric circuit. The system is converted to a combination of magneto-motive force sources and reluctances (equivalent to voltage and resistance in an electric circuit). The reluctances and sources for a system are derived using the magnetostatic equations given above. Important assumptions for the use of electric equivalent components include that the magnetic field strength vector,  $\mathbf{H}$ , is parallel to the magnetic flux path and that there is negligible leakage of flux outside of the circuit. Although these conditions are near impossible to achieve in a real system, this modelling technique can often provide a good insight into the system's behaviour.

$$\sum_a \mathfrak{R}_a \Phi_a = \sum_b n_b i_b \quad (2.10)$$

$$\sum_a \Phi_a = 0 \quad (2.11)$$

Where:

$\mathfrak{R}$	Reluctance (A*turns/Wb)
$\Phi$	Total flux (Wb)
$n$	Number of turns
$i$	Current (A)

The magnetic circuit laws which dictate the circuit's behaviour and are used for analysis are given by Equations 2.10 and 2.11 [24]. These are analogous to Kirchhoff's current and voltage laws for electrical circuits. Note the reluctance term,  $\mathfrak{R}$ , which is introduced as an analogous term to electrical resistance. For an element with a linear response, of length  $l$ , and of constant cross-sectional area  $A$ , the reluctance is defined in Equation 2.12.

$$\mathfrak{R} = \frac{l}{\mu A} \quad (2.12)$$

The magneto-motive force of a magnet can be given in terms of its reluctance and flux in Equation 2.13.

$$\text{MMF}_{\text{magnet}} = \mathfrak{R}_{\text{magnet}} \Phi_{\text{magnet}} \quad (2.13)$$

An EPM in either its "off" state or "on" state (when latched onto a ferromagnetic material) can be reasonably modelled using this method when the air gaps in the system are small [38].

### 2.7.1.2 Magnetic charge model

The magnetic charge model can be used for the analysis of permanent magnets. It involves converting the magnet into an equivalent distribution of magnetic monopoles/charges. In a magnetic system, each "positive" monopole requires a "negative" counter-part. To date no such particle has been discovered that exhibits such behaviour yet this approach is useful for predicting the behaviour of magnetic systems. The introduction of a new term,  $\varphi_m$ , called the scalar magnetic potential is required, the divergence of which is defined as the negative of field strength in Equation 2.14.

$$\mathbf{H} = -\nabla \varphi_m \quad (2.14)$$

Using Equation 2.14 and inserting the value of flux density from its relation to field strength in Equation 2.7 and Gauss' law for magnetism in Equation 2.9, leads to Equation 2.15.

$$\nabla \cdot (-\nabla \varphi_m + \mathbf{M}) = 0$$

or

$$\nabla^2 \varphi_m = \nabla \cdot \mathbf{M} \quad (2.15)$$

The relation between the magnetisation and the scalar potential is observed to be in the form of Poisson's equation and may be solved by using a Green's function. If the magnet is considered in free space and magnetisation exists solely in the magnet, the expression in Equation 2.16 for the scalar product is valid [24].

$$\varphi_m(\mathbf{x}) = -\frac{1}{4\pi} \int_v \frac{\nabla' \cdot \mathbf{M}(\mathbf{x}')}{|\mathbf{x} - \mathbf{x}'|} dv' + \frac{1}{4\pi} \oint_s \frac{\mathbf{M}(\mathbf{x}') \cdot \hat{\mathbf{n}}}{|\mathbf{x} - \mathbf{x}'|} ds' \quad (2.16)$$

For many permanent magnets there is a uniform magnetisation throughout the material. In this scenario, the volume integral has zero value due to the fact that  $\nabla \cdot \mathbf{M} = 0$  leaving only the surface integral component. Returning to the original relation in Equation 2.14, the magnetic field strength vector at point  $\mathbf{x}$  can now be solved contributions at points  $\mathbf{x}'$  along the surface  $s$ , see Equation 2.17

$$\mathbf{H}(\mathbf{x}) = \frac{1}{4\pi} \oint_s \frac{\mathbf{M}(\mathbf{x}') \cdot \hat{\mathbf{n}}(\mathbf{x} - \mathbf{x}')}{|\mathbf{x} - \mathbf{x}'|^3} ds' \quad (2.17)$$

For a singular magnetic point charge with a surface area,  $\Delta A$ , the magnetic field strength can be described as in Equation 2.18. Using the earlier assumption that the magnet is in a medium with magnetic permeability  $\mu_0$ , the magnetic flux density can be easily deduced per Equation 2.19.

$$\mathbf{H}(\mathbf{x}) = \frac{1}{4\pi} \frac{Q_m(\mathbf{x}') \cdot \hat{\mathbf{n}}(\mathbf{x} - \mathbf{x}')}{|\mathbf{x} - \mathbf{x}'|^3} \quad (2.18)$$

$$\mathbf{B}(\mathbf{x}) = \frac{\mu_0}{4\pi} \frac{Q_m(\mathbf{x}') \cdot \hat{\mathbf{n}}(\mathbf{x} - \mathbf{x}')}{|\mathbf{x} - \mathbf{x}'|^3} \quad (2.19)$$

Where the surface point charge,  $Q_m$ , has been introduced as in Equation 2.20.

$$Q_m(\mathbf{x}') = (\mathbf{M}(\mathbf{x}') \cdot \hat{\mathbf{n}}) \Delta A \quad (2.20)$$

The magnetic charge model facilitates a very neat solution for the force between magnets. Analogous to the force between electric point charges, an equation for the force between magnetic point charges can be derived [24]. Referred to as Coulomb's law for magnetism Equation 2.21, describes the force between point charges located at vectors defined by  $\mathbf{x}_1$  &  $\mathbf{x}_2$ .

$$\mathbf{F} = \frac{\mu_0}{4\pi} \frac{Q_m(\mathbf{x}_1) Q_m(\mathbf{x}_2) (\mathbf{x}_1 - \mathbf{x}_2)}{|\mathbf{x}_1 - \mathbf{x}_2|^3} \quad (2.21)$$

Modelling the fields and forces between permanent magnets with single magnetic charges at the poles is a gross simplification for the majority of systems as the area of the charge will not be negligible with respect to the air gap size. However, the surface of a magnet can be divided into a finite number of smaller sections leading to a distribution of magnetic surface charges. For sufficiently small charge areas, the magnetic field/force even close to the magnets surface can be evaluated

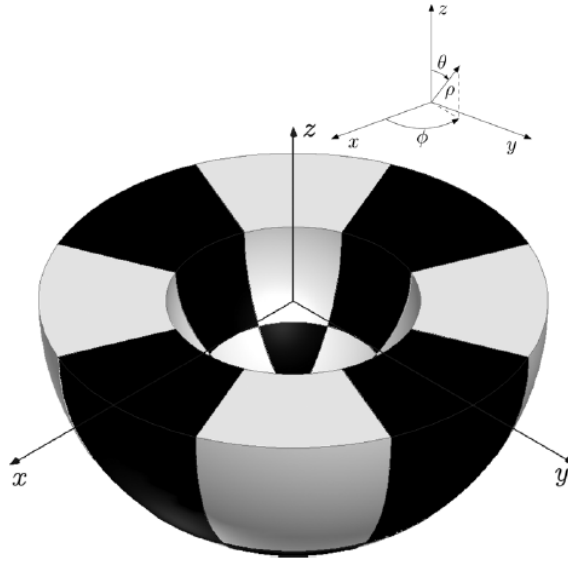


Figure 2.33: Cut view of spherical magnet array, magnetised radially, analysed using the magnetic charge model [47].

through summing the contribution of each charge.

B. van Nindhuijs et al. [47] make use of this model for the analysis of spherical magnet arrays. A cut-section of an analysed magnetic system is shown in Figure 2.33 for which an analytical solution of the magnetic field was produced. The magnet array consists of radially magnetised tiles and the final solution for the magnetic field is calculated as the contribution of each individual tile and the field of each tile is a further sum of the contributions of the faces of the tile. The same system was analysed using the numerical finite element analysis discussed later and found to differ by less than 3% whilst requiring far more time than the analytical approach. However, both this paper and the derivation of the model above make the assumption that all elements have unity relative permeability which, despite being a close approximation, does not perfectly align with many permanent magnet materials. This shortcoming has been investigated and addressed by several researchers such that analysis more closely fits reality [48], [49].

### 2.7.1.3 Magnetic current model

The magnetic current model involves converting a permanent magnet to a series of currents. Using these currents and the magnetostatic field equations the fields of permanent magnets can be obtained. Generally, several currents make up the equivalent of the magnet field where each current source is combined in order to

represent the total field of the magnet. The derivation follows a similar approach to the charge model described in the previous section. The vector potential,  $\mathbf{A}$ , is first introduced and then, using a combination of the magnetostatic equations and the relation between  $\mathbf{B}$  and  $\mathbf{H}$ , an equation in the form of Poisson's equation is obtained from which the flux density field equation is developed. As in Equation 2.22, the curl of the vector potential is defined to be equal to the magnetic flux density in the magnet.

$$\mathbf{B} = \nabla \times \mathbf{A} \quad (2.22)$$

By replacing the flux density term in Equation 2.22 with its relationship to field strength in Equation 2.7, a relationship between the vector potential and magnetic current density can be formed as shown in Equation 2.23.

$$\nabla^2 \mathbf{A} = -\mu_0 (\nabla \times \mathbf{M}) = -\mu_0 \mathbf{J}_m \quad (2.23)$$

$\mathbf{J}_m$  represents an equivalent magnetic current density from the magnetisation of the magnet. Note that the free current density term is zero for a permanent magnet system. If the further assumption is made that the system is in a medium defined by  $\mu_0$  then Green's function for free space may be applied to Equation 2.23. After applying Green's function, vector calculus identities, and the original relation between  $\mathbf{B}$  and  $\mathbf{A}$ , a neat expression for the magnetic flux density at point  $\mathbf{x}$  due to contributions at points  $\mathbf{x}'$  in the volume  $v$  and along the surface  $s$  is produced, see Equation 2.24 [24].

$$\mathbf{B}(\mathbf{x}) = -\frac{\mu_0}{4\pi} \int_v \mathbf{J}_m(\mathbf{x}') \times \frac{\mathbf{x} - \mathbf{x}'}{|\mathbf{x} - \mathbf{x}'|^3} d\mathbf{v}' + \frac{\mu_0}{4\pi} \oint_s \mathbf{j}_m(\mathbf{x}') \times \frac{\mathbf{x} - \mathbf{x}'}{|\mathbf{x} - \mathbf{x}'|^3} ds' \quad (2.24)$$

Where  $\mathbf{j}_m$  is the equivalent surface current density from the magnet's magnetisation.

$$\mathbf{j}_m = \mathbf{M} \times \hat{\mathbf{n}} \quad (2.25)$$

Since the relation between the volume and surface current densities to the magnetisation is known, the field can be calculated at any point provided that the magnetisation value is known. A further simplification exists if the magnetisation



is homogeneous and uniform as is the case for most permanent magnets. In this scenario the volume current density becomes zero and only the surface charge density term remains, Equation 2.26.

$$\mathbf{B}(\mathbf{x}) = \frac{\mu_0}{4\pi} \int_s \mathbf{j}_m(\mathbf{x}') \times \frac{\mathbf{x} - \mathbf{x}'}{|\mathbf{x} - \mathbf{x}'|^3} ds' \quad (2.26)$$

Both the solutions of the magnetic charge model and the magnetic current model align, with the application of one over the other stemming purely from which is easier to implement for a particular system topology.

### 2.7.2 Numerical Analysis

Numerical analysis is a popular approach for analysing magnetic systems. It is particularly advantageous for magnetic systems with complex geometries which would otherwise be too tedious for theoretical analysis. Numerical analysis has proven itself to be a reliable method of analysis, often providing results close to that observed experimentally. Finite element analysis (FEA) [50], finite volume method (FVM) [51], and the finite difference method (FDM) [52] are three such methods, although the popularity of FEA far exceeds that of the latter two methods. To analyse a system using FEA it must first be discretised in space using a mesh, where approximate field equations are applied to each section. The mesh must be sufficiently fine such that the field and potentials in each region can be considered constant. Using these regions, system equations can be produced and in turn solved for. Whilst this method can handle an extremely versatile set of systems, it is computationally expensive. Due to the computationally expensive nature of the model it can take extended periods of time to solve the fields of a system. The Finite Elements Method Magnetics (FEMM, David Meeker) software is a free open-source FEA solver capable of simulating 2D and axisymmetric 3D magnetostatic problems. More advanced numerical analysis software for electromagnetic problems is also available, with COMSOL Multiphysics (COMSOL AB, Stockholm, Sweden) and Ansys Maxwell (Ansys Inc., Canonsburg, Pennsylvania, U.S.) being two of the most popular.

# Chapter 3

## Preliminary Device Design

The work included in this section relates to an early approach to the design of a controllable device for safer magnetic coupling in surgical applications. At the discretion of the reader, this section of work may be skipped without loss of continuity with regard to the main device design in the following chapter. This device design consists of an array of electropermanent magnets cells. Each electropermanent magnet cell is individually controlled in order to achieve a desired array state. Safer magnetic behaviour is then ideally achieved by interacting specific array states with each other. Following the production of a prototype, limitations of electropermanent magnets to achieve safer magnet behaviour were discovered. Whilst the device demonstrated the suitability to other applications, it was ultimately decided to retire the device in order to focus on a variable magnetism technology better capable of achieving safer magnetic behaviour.

### 3.1 Device Simulation Method

A single core electropermanent magnet consists of a permanent magnet surrounded by a coil. The magnetisation of the permanent magnet core can be permanently altered by powering the surrounding coil. To facilitate this, with an interest in using a smaller sized coil and less power, a permanent magnet with a lower coercivity is used. The single core electropermanent magnet can be modelled as a permanent magnet for the purpose of field and force calculations when it is not switching states. This modelling simplification can be extended to arrays of magnets interacting with one another when they are not switching.

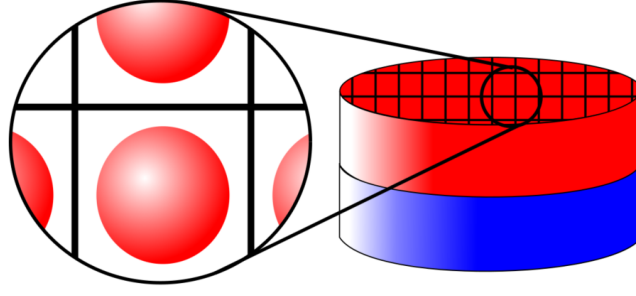


Figure 3.1: Simple rod magnet with the pole surface divided into small facets of area  $\Delta A$  with a "magnetic charge".

Permanent magnet modelling is used for the analysis of the electropermanent device. The magnetic charge model, presented in section 2.7.1.2, is continued to allow for many point charges interacting with one another. The derived equation for the force between 'magnetic charges', Equation 2.21, allows for the forces between magnets to be calculated through the division of the magnetic faces into small areas of magnetic charge (Figure 3.1) and applying the principle of superposition, summing the force contribution from each charge. This method is not restricted to magnets of a single magnetisation direction but can be applied to calculate the forces between arbitrarily patterned magnetic faces. This is achieved by assigning a polarity to each of the magnetic charge regions depending on the polarity of the magnet at that point. The same assumptions are carried through from the derivation of the equation, i.e. that the magnets have a uniform magnetisation and that the magnetic material and the surrounding area have a relative permeability of free space. The term for the 'surface point charges',  $Q_m$ , is dependent on the magnetisation of the magnet and on the surface areas of the magnetic charges as per Equation 2.20. The magnitude of magnetisation of the magnetic material is approximated by Equation 3.1, allowing the surface point charge to be calculated as in Equation 3.2

$$|\mathbf{M}| = \frac{B_r}{\mu_0} \quad (3.1)$$

$$Q_m(\mathbf{x}') = \frac{B_r}{\mu_0} \Delta A \quad (3.2)$$

Where:  $B_r$  Residual flux density (T)  
 $\Delta A$  Facet area (m<sup>2</sup>)

Given the dimensions and magnetisation patterns of any two permanent magnets, the force exerted on one due to the other may now be calculated as per Equation 3.3 where magnet A is represented by the surface charges at points  $\mathbf{x}_1$  to  $\mathbf{x}_n$  and magnet B is represented by surface charges at points  $\mathbf{x}_{n+1}$  to  $\mathbf{x}_m$ .

$$\mathbf{F}_{A \rightarrow B} = \sum_{\mathbf{x}_a=\mathbf{x}_1}^{\mathbf{x}_n} \sum_{\mathbf{x}_b=\mathbf{x}_{n+1}}^{\mathbf{x}_m} \frac{\mu_0 Q_m(\mathbf{x}_a) Q_m(\mathbf{x}_b) (\mathbf{x}_a - \mathbf{x}_b)}{4\pi |\mathbf{x}_a - \mathbf{x}_b|^3} \quad (3.3)$$

The summation stages of this equation involves breaking the magnets into their regions of surface charge and taking the ‘magnetic point charges’ to be at the centre of these regions. There are two strategies for which each magnet can be broken into these regions;

1. The division of the magnets surfaces can be tailored to the particular magnet shape and magnetic pattern
2. Approximating the shape and patterns of the magnets to fit the cells of a predefined grid

Figure 3.2 demonstrates the two different area division methods. Despite the accuracy advantage of the tailored approach, the general approach can give suitable accuracy whilst remaining far more versatile for different shapes and arrays of magnets. Once the magnets surfaces have been divided into small regions of charge, the magnetic charge model equations derived earlier can be used to

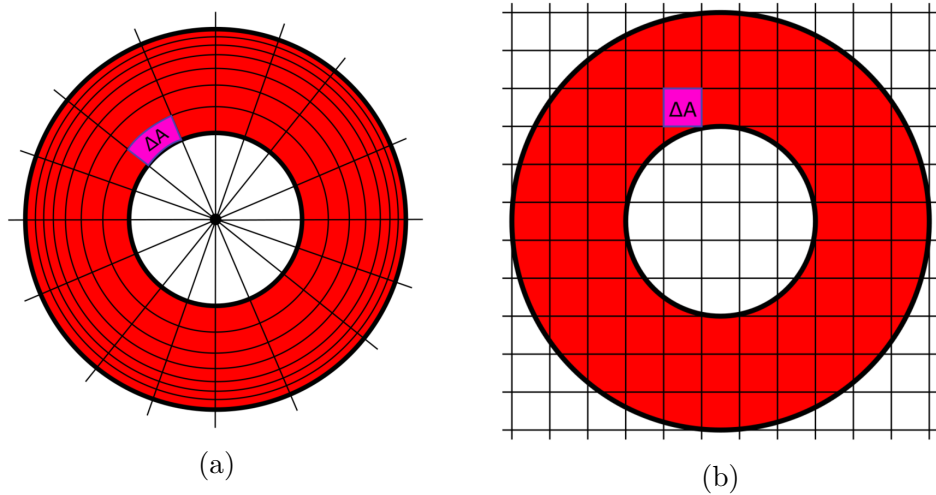


Figure 3.2: Annular permanent magnet surface division using: (a) a tailored approach and (b) a general predefined grid. Magnet shape is approximated when using general, i.e. an area that is mostly north pole will be assumed to be all north pole.

determine the forces experienced between magnets. Matlab (The MathWorks, Inc., Natick, Massachusetts, United States) was used to write scripts for both area division and force calculation using the magnetic charge model. Figure 3.3 shows the force separation plots obtained using both surface division approaches for an annular ring N40 magnet. The results from the charge model are also compared to that of a standard magnetics simulation software, FEMM (David Meeker, <http://www.femm.info/>). There is very close agreement between the results of all the methods.

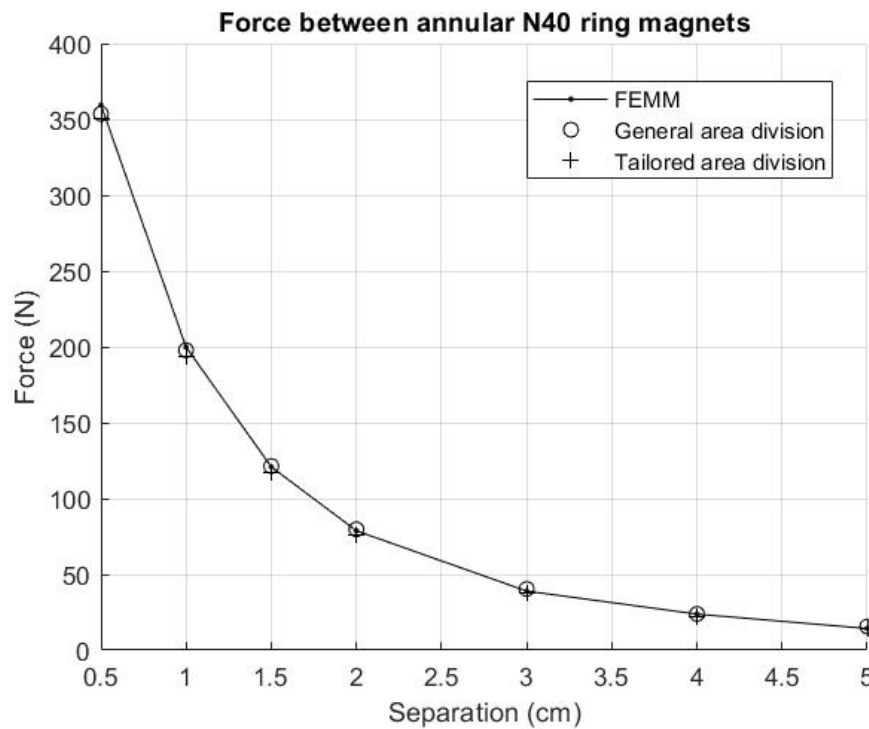


Figure 3.3: Comparison of predicted forces between a tailored and general surface division approach. The approaches are further compared to results from FEMM software. Forces refer to two annular N40 permanent magnets with inner radius of 2 cm, outer radius of 4 cm, and thickness of 1 cm.

The FEMM method required that the magnetics issue was a 2D problem or axially symmetric in 3D. However, as magnetic patterns of interest may not satisfy these conditions, this method is not suitable for general problems. The tailored area division approach offers quick simulation times for problems however, this method can be time consuming to produce the unique approach for each particular case if the geometries are changing beyond that of simple scaling. Therefore, the general area division method was chosen due to the ease of which new patterns can be investigated. The general area division method approximates the geometries to be simulated in a process similar to pixelation. The degree of pixelation and the

size of the magnetic surface charges relative to the gap between the magnets, play a significant role of the accuracy of simulated results. In the case where magnets with curved edges are being simulated, such as for the surfaces of an axially magnetised cylinder, the degree of pixelation can lead to distortions of the actual magnet geometry. The amount of distortion can lead to results that no longer represent the magnet of interest. Figure 3.4 shows how the top surface of a cylinder magnet can be approximated using fine and coarse grid sizes.

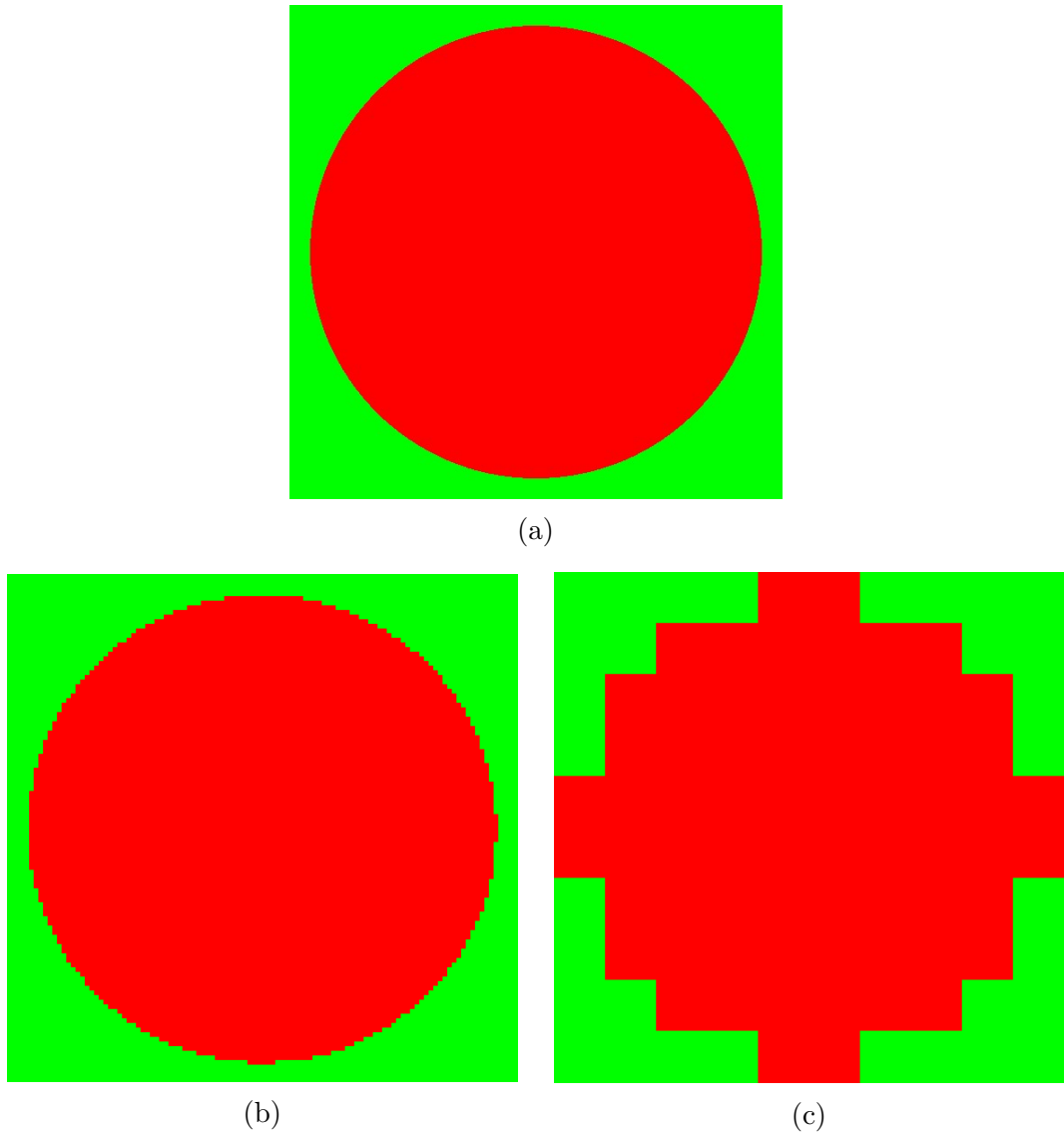


Figure 3.4: Surface of a cylindrical magnet where red colouring denotes magnetic north pole, blue colouring denotes magnetic south poles, and green colouring denotes free space. The original image (a) consists of 550x550 pixels. Image (b) is a fine grid approximation of the cylinder consisting of 110x110 pixels. Image (c) is a coarse 10x10 grid approximation of the cylinders top surface.

Table 3.1: Summarised results for a force simulation between two cylindrical N40 magnets with a diameter and height of 36.6 mm at a separation distance of 10 mm. The force between the magnets was measured as they were rotated relative to one another at a constant separation distance.

Simulation type	Mean force	Rotation force variation	Single sim time
Fine mesh	211.65 N	0.012 N	$\sim 5$ s
Coarse mesh	219.2 N	0.260 N	$\sim 10$ ms
FEMM	211.36 N	-	-

Table 3.1 summarises the results of simulations between two cylindrical magnets which are held at a constant separation distance and rotated around their central axis. This can be thought of as one magnet spinning while the second is held in place. For perfectly aligned magnets, the force should not vary as the magnet rotates. However, due to pixelation, there is a variation in the force between the magnets as one rotates. With reference to column 3 of the table, the coarse mesh produces a far greater force variation than when a fine mesh is used. This is largely due to the coarse mesh not accurately reflecting the shape the magnets of interest. The degree to which a magnet surface can be pixelated also depends of the simulated separation distance between the magnets. Column 2 of Table 3.1 shows that, if FEMM simulations are used as a reference, there is far greater error in the simulated mean force for a coarse mesh. This is due to the distortion of the magnet geometry and the size of the magnetic charge areas relative to the separation gap. The magnetic charge length is the square root of the charge area. Once the geometry is adequately captured by the mesh density, it was found from testing that a magnetic charge length 4-5 times smaller than the separation gap results in good accuracy. It is also of note that fine meshes require far longer time per simulation than coarse mesh sizes. When simulating a large number of scenarios a mesh size as large as possible whilst retaining reasonable accuracy should be selected to reduce computation time.

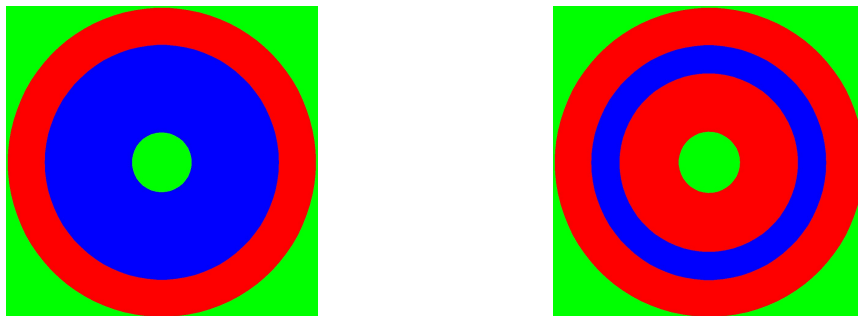


Figure 3.5: Interacting surface magnetisation patterns for an annular set of magnets based off the spring magnet demonstration produced by CMR Polymagnets.

## 3.2 Safer Magnetic Behaviour for Arrays

For more comprehensive coverage of safer magnetic behaviour please refer to section 4.1. The main feature of safer magnetic behaviour is that the force between magnets does not increase exponentially as the gap between them reduces. This can be achieved to varying degrees in the form of:

- Linear increase in force with reduced separation.
- Peak force achieved at a non-zero separation.
- Zero force crossing point.

A commercially available example of such a response can be seen in the ‘Spring’ type polymagnets from CMR. Figure 3.5 shows the magnetisation patterns of the interacting faces of the spring magnet demonstration. A custom vice was designed to hold the magnets so that their force profile could be measured using in a tensile testing machine (‘TA.HD plusC Texture Analyser’ by Stable Micro Systems) as shown in Figure 3.6. The custom vices were designed consisting of two main pieces: an inner 3D printed casing fitting to the form of the demonstration magnet, and an outer case which keeps the inner case compressed on the magnet and attaches to the testing machine. The overall design and material choice for the vice allows the magnets to be held flat, restricts the rotational motion of the magnet and minimises the effect of unwanted force contributions from nearby

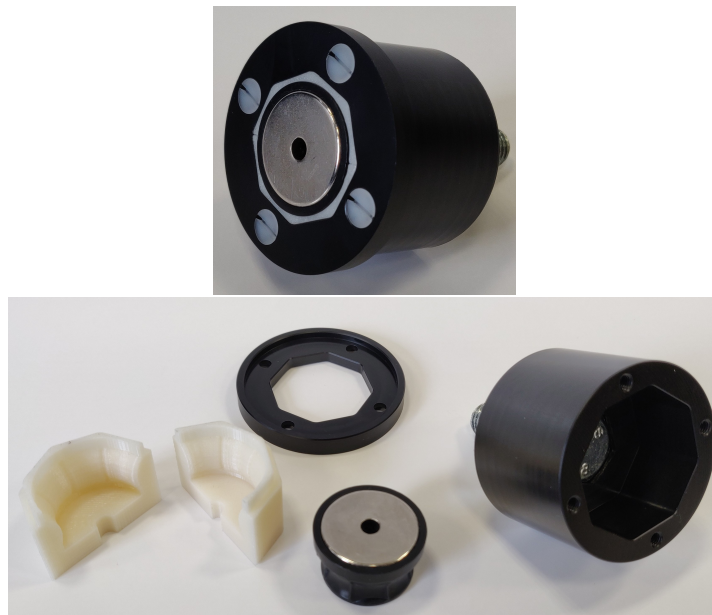


Figure 3.6: Custom magnet vice used to hold spring polymagnet demonstration during tensile testing.



ferromagnetic materials. The tensile test was also run with only one magnet to measure any force contributed by the coupling between the stainless steel bolt in the vice and the polymagnet. The force contributions from the bolt coupling was minimal but was still removed from the results of the tensile test for the magnets coupling to each other. Figure 3.7 demonstrates the ability of these patterned magnets to both attract and repel each other depending on their separation distance. At larger separations ( $\sim 10$  mm) there is very little interaction between the magnets, experiencing weak attraction of less than 1 N. The attractive force between the magnets continues to increase as they move closer together until it reaches its maximum attractive force at 5 mm separation ( $\sim 2$  N). The attractive force between the magnets transitions into a repulsive force as the separation distance is further reduced, with the zero force crossing point between the magnets occurring around 2.7 mm separation. Following the zero force crossing point the repulsive forces greatly increase for any further reduction in separation distance.

Whilst polymagnets are very successful at achieving safer magnetic behaviour, it is a permanent magnet device with no controllability. An array of on-the-go programmable magnetic cells could transition between multiple safer magnetic states depending on the magnetisation pattern.

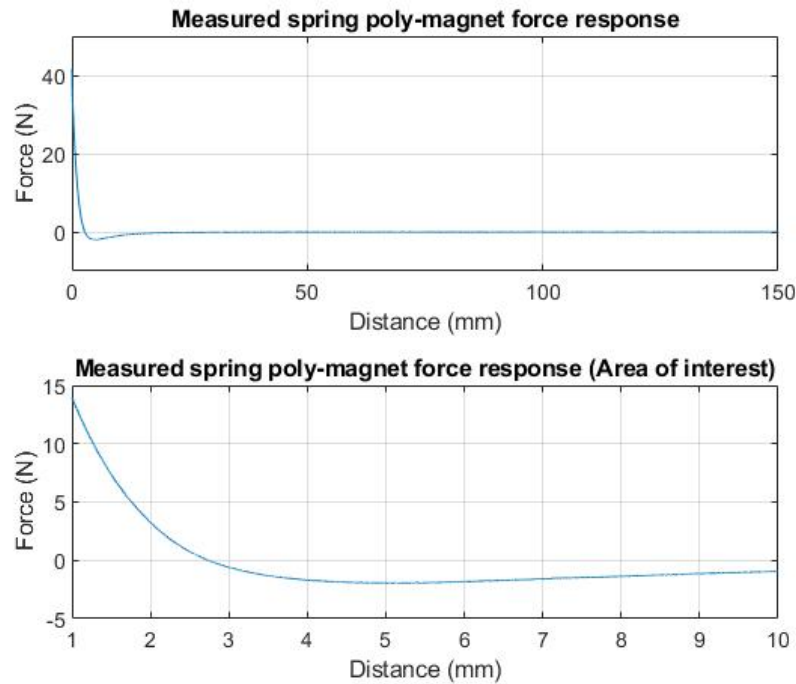


Figure 3.7: Net measured force between spring polymagnets using tensile testing equipment.

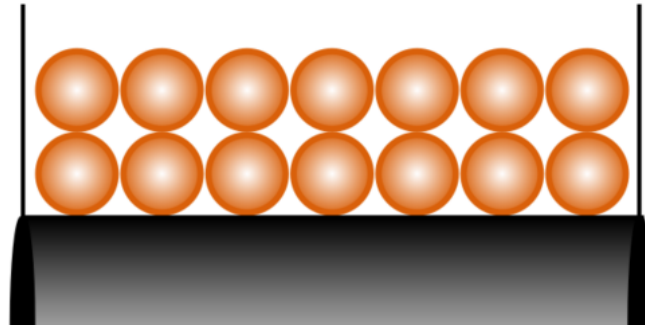


Figure 3.8: Square wire packing around bobbin.

### 3.3 Electropermanent Magnet Array Design

#### 3.3.1 Design Considerations

A single cell electropermanent magnet consists of a single permanent magnet material surrounded by a coil. AlNiCo 5 is selected as the core material as it has a high residual flux density (similar to that of N40) and a relatively low coercivity of around 50 kA/m (N40 has a coercivity nearly 20 times greater). This material selection should allow for strong forces whilst being controllable by a passively cooled coil. A field 3-5 times the strength of the coercivity of a magnet material is regarded as the rule of thumb for fully reversing the magnetisation direction. For AlNiCo 5, this means its surrounding coil must be capable of producing a field strength of 150 - 250 kA/m. Square packing of the wire around the bobbin (see Figure 3.8) is assumed for all calculations in this section.

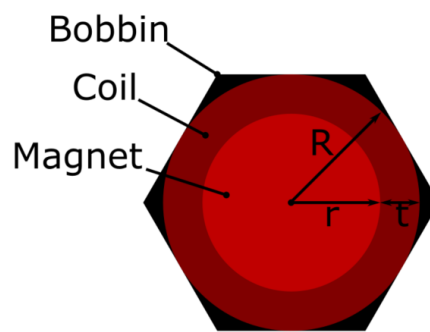


Figure 3.9: Labeled top view diagram of a hexagonal electropermanent cell. The outer radius of the coil,  $R$ , is the sum of the magnet radius,  $r$ , and the coil thickness,  $t$ .

To physically build a prototype, coils are wound around bobbins within which the magnet core will be placed. The bobbin ends are shaped like hexagons to give the best packing efficiency and facilitate easy construction of arrays. A labeled top view diagram of one of these cells is shown in Figure 3.9. The radius of

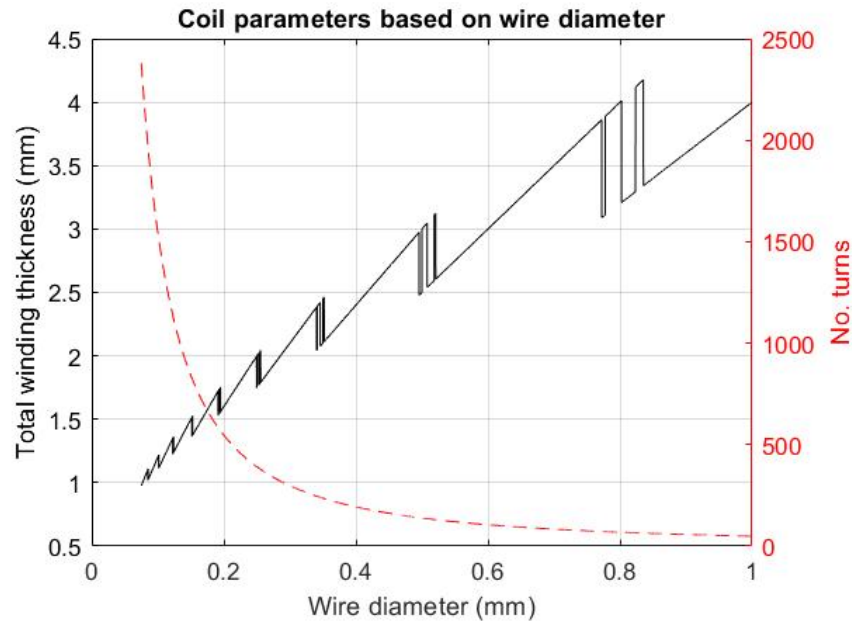


Figure 3.10: Variation in winding thickness and the total number of turns required for changing wire diameter.

the circle inscribing the hexagonal cell is the sum of the magnet radius and coil thickness. The total number of turns and thickness of the magnetising coil are plotted against increasing wire diameter in Figure 3.10. Note the jumps in the total thickness plot are due to the integer number of turns that can fit on a coil of a max height, i.e. some wire diameters will fit the max coil height without any remainder space. It is observed that a thinner total winding thickness is achieved for the smaller diameter winding wire. However, that comes at the cost of more turns due to the lower current capacity of small wires. An additional downside of using a smaller wire is that the coil will have a higher resistance, requiring a larger driving voltage. If the hexagonal cell size is constant, the larger wire diameter produces a thicker coil which reduces the size the magnet core. It is important to consider how much of the device's interacting face is magnet area as this will dictate the maximum forces achievable. Figure 3.11 shows an example of how the individual electropermanent magnet cells join together to form an array. Ideally, the majority of the device would be magnet area as this would increase the range of forces achievable and reduce the variation in force as interacting arrays are rotated relative to each other. For a particular wire choice, an increase in the size of the core magnet will increase the total cell size and increase the magnet percentage area of the device (i.e. the light red area relative to the total array footprint in Figure 3.11). The variation in magnet percentage area of the device with the core magnet radius is shown in Figure 3.12.

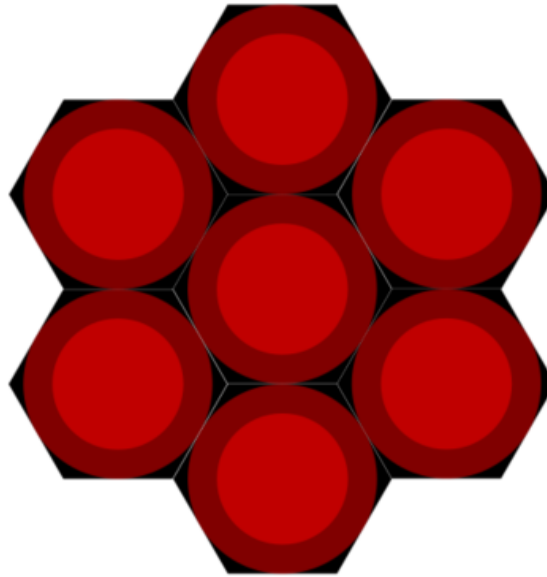


Figure 3.11: Diagram of a seven cell electropermanent array where the light red represents magnet area, dark red represents coils, and black represents the hexagonal bobbin.

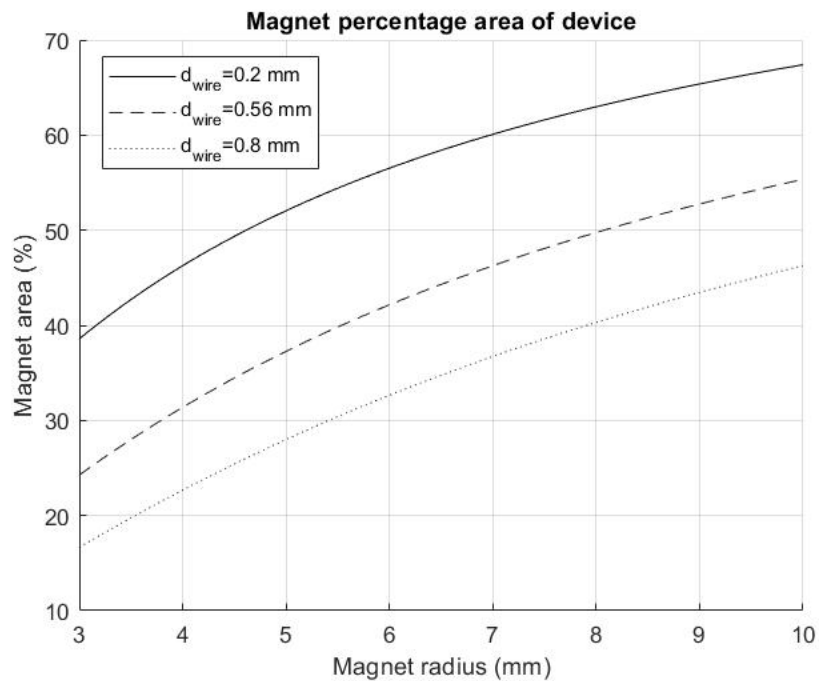


Figure 3.12: Relation of magnet area to total device footprint for increasing core magnet sizes. A selection of coil wire diameters show the trend of smaller wire diameters leading to greater percentage area of magnets.

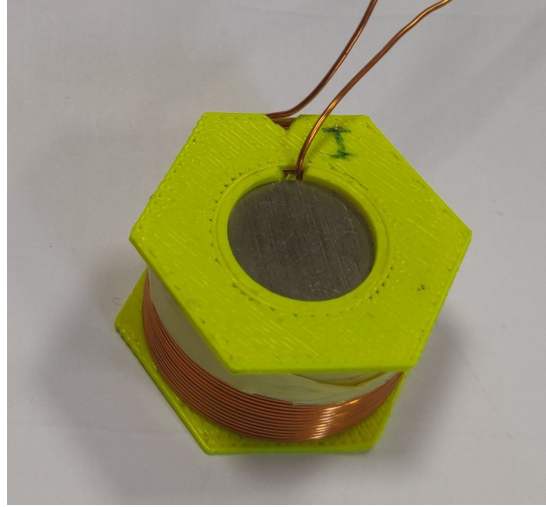


Figure 3.13: Prototype hexagonal electropermanent magnet cell using a cylindrical AlNiCo 5 magnet core and 220 turns of 0.56 mm wire.

The prototype electropermanent magnets cells, see Figure 3.13, made use of a cylindrical AlNiCo 5 core magnet with a height and diameter of 14 mm. The coil with a height of 14 mm consists of 220 turns of 0.56 mm wire. The hexagonal cell has a total height of 16 mm and the circle that inscribes the hexagonal bobbin has a diameter of 28 mm.

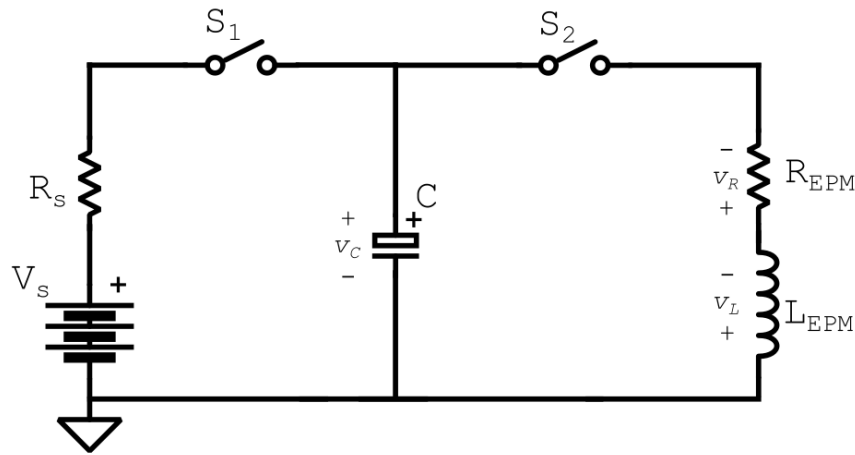


Figure 3.14: Simplified schematic for a capacitor discharge circuit.

### 3.3.2 Power Delivery Design

Electropermanent magnets are often considered to be low power devices as they use no power unless they are switching states. However, the impulse power required to fully reverse the magnetisation direction of the core magnet can be quite high. Due to the speed at which the domains within a magnet align when

exposed to a suitably strong field, only a short pulse field is required. For this reason a capacitor discharge circuit was designed to generate a current pulse in the electropermanent magnet coil. A simplified view of a capacitor discharge circuit is shown in Figure 3.14. The capacitor,  $C$ , is charged up to the supply voltage,  $V_s$ , by closing switch 1. The rate at which the capacitor charges depends on the value of the resistor,  $R_s$ . Once the capacitor is charged, switch 1 is opened. The circuit is now ready to generate a current pulse in the electropermanent magnet. When a pulse is required, switch 2 is closed, connecting the charged capacitor to the electropermanent magnet (modelled as resistance,  $R_{EPM}$ , and inductance,  $L_{EPM}$ ). While switch 2 is closed, the circuit is simply a RLC circuit with an initial charge on the capacitor. The voltages on each of the components is defined by Equations 3.4 to 3.6.

$$v_C = \frac{1}{C} \int i \, dt \quad (3.4)$$

$$v_R = i R_{EPM} \quad (3.5)$$

$$v_L = \frac{di}{dt} L_{EPM} \quad (3.6)$$

Where:  $v_C$  Voltage on the capacitor (V)  
 $v_R$  Voltage on the resistor (V)  
 $v_L$  Voltage on the inductor (V)

Applying Kirchhoff's Voltage Law to the RLC loop and substituting in the relationships in the above equations leads to Equation 3.7. Differentiating the whole equation produces a second order differential equation, see Equation 3.8.

$$v_L + v_R + v_C = 0$$

$$\frac{di}{dt} L_{EPM} + i R_{EPM} + \frac{1}{C} \int i \, dt = 0 \quad (3.7)$$

$$\frac{d^2 i}{dt^2} L_{EPM} + \frac{di}{dt} R_{EPM} + i \frac{1}{C} = 0 \quad (3.8)$$

The current pulse used for magnetising the magnet core should be overdamped to eliminate any unwanted demagnetisation. The second order differential equation can be solved assuming an overdamped response. An overdamped response is also preferred when MOSFETs are used as the switches to ensure a continuous circuit for the duration of the pulse. By comparing Equation 3.8 to the characteristic equation for a second order system, the damping factor,  $\zeta$ , can be predicted using Equation 3.9. For an overdamped response, the damping factor must be greater than 1. As the electropermanent magnet will dictate resistance and inductance, the capacitance is the design variable to achieve the desired response. The criteria for capacitance to achieve an overdamped response is given in Equation 3.10.

$$\zeta = \frac{R_{EPM}}{2} \sqrt{\frac{C}{L_{EPM}}} \quad (3.9)$$

$$C > \frac{4L_{EPM}}{R_{EPM}^2} \quad (3.10)$$

The schematic for the capacitor discharge supply used to magnetise the prototype electropermanent magnet cells is shown in Figure 3.15. The component names and values are given in Tables 3.2 to 3.7.

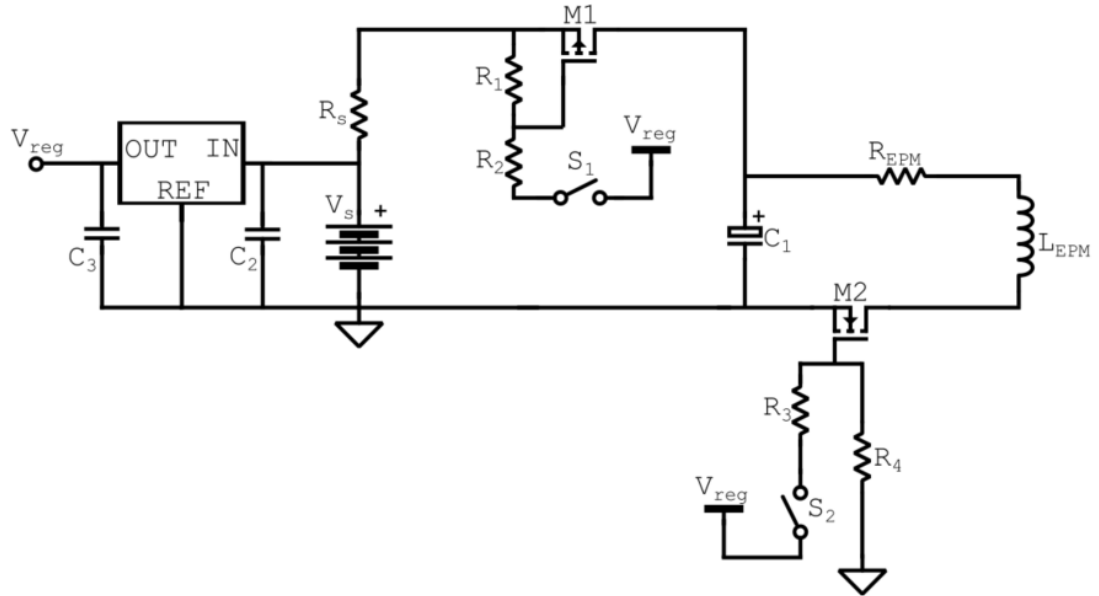


Figure 3.15: Capacitor discharge supply schematic.

Table 3.2: Voltage values for power schematic.

Voltage	Value (V)
$V_s$	35
$V_{reg}$	15

Table 3.3: Voltage regulator used for power schematic.

Voltage Regulator	Product code
$V_{reg}$	L7815CV

Table 3.4: Resistance values for power schematic.

Resistance	Value ( $\Omega$ )
$R_1$	10k
$R_2$	220
$R_3$	220
$R_4$	12k
$R_s$	100
$R_{EPM}$	$\sim 1.1$ (measured)

Table 3.5: Capacitance values for power schematic.

Capacitance	Value ( $\mu\text{F}$ )
$C_1$	4566 (measured)
$C_2$	0.33
$C_3$	0.1

Table 3.6: Inductance values for power schematic.

Inductance	Value ( $\mu\text{H}$ )
$L_{EPM}$	940 (measured from coil with 220 turns)

Table 3.7: MOSFETs used for power schematic.

MOSFET	Product code
$M_1$	SUP75P05-08
$M_1$	FQP70N10



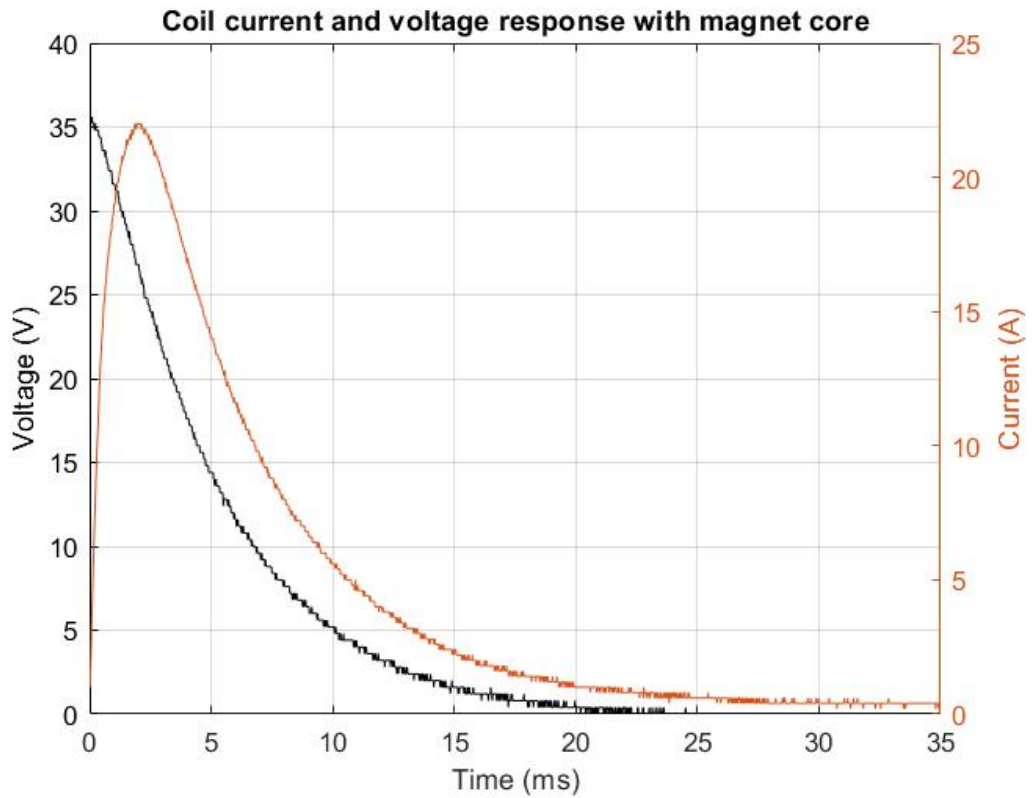


Figure 3.16: Measured voltage and current pulse through an electropermanent magnet cell (with AlNiCo 5 core material) from the capacitor discharge circuit. Capacitors had an initial voltage of 35 V.

Figure 3.16 shows measured values for the voltage across the capacitor and current through the cells coil during a current pulse. The measured current pulse closely matches the theoretically expected current for the measured component values ( $R_{EPM}$ ,  $C_1$ , and  $L_{EPM}$  from Tables 3.4 to 3.6). The circuit was capable of reversing the magnetisation direction of the magnet cores in the electropermanent magnet cells. The magnetic field density was measured at the centre of the top surface of the magnet using the GM08 Gaussmeter (Hirst Magnetic Instruments Ltd, Falmouth, United Kingdom). The flux density was first measured as 40.5 mT. Following a current pulse in the coil, the flux density was measured as -43.5 mT. A current pulse in the opposite direction then returned the magnetisation to the original direction with a measured flux density of 40.7 mT. However, it was observed that the flux density at different points on the top surface of the magnet varied significantly in value. This is addressed in more detail later in the chapter, see section 3.5.

### 3.4 Predicted Electropermanent Magnet Array Performance

For the purpose of simulations, the array of electropermanent magnets are simplified to an array of permanent magnets. This assumption is made as the majority of interaction between arrays depends on forces due to the permanent magnet cores. The cells are only occasionally powered to magnetise the core as desired, after which, the electropermanent magnet cells will again magnetically operate as permanent magnets. In Figure 3.17, the seven cell array (presented earlier in Figure 3.11) is reduced to just its permanent magnets and the polarity of the magnet cores at the interacting surfaces are indicated. In the case of Figure 3.17a, all the magnets are given the same polarity, with their north pole (marked red) at the interacting surface. The magnetisation pattern is the term used to describe a particular array magnetisation state. Although the pattern in Figure 3.17b also consists of cells magnetised in the same direction, it is considered a different magnetisation pattern as they have south poles at the interacting surface. Other magnetisation patterns can be achieved by altering one or more cell magnetisation directions.

Figure 3.18 shows how the force, between the interacting magnetic patterns of Figure 3.17, varies as the arrays are separated and rotated relative to one another. Due to the cell nature of the design, the magnetic patterns are not axially symmetric, leading to large variations in force as the arrays are rotated relative to one another for a specific separation distance. The strongest forces are obtained when the magnets from each array overlap each other. For a seven cell array, this occurs every 60 degrees of relative rotation. The weakest force occurs when there is the least amount of overlap between the magnets of the interacting arrays. At a separation distance of 3 mm, the weakest force between the arrays occurs at  $\pm 30^\circ$  of relative rotation and is only 28% of the strength when compared to when the magnet arrays fully overlap.

The magnetic patterns of the arrays are varied to achieve safer magnetic responses. The magnetisation strength of individual cells is another parameter that can be varied to assist in achieving safer magnetic behaviour. The magnetic strength on cells can be modified by using smaller pulse currents. For particular relative rotations, safer magnetic behaviour can be simulated using the seven cell array. However, due to the non-axially symmetric nature of the device, the device will rotate, no longer producing a safer magnetic response.

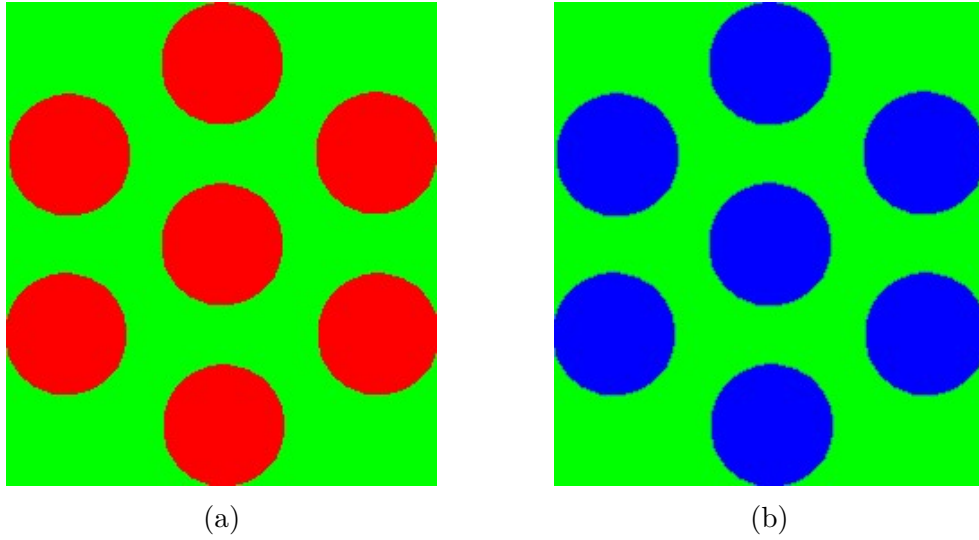


Figure 3.17: Permanent magnet simulated layouts for a seven cell electropermanent magnet array. Both magnetisation patterns shown consist of magnet cores with the same polarity, (a) with north poles at the interacting surface, (b) with south poles at the interacting surface.

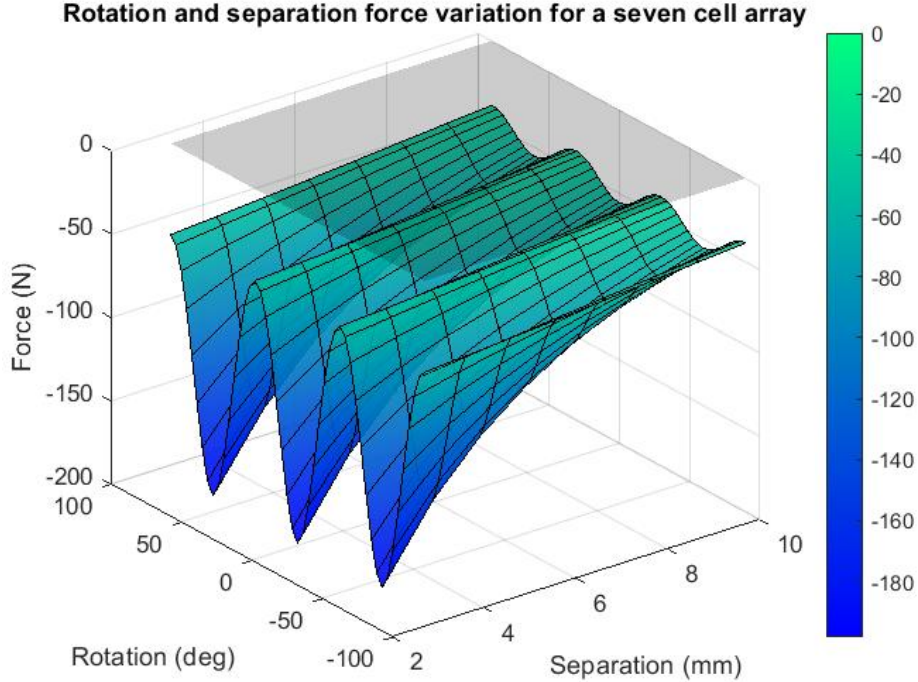


Figure 3.18: Simulated maximum attractive force between two seven cell electropermanent magnet arrays. Magnetic patterns used for the simulation of two interacting arrays are shown in Figure 3.17. Zero force plane is shown as a translucent black plane.

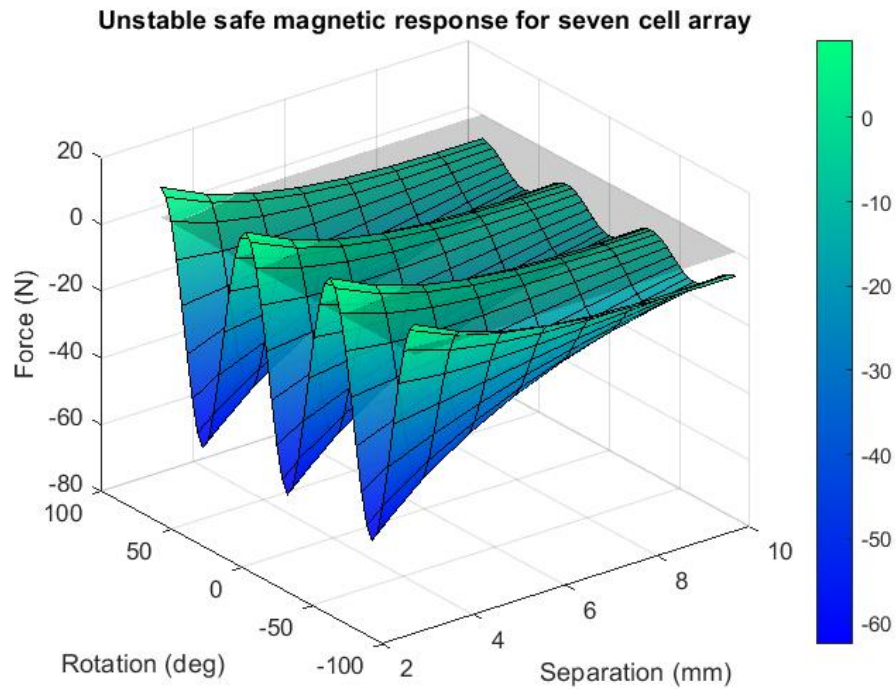


Figure 3.19: Simulated example of a seven cell array demonstrating safe magnetic behaviour (repulsive at close separations, attractive at further separations) along certain relative rotations. Safe magnetic behaviour is unstable as arrays will rotate away from repulsion to the relative rotations that are most attractive.

Figure 3.19 is an example of such a response for a particular set of interacting magnetic patterns. The force response shows safer magnetic behaviour when the magnets least overlap (i.e. relative rotation of  $\pm 30^\circ$ ,  $\pm 90^\circ$ , ...) as the force transitions from repulsive at very close separations, to attractive at further separations. However, if rotational movement of the magnet arrays is not restricted, then the magnets will tend to rotate to relative rotations where there is purely attractive forces. This is further captured if the energy of the interaction is analysed, see Figure 3.20. The magnet arrays will tend to move so as to reduce the system energy. The minimum energy along the safe magnetic response relative rotations is at the zero force crossing point meaning that, if the rotational motion of the arrays was restricted, the arrays would move to the separation distance where the zero force crossing point occurs. However, if the rotational motion of the arrays is not restricted then they will rotate to a lower energy position (i.e. relative rotation with a stronger attractive force).

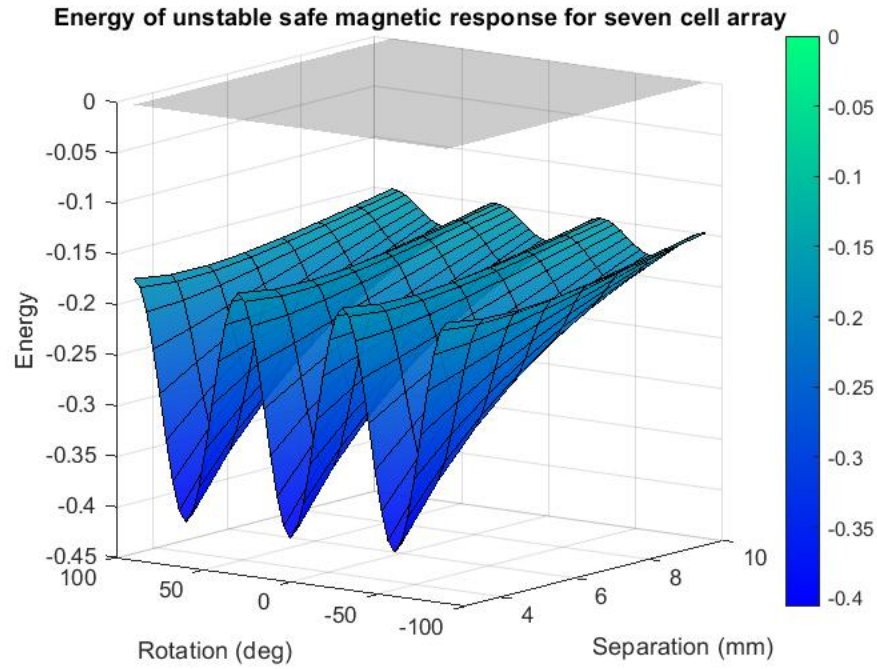


Figure 3.20: Simulated energy of the unstable safe magnetic response for a seven cell array.

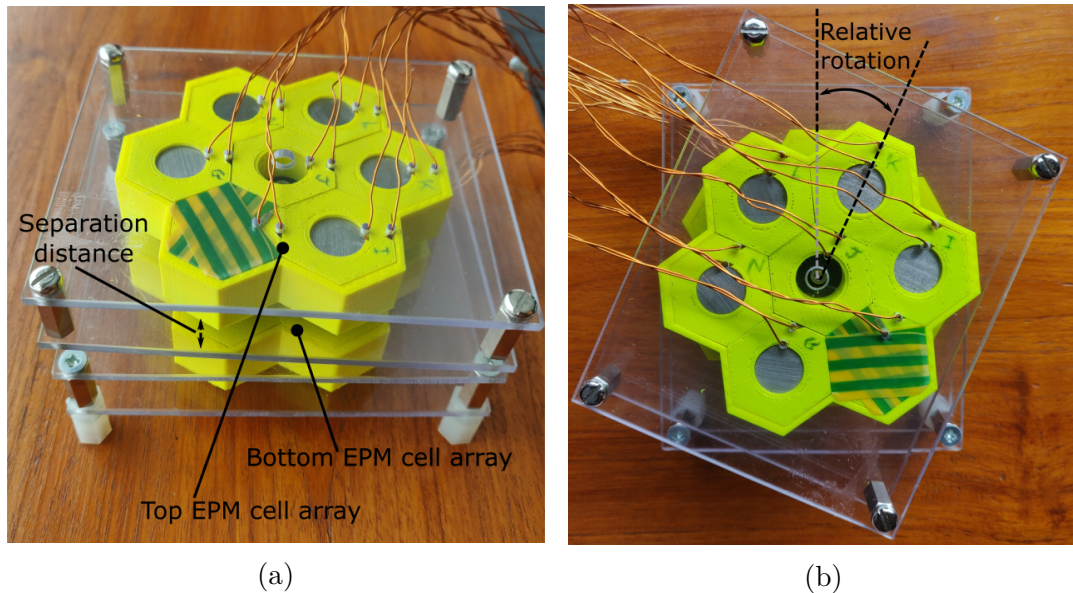


Figure 3.21: EPM cell array prototype side (a) and top (b) views. Points of measurement for separation distance and relative rotation between the two cell arrays are shown. The magnet core of the central cell in each array has been replaced by a bar and bearing to restrict separation but allow for relative rotation.



A prototype for the seven cell configuration of electropermanent magnets was produced, see Figure 3.21. In the rig, the magnet core of the central magnet was replaced by a connecting bar and bearing. This allowed for the separation distance to be fixed and allow free rotational movement. Extensive testing of this prototype was not carried out largely due to the poor performance of the core magnets with respect to their magnetisation strength, magnetisation uniformity, and resistance to unwanted demagnetisation (explained in section 3.5). Whilst not capable of performing safer magnetic coupling behaviour, the prototype does tailor itself to possible motor applications or those requiring rotational positioning.

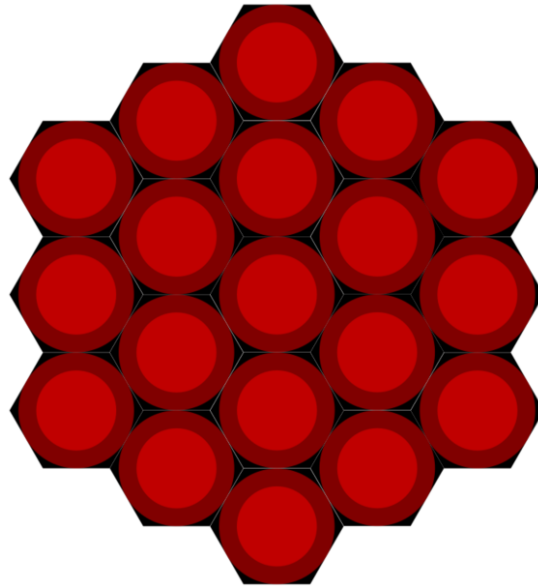


Figure 3.22: Diagram of the larger electropermanent array consisting of nineteen cells. The light red represents magnet area, dark red represents coils, and black represents the hexagonal bobbin.

Prior to the production of the seven cell array prototype, larger array sizes were simulated to try achieve stable safer magnetic behaviour in theory. An extra layer of electromagnets was added, see Figure 3.22. The larger array is made up of nineteen electromagnet cells. It was found that stable safe behaviour could be simulated for this larger array for a particular set of magnetic patterns by tuning the magnetisation strength of the cells. The variation in force for changing separations and rotations for the stable safe behaviour is shown in Figure 3.23. At relative rotations of  $\pm 11.25^\circ$ ,  $\pm 48.75^\circ$ , ... the force is observed to act repulsively at close separations and transition to attractive at further separations. The magnet arrays would not rotate out of this relative rotation as, if the arrays are rotated in either direction, there is a stronger repulsive force. Whilst this shows that there

are cases where safe magnetic behaviour can be achieved, it does not represent a array state that can be physically implemented. The magnetic patterns which created the safe force response requires too strict control of the magnetisation strength of the individual cells (accuracy of  $\sim 10\%$  for cell magnetised to 6% of maximum strength). Additionally, the attractive force along the safe magnetic force rotation is  $<1$  N and therefore has little practical use given the scale of the device.

Due to problems with the prototype magnets and the difficulties mentioned above, the electromagnet cells were no longer pursued as a method of achieving safer magnetic force responses. Further details on the problems with the prototype magnets can be found in section 3.5.

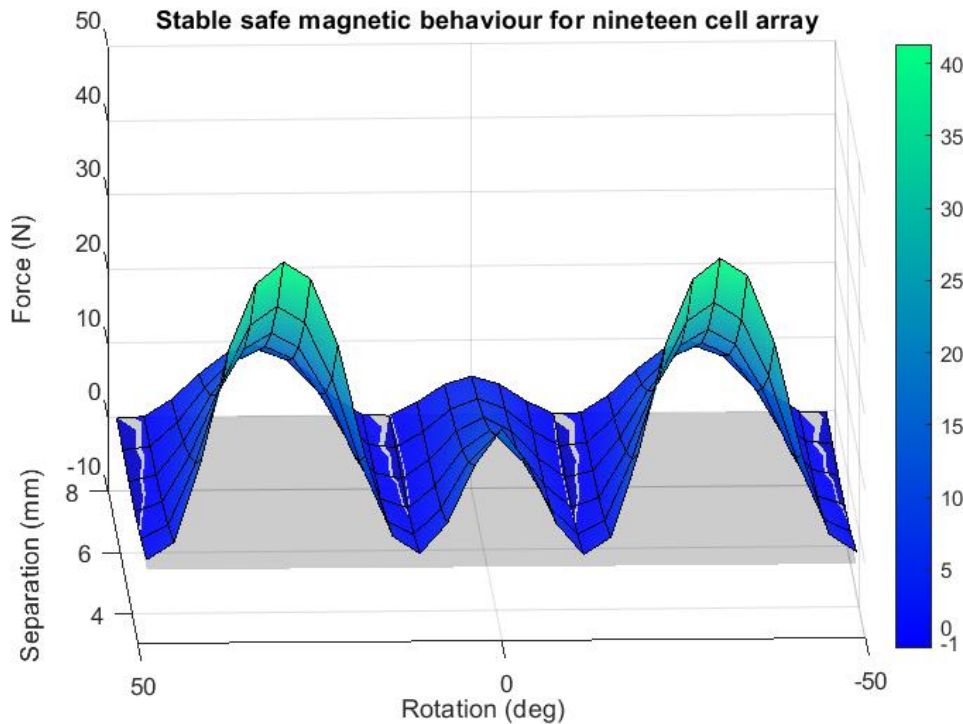


Figure 3.23: Simulated nineteen cell array demonstrating stable safe magnetic behaviour. The zero force plane assists in highlighting where the force transitions from repulse to attractive as the separation increases.

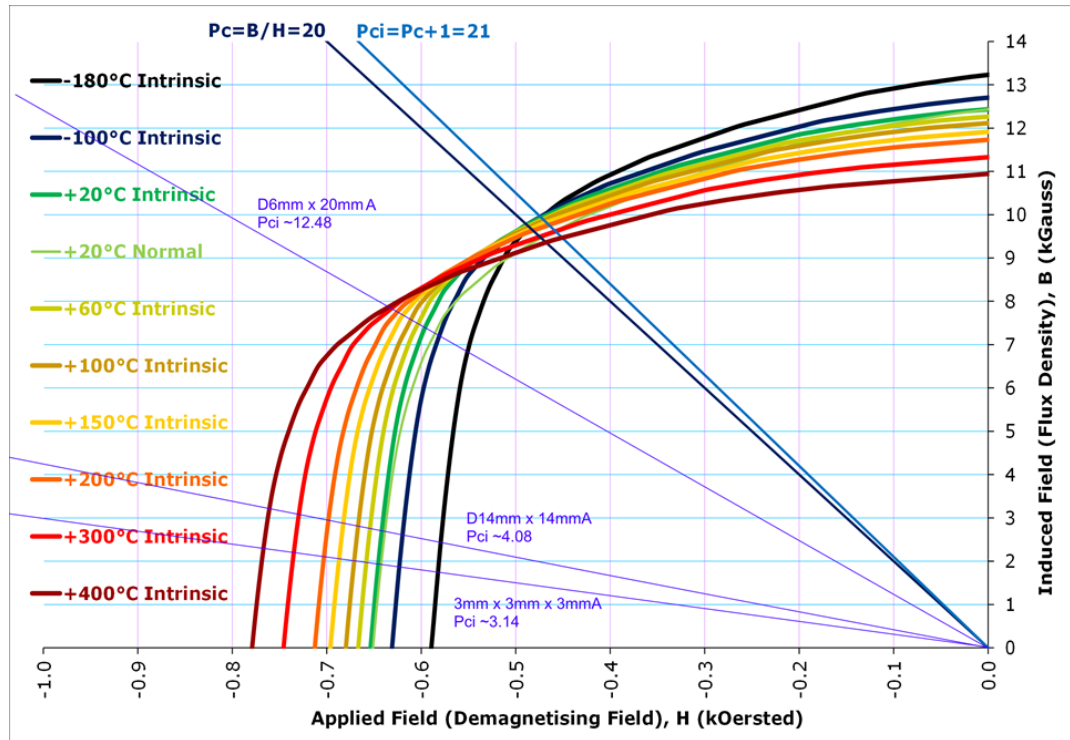


Figure 3.24: Permeance coefficient and load lines for different AlNiCo 5 magnet geometries, courtesy of Eclipse Magnetics (Eclipse Magnetics Ltd, Sheffield, UK).

### 3.5 Limitations of the Electropermanent Magnet Device

The prototype used cylindrical AlNiCo 5 magnets with a diameter and height of 14 mm. The magnets were supplied by Eclipse Magnetics (Eclipse Magnetics Ltd, Sheffield, UK). The adverse effects of a poor permeance coefficient were not taken fully into account during the magnet selection process. A detailed review of how the permeance coefficient of a magnet can effect its operation can be found in section 2.4.1.1. Figure 3.24 shows the operating lines for different AlNiCo 5 geometries. It can be seen that for a cylindrical magnet of height and diameter 14 mm, an intrinsic permeance coefficient,  $P_{ci}$ , of around 4.08 is expected. This magnet operates well below the knee of the demagnetisation curve leading to a far lower emitted flux density. The magnets are also extremely susceptible to demagnetisation when exposed to repelling fields. These magnets are not suitable for producing safer magnet behaviour as it requires repulsion between the arrays of magnets. When exposed to the repelling fields, the magnets demagnetise and attractive force components of interacting patterns dominate, causing the magnet arrays to no longer demonstrate safe behaviour but instead simply attract each other.



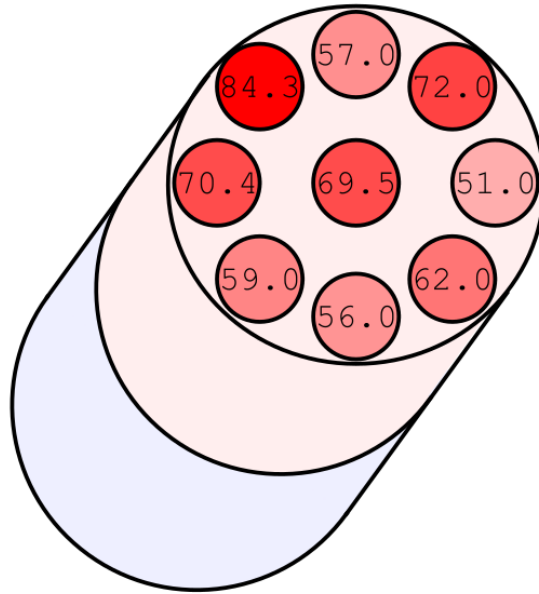


Figure 3.25: Measured flux density at points on the surface of the north pole of a single prototype magnet. Measured values are in mT and were obtained using the GM08 Gaussmeter from Hirst Magnetic Instruments.

In addition to emitting a lower magnetic flux density, the flux density was found to vary significantly across the surface of the magnets poles. Figure 3.25 shows the measured values for flux density at points around the surface of the north pole. The average flux density at the surface was 64.6 mT and had a standard deviation of 10.3 mT. As previously noted, fine control of the magnetisation strength is require to achieve safer magnetic behaviour. The prototype magnets are therefore unsuitable for achieving safer magnetic behaviour.

### 3.6 Final Comments

A device consisting of arrays of electropermanent magnet cells was developed. The magnetisation direction of each cell could be reversed in order to create different magnetisation patterns. Simulations of interacting magnetic patterns displayed the ability to achieve safer magnetic behaviour. In a physical system, these results could not be replicated due to both, poor magnet performance, and a conflict between electropermanent magnet design and the conditions required for safer behaviour. The repelling operating conditions for the magnets when producing safer magnetic behaviour conflicts with the need for a low coercivity magnet material in the electropermanent magnet which is required for remagnetisation.

## Chapter 4

# Simulation Methods for Device Design

An incremental simulation-based design process was followed for the design of the electromagnet colorectal anastomosis compression device. The finite element analysis software Finite Elements Method Magnetics (FEMM, David Meeker) is used to model and analyse the device performance. Device designs that, during this process, demonstrate safer magnetic behaviour are judged on their ability to achieve the pressures required for successful anastomosis. An earlier approach made use of electropermanent magnet technology, see Chapter 3 *Preliminary Device Design*. However, following initial testing, this technology approach was found to have limited practical use for achieving the behaviour desired. Returning to the technology review there were two other sources of variable magnetism: mechanically variable systems and electromagnets/combinational magnets systems. Electromagnetic based approaches are considered more desirable due to their ability to be electrically controlled and their absence of moving parts.

### 4.1 Safer Magnetic Behaviour

Typically, as magnets approach each other the force between them increases non-linearly. This behaviour can be captured on a force-separation plot. Figure 4.1 shows sample force profiles for N40 disk magnets and ring magnets from K&J magnetics (K&J Magnetics, Inc., Pipersville, United States). It is convention in this report that negative values of force describe an attractive force between magnets. For both sets of sample magnets in Figure 4.1 the force is observed to increase exponentially as the separation distance between them decreases. For

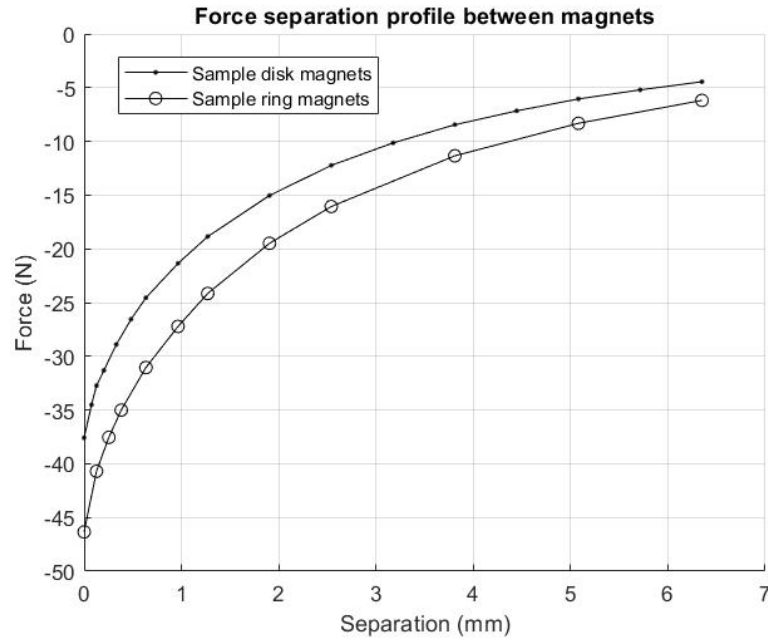


Figure 4.1: Sample force-separation plot for two different sets of N40 magnets from K&J Magnetics. Sample disk magnets have a diameter and thickness of 10 mm. Sample ring magnets have an outer diameter of 15 mm, inner diameter of 10 mm, and thickness of 10 mm.

medical applications where magnets are working across tissue with an air-gap failures can be catastrophic. Should the anchored clip begin to rip or overly pull on the tethered organ, then the separation distance between the external and internal magnets will reduce, leading to a vastly stronger pulling force, which reinforces the initial problem. Additionally, if the tether was to fail and the internal magnet was to accelerate towards the external magnet, the tissue separating the magnets would be highly compressed and damaged. Such magnet behaviour is also non-ideal for compression anastomosis applications. For the magnetic anchoring device proposed in [53] where one magnet is held externally and the other is tethered internally (see Figure 4.2), there are minimum limits on the tissue thickness due to concerns about the magnets applying too much pressure and damaging the tissue. Low compression pressures can lead to a failure in anastomosis as the magnets can easily decouple and become displaced. Pressures which are very high can also be dangerous, compressing at too great of a rate for the site to heal and may even cut through the compressed tissue causing leakage [54]. It is therefore desirable to have high enough initial forces to achieve strong coupling between the magnets without exceeding acceptable levels as compression progresses. According to G. Zhao et al. [54] this optimal pressure range is between 79.8 kPa - 169 kPa for dog intestinal tissue.

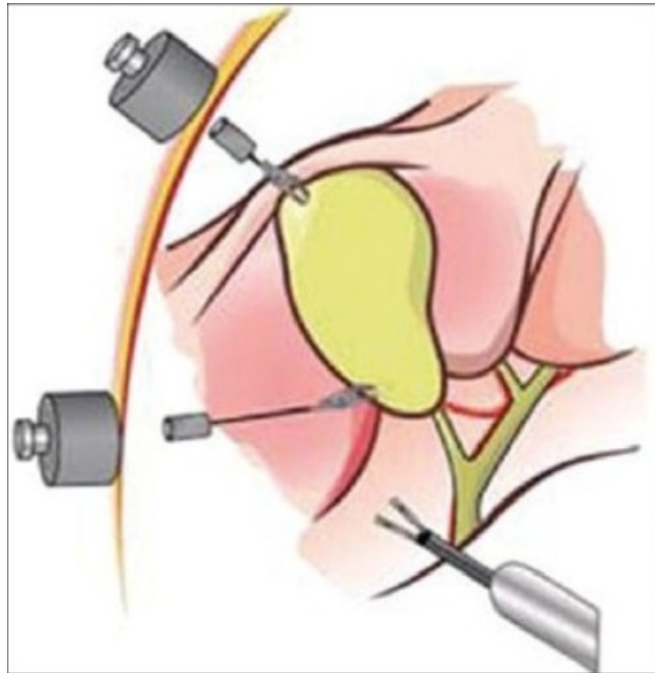


Figure 4.2: Modified image of magnetic anchoring system from a report by G. Domingues et al. [53] showing the Imanlap system. External magnets pull on smaller internal magnets, which are tethered to an organ.

For magnetic anchoring and colorectal anastomosis applications, alternative safer magnetic behaviour, where the force does not increase exponentially, can mitigate such dangers. There are three key improvement stages for achieving safer attractive magnetic behaviour as listed below:

1. Linear increase in force with reduced separation.
2. Peak force achieved at a non-zero separation.
3. Zero force crossing point.

These safer magnetic behaviours are considered for how they reduce the risks posed by typical magnets in a medical device setting. These behaviours are achievable through the modification of the shapes of interacting magnets as well as their magnetisations. To date, some of these safer magnetic behaviours have been physically shown with Polymagnets, a multi-pole magnet designed and produced by Correlated Magnetics (Correlated Magnetics Research, LLC, Huntsville, Alabama, United States) .

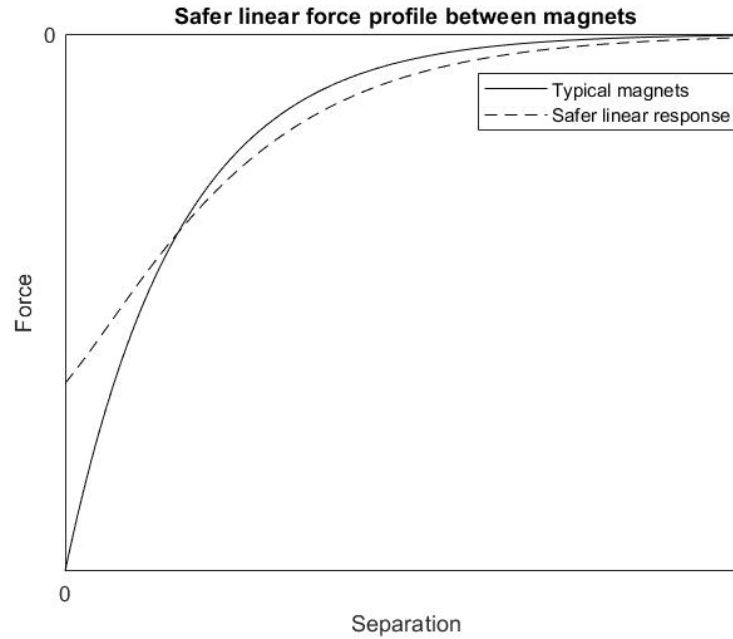


Figure 4.3: A safer linear force response compared to a force response from typical magnets.

#### 4.1.1 Linear Increase in Force with Reduced Separation

The first step to improving the safety of magnetic attraction is to reduce the rate at which force increases as the separation decreases. Figure 4.3 shows both a typical magnetic force profile and one where the force increases linearly at close separations. This behaviour reduces the peak force achievable from the same magnet footprint. However, for many medical applications magnet size is not a limiting factor as suitable forces can be achieved within the space available. In the case of compression applications, the linear relationship between the force and separation may allow for greater initial forces whilst not exceeding acceptable forces as the compression progresses.

#### 4.1.2 Peak Force Achieved at a Non-Zero Separation

Focusing on compression applications, coupling magnets that can produce a peak force at a non-zero separation point are desirable. Figure 4.4 shows this safer magnetic behaviour compared to that of typical magnets. This behaviour allows for even greater initial compression forces whilst limiting the peak compression force. An additional benefit of such magnetic behaviour is that the magnets can have a far greater coupling force over larger separations. The reduction in force at very close separations also lends itself for anchoring applications where the

peak force can be set to the maximum desired pulling force. Should the internal tether start to rip or over-pull the organ, the decrease in separation will result in a lower force, which in turn should slow or even stop the tether from ripping.

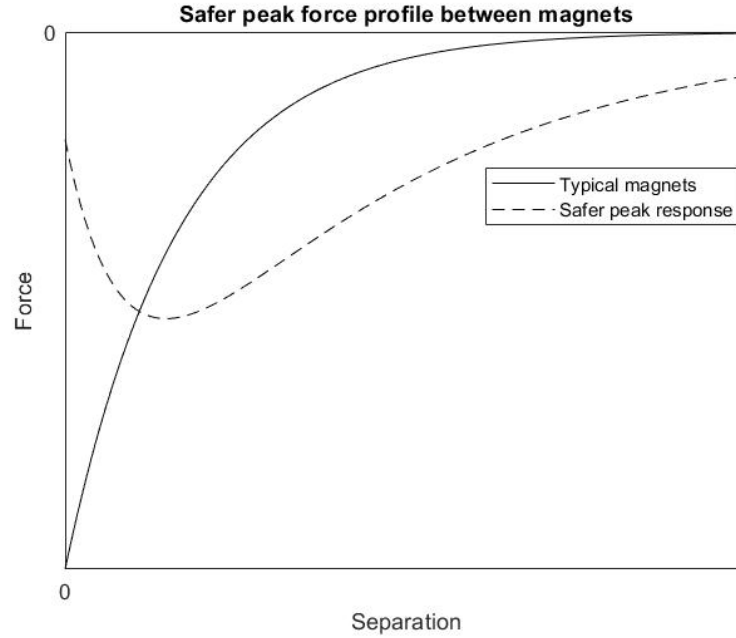


Figure 4.4: Force response from typical magnets compared to a safer magnetic behaviour where the peak force is achieved at a non-zero separation.

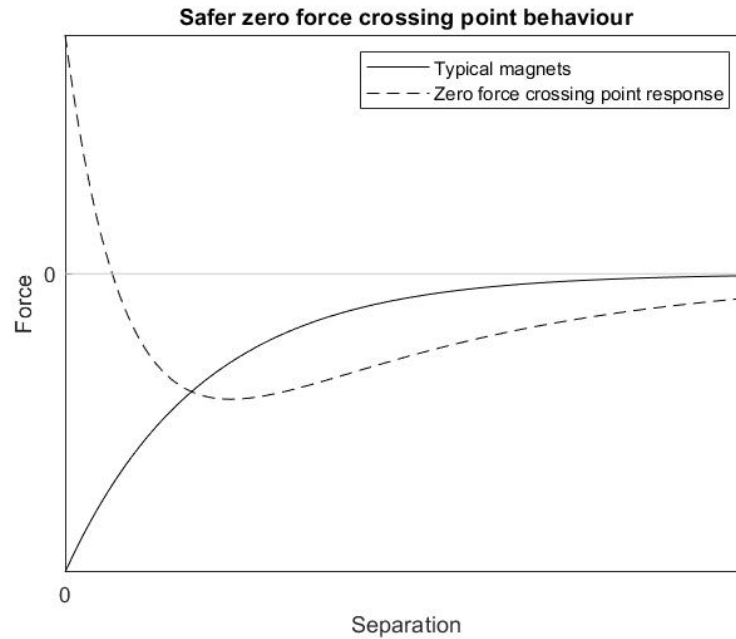


Figure 4.5: Force response from typical magnets compared to a safer magnetic behaviour where the force between magnets changes from attractive to repulsive. A zero force crossing point is introduced due to this behaviour.

### 4.1.3 Zero Force Crossing Point

The most complex of the safer magnetic behaviours proposed is that which displays a zero force crossing point, such as that shown in Figure 4.5. Here the magnets attract each other at larger separations but when the separation distance becomes very small the magnets transition to repelling each other. As the force changes from an attractive to a repulsive state, a separation point where there is no net force between magnets is produced. This behaviour results in greatly reduced peak compression forces when compared to traditional magnets and is therefore not best suited to compression applications. This magnetic behaviour best addresses the possible dangers of anchoring as, should the internal magnet detach from its tether, there will be no damage to the tissue between the magnets due them not snapping together. Separations closer than the zero force point cause the the magnets to repel each other and separations further than this point cause the magnets to attract each other leading to a stable separation distance between the magnets. Correlated Magnetics have designed ploymagnets to produce such a force response which they have called magnetic spring behaviour. An example of the multipole patterning used to create this behaviour is shown in Figure 4.6. However, once patterned, there is no additional control of the force response.

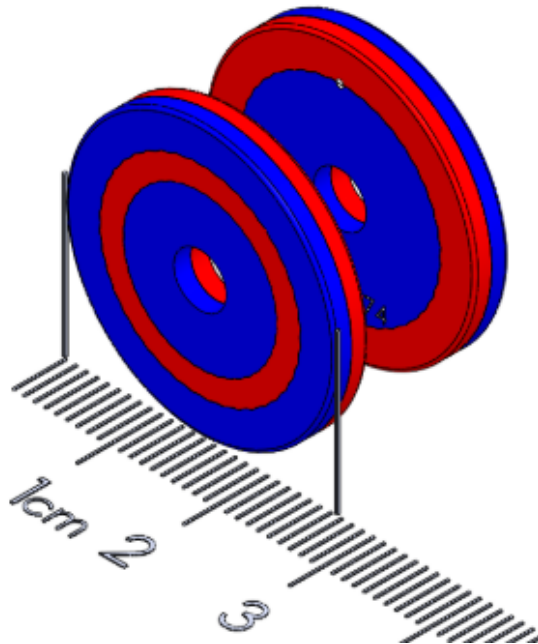


Figure 4.6: Set of Polymagnets by Correlated Magnetics used to demonstrate magnetic spring behaviour where north poles are coloured red and south poles coloured blue.

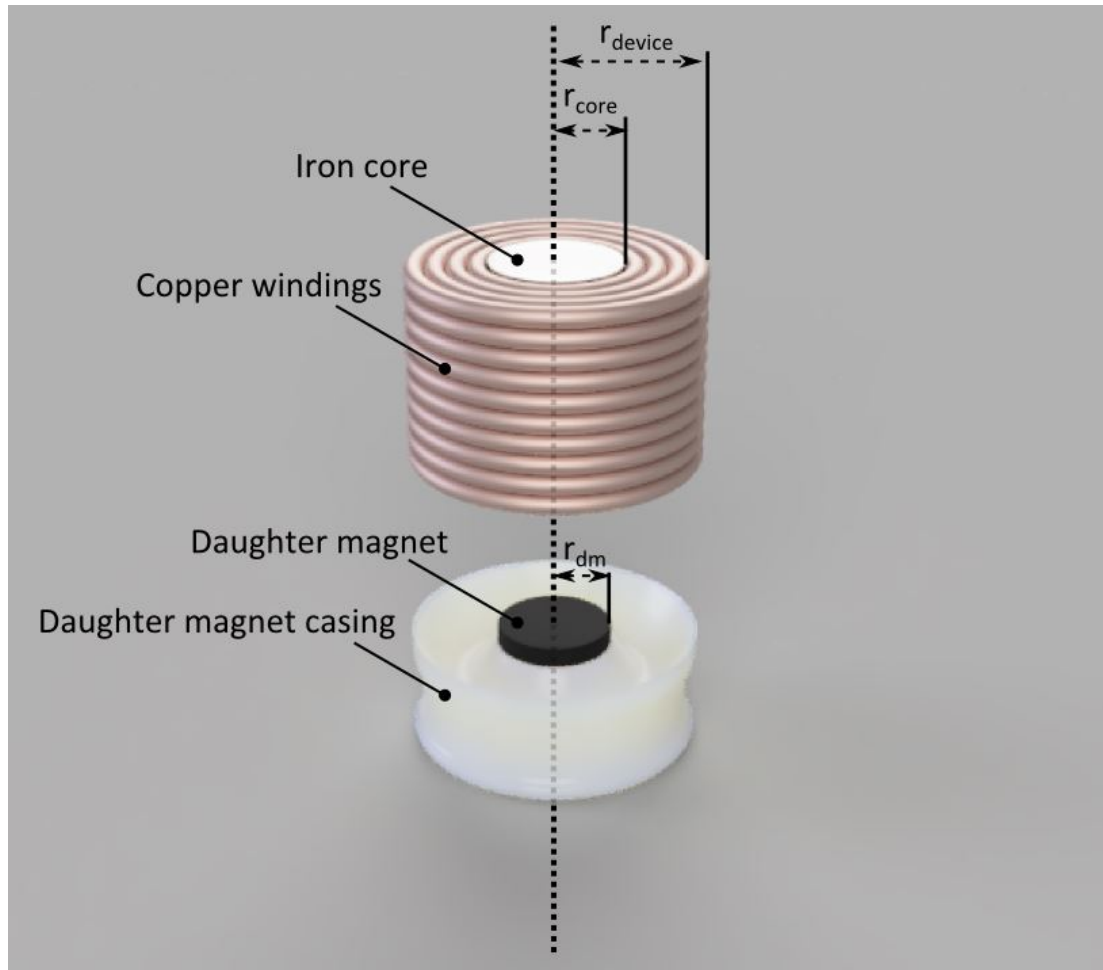


Figure 4.7: Annotated render of the proposed electromagnet anastomosis device, where  $r_{dm}$  is the radius of the daughter magnet,  $r_{core}$  is the radius of the iron core, and  $r_{device}$  is the radius of the full electromagnet device.

## 4.2 Anastomosis Device Constraints

One potential solution to the lack of control in the existing Polymagnet design is shown in Figure 4.7, where the compression forces are produced between the mother magnet, i.e. iron core electromagnet, and the daughter magnet. The design process for the device is captured in Figure 4.8. Constraints on the size of the device and the heat it can produce form the initial specifications of the electromagnet design. Parameters of the electromagnet and daughter magnet design are varied and the resultant performance analysed. Following the optimisation of the electromagnet and daughter magnet for high degrees of control, modifications to the electromagnet are investigated for their ability to improve the safe magnetic behaviour of the device when it is not powered whilst retaining as much control of the pressure as possible when the device is driven by a current.



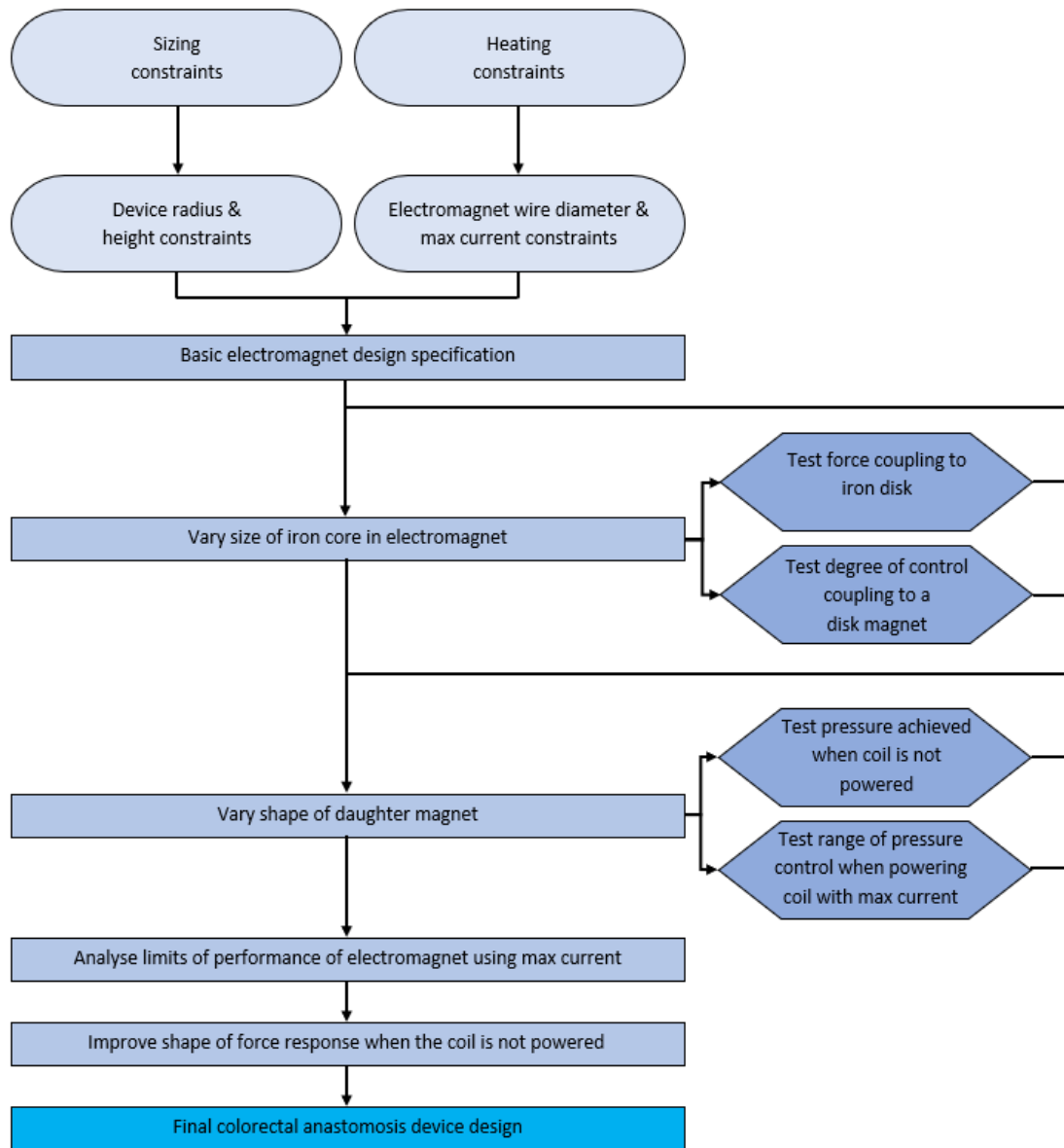


Figure 4.8: Process flow diagram for the design of an electromagnet colorectal anastomosis compression device.

The device constraints are summarised in Table 4.1. The existing devices used for colorectal anastomosis (reviewed in section 2.2) are used as reference for sizing constraints of the final device. The overall dimensions of the device are to be roughly 30 mm in both diameter and height to allow for suitable anastomosis sizes and for the device to be inserted and removed via natural orifices.

The force achieved by an electromagnet largely depends on the number of windings and the amount of current. Ignoring for now the effects of a saturated core material, increasing either the number of windings or the current will result in a stronger electromagnet. The stronger forces achieved by doing so lead to a higher

production of heat. For a device that will be inserted into a patient there is a limit to how much heat energy can be generated and expected to dissipate safely. For any particular wire choice, there is a maximum current that can be reached such that the temperature increase over time lies within a constraint. An increase of 3°C per minute is a conservative estimate for the maximum heat production of the device which can safely be dissipated in a colorectal anastomosis setting.

Table 4.1: Colorectal anastomosis device constraints.

Constraint parameter	Constraint value
Device Diameter	30 mm
Device Height	30 mm
Temperature increase	3°C/min

For a change in temperature,  $\Delta T$ , in a time period,  $\Delta t$ , the relation between current and the wire diameter is described by equation 4.1:

$$I = \pi \left( \frac{d_{wire}}{2} \right)^2 \sqrt{c \left( \frac{\rho_d}{\rho_r} \right) \left( \frac{\Delta T}{\Delta t} \right)} \quad (4.1)$$

Where:

- $d_{wire}$  Diameter of the electromagnet wire in m
- $c$  Specific heat capacity of copper in J/(kg K)
- $\rho_d$  Density of copper in kg/m<sup>3</sup>
- $\rho_r$  Resistivity of copper in  $\Omega\text{m}$

The amp-turns that can be achieved given the temperature constraint and sizing constraint above are shown in Figure 4.9. Figure 4.9 includes the loss in packing efficiency obtained using small diameter wires. Due to this packing constraint, superior amp-turns can be achieved at larger wire diameters. Twelve gauge wire is initially selected as this achieves a high amp-turn value within the sizing constraints and has a current that can be easily produced by commercially available equipment. The electromagnet device parameters are given in Table 4.2.

Table 4.2: Electromagnet parameters given size and temperature constraints.

Wire diameter (AWG)	(mm)	Max steady state current (A)	Electromagnet height (mm)
12	2.05	10.45	20.5

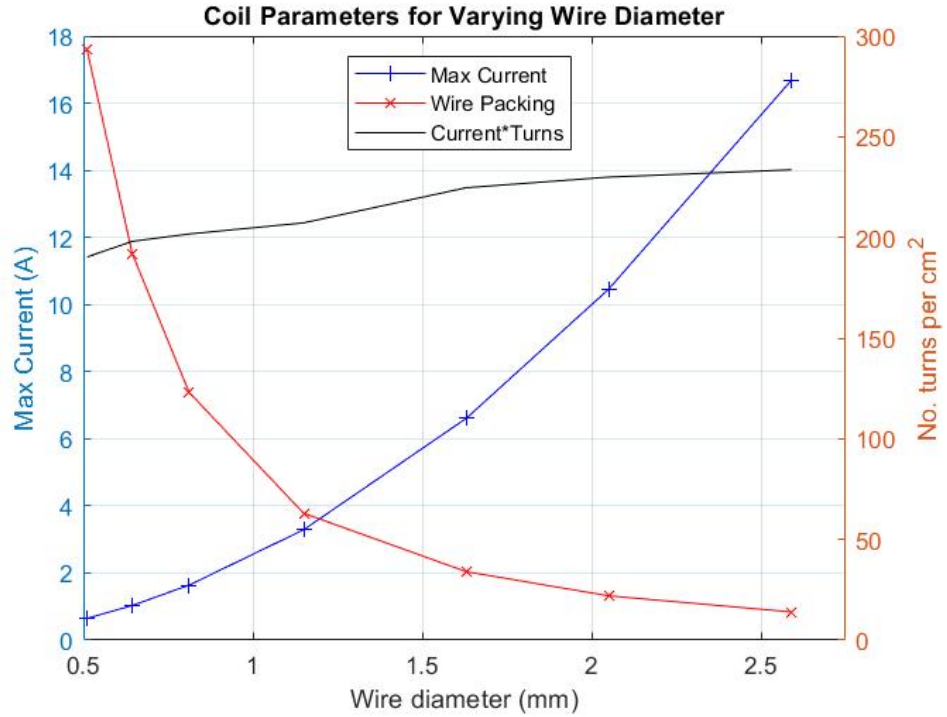


Figure 4.9: Amp-turns achievable given temperature and sizing/packing constraints (assuming packing factor from "Principles of Power Electronics" by J.G. Kassakian, et al. [55])

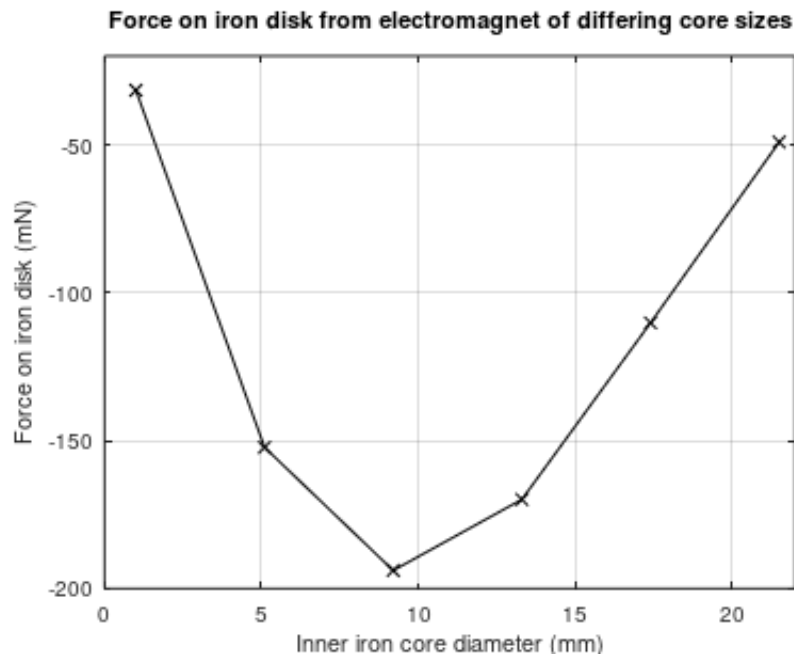


Figure 4.10: Simulated force on a iron disk (10 mm thick, 30 mm wide) due to an electromagnet of fixed outer dimensions for varying iron core sizes.

### 4.3 Electromagnet Optimisation

Prior to designing with a safe force response in mind, the limitations of an electromagnet under the constraints on size and temperature must be tested. The aim is to produce an electromagnet with the largest degree of force control given the current limits. This will allow for the force-separation profile to be best altered to achieve safe magnetic compression. The size of the iron core in the electromagnet is varied to investigate the trade-off between core size and force control. As the outer diameter of the device is constrained, an increase in the diameter of the iron core reduces the number of turns. In Figure 4.10 there is a clear point where the ratio of iron core to windings produces the maximum force. Cores of diameters between 9 mm and 13 mm give the largest forces when the powered electromagnet is coupling to an iron disk. Repeating this analysis when the electromagnet is coupling to a permanent magnet of the same dimensions leads to the results in Figure 4.11. The attractive force between the electromagnet and permanent magnet continues to increase as the core diameter increases. This is due to attraction between the permanent magnet and ferromagnetic core. The range of force control peaks between core diameters of 9 mm to 17 mm.

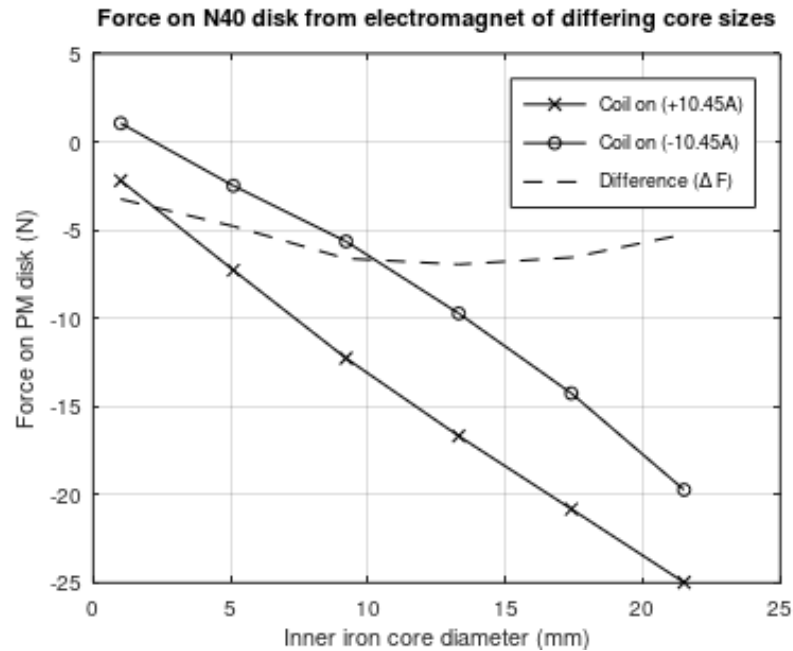


Figure 4.11: Simulated force on a N40 disk (10 mm thick, 30 mm wide) due to an electromagnet for varying iron core sizes with the coil operating in both directions (at the current limit) and the net force control range.

The electromagnet with iron core of diameter 13 mm is selected as it achieves the largest degree of force control ( $\approx 7$  N). The peak pressures achievable between this electromagnet design and a daughter magnet is investigated by varying the inner and outer diameters of the daughter magnet. Figures 4.12 and 4.13 show the forces and pressures experienced by ring daughter magnets of varying inner diameters. The pressure plot is found to mostly follow the shape of the force response in that it is reduced as the inner diameter of the ring daughter magnet is increased. The outer diameter of the disk daughter magnet was varied and the force and pressure responses are shown in Figures 4.14 and 4.15 respectively. In general, the force trends to increase as the outer diameter of the daughter magnet increases. However, the pressure is observed to peak at 65 kPa for an outer diameter of 12 mm.

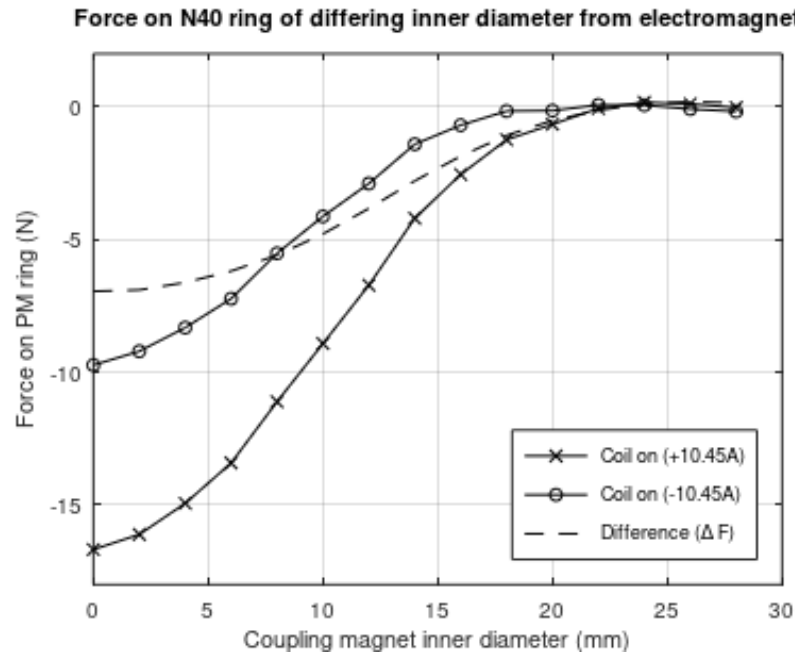


Figure 4.12: Simulated force on a N40 ring magnet (10 mm thick, 30 mm outer diameter) of differing inner diameters due to an iron core electromagnet.

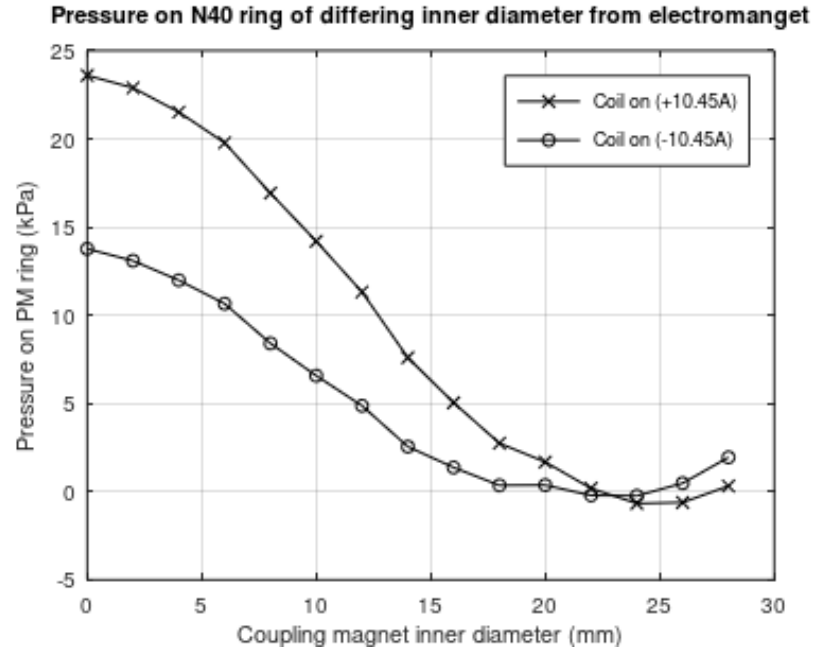


Figure 4.13: Simulated pressure on a N40 ring magnet (10 mm thick, 30 mm outer diameter) of differing inner diameters due to an iron core electromagnet.

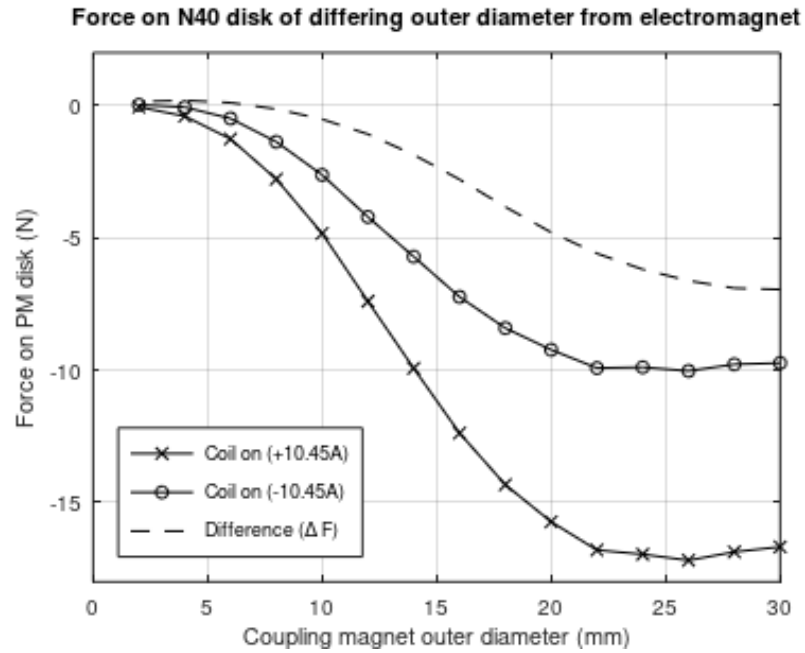


Figure 4.14: Simulated force on a N40 disk magnet (10 mm thick) of differing outer diameters due to an iron core electromagnet.

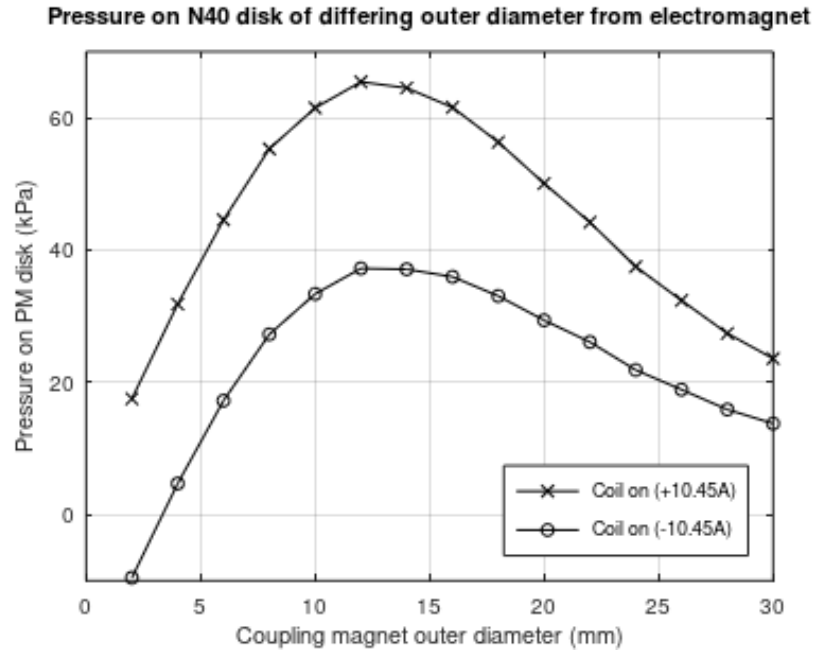


Figure 4.15: Simulated pressure on a N40 disk magnet (10 mm thick) of differing outer diameters due to an iron core electromagnet.

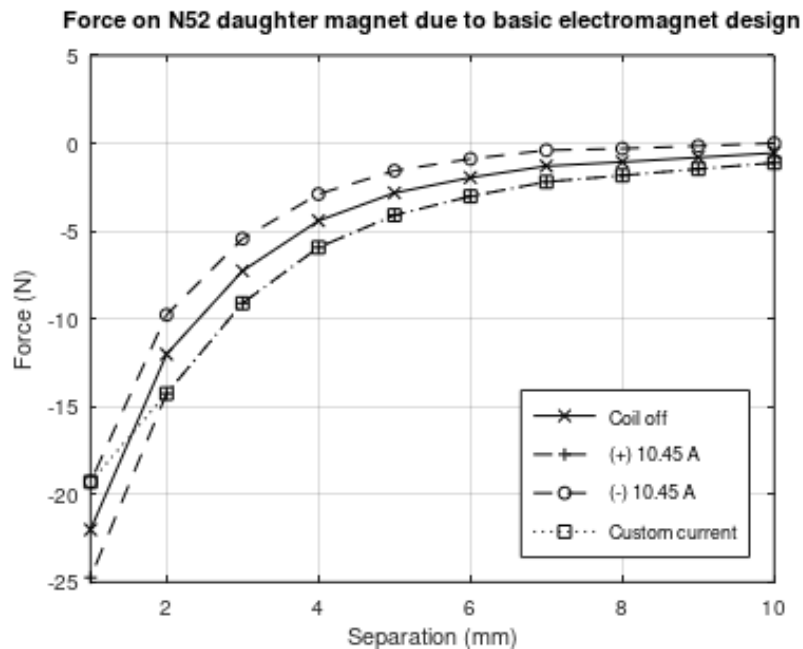


Figure 4.16: Simulated force-separation plot between a N52 disk daughter magnet (OD=12 mm) and the basic iron cored electromagnet design. Steady state limits of control are shown with the coil operating in both directions. A custom control current between the limits shows a possible controlled response.

## 4.4 Modification of Electromagnet to Achieve Safer Magnetic Behaviour

The simple electromagnet to daughter magnet coupling device described in section 4.3 was found to provide forces suitable for colorectal anastomosis. Figure 4.16 shows the simulated force-separation plot for the optimised electromagnet with a core diameter of 13 mm coupling to a N52 daughter magnet of outer diameter 12 mm. It can be seen that this design produces an exponential increase in force as the separation distance is decreased. Controlling the electromagnet with a custom current within the steady state limits (10.45 A as per Table 4.2) allows for some control of the force response, reducing the rate of increase in force from over 9 N/mm to just 4 N/mm over the 1 mm - 2 mm gap. Whilst this is a clear improvement, it differs significantly from the safer force responses of interest and requires the full range of current control. Design modifications are pursued in order to achieve a safer force response for zero power dissipation which allows the range of current control to be used for fine tuning of the device for variations in a particular patient's biology (e.g. thinner colon walls). In order to achieve the safer magnetic behaviour, additional magnets can be added to the electromagnet. The force contribution of these added magnets can have two forms depending on whether they are attracting or repelling the daughter magnet. If the magnets are working in conjunction with the electromagnet to attract the daughter, then the force between the added magnet and daughter magnet must be of the form shown in Figure 4.17. The added magnet and daughter magnet interact in such a way that there is a peak attractive force at a non zero separation point. For the overall device force response, this works to increase the attractive force at further separations more than the close separations thereby reducing the slope of the overall force response. If the added magnets are instead repelling the daughter magnet, then the force contribution from the added magnet must follow that shown in Figure 4.17. The main feature of this force contribution is that the gradient must be larger than that between the electromagnet and the daughter magnet. This leads to a greater reduction in electromagnet-daughter magnet force at close separations than at farther separations thereby achieving safer magnetic force responses. In reality, configurations where the added magnets suitably repel the daughter magnet are far more promising, with a wider variety of configurations demonstrating suitable behaviour as well as showing less sensitivity to component tolerances. For this reason the following body of work focuses on added magnets which repel the daughter magnet.



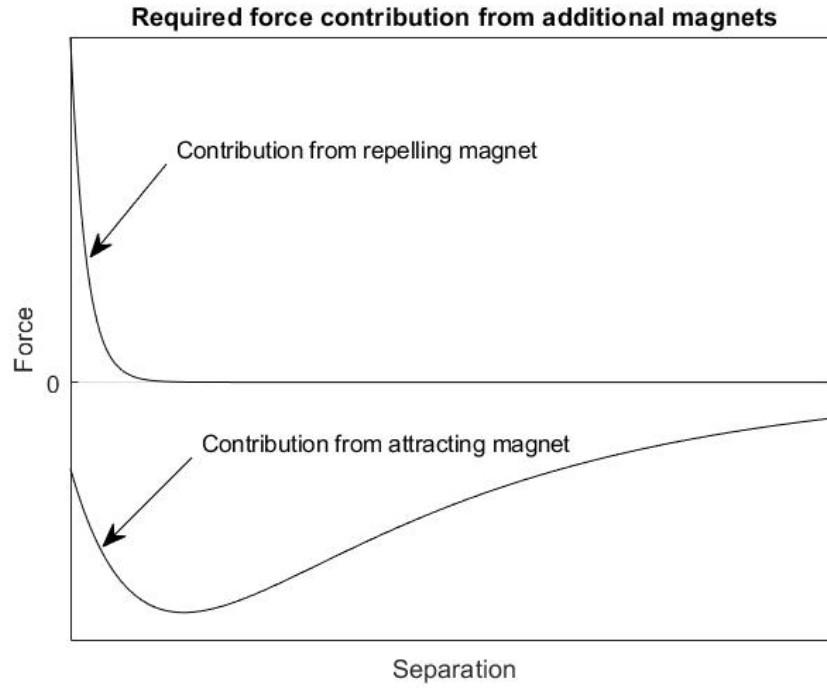


Figure 4.17: Required force contribution shape from added magnets to achieve safer magnetic force response from electromagnet design.

Possible modifications to the electromagnet design to include additional magnets are shown in Figure 4.18. Table 4.3 outlines the shape and size limits for the different types of embedded and interface magnets.

Table 4.3: Characteristics of the additional magnet types to improve device performance.

Added Magnet	Shape	Inner radius limit	Outer radius limit
Interface A	Disk or Ring	-	$< r_{dm}$
Interface B	Ring	$< r_{dm}$	$> r_{dm}$
Interface C	Ring	$> r_{dm}$	$< r_{device}$
Embedded A	Rod	-	$< r_{core}$
Embedded B	Ring	$> 0$	$< r_{core}$

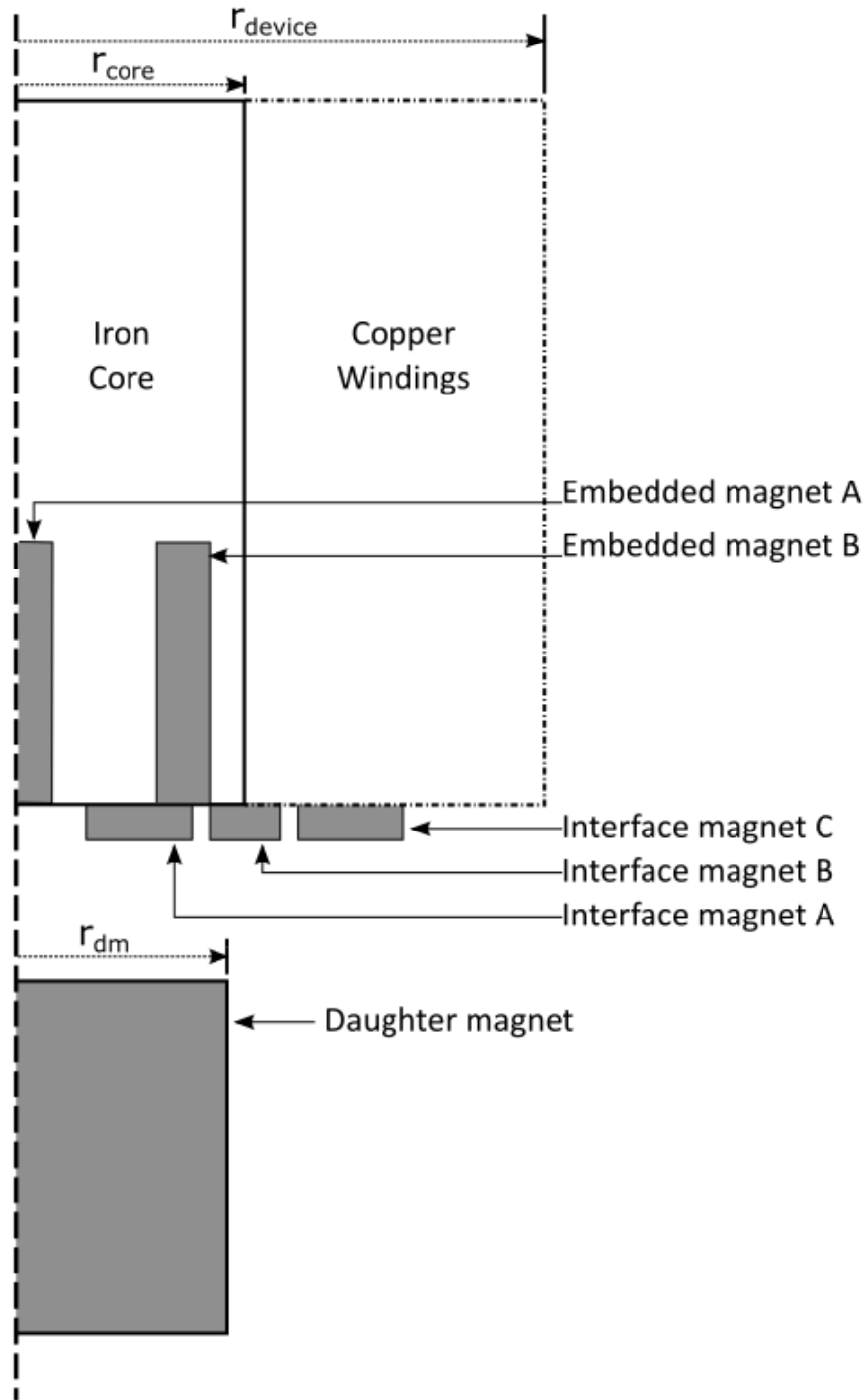


Figure 4.18: 2-D Planar cut of device design with possible additional magnets (Interface and Embedded) for tuning of force response shape. Shaded regions mark device permanent magnets.

#### 4.4.1 Interface Magnets

Magnets placed at the interface between the electromagnet and the daughter magnet were first tested for their ability to achieve safer magnetic behaviour. At first, the simulations for how interface magnets effect the device performance were run in parts. The force response between the iron cored electromagnet and daughter magnet was simulated using FEMM and the force response between the interface magnets and the daughter magnet was simulated using a custom magnetic charge-based Matlab script. It was initially assumed that the full device force behaviour would be obtained from the superposition of these results however this did not align with full FEMM based solutions. This is likely due to the self-coupling of the interface magnets through the iron core of the electromagnet that it rests against. This approach had further limitations in that the interface magnets had very poor permeance coefficients. This would lead to demagnetisation during the operation of the device and it would no longer act to provide a safer magnetic force response. Finally, in addition to the issues above, placing magnets in the compression gap between the electromagnet and daughter magnet increases the separation between the two leading to reduced overall forces and reduced force control.

#### 4.4.2 Embedded Magnets

Embedded magnets are placed within the iron core of the electromagnet. They strongly couple with themselves through the iron core, ruling out the suitability of permanent magnet based simulations. Therefore, FEMM was used for the full modelling of the device as it allows for ferromagnetic and permanent magnet materials as well as electromagnet behaviour to be simulated.

The device behaviour was investigated when embedded rod magnets, like type A per Figure 4.18, were added to the device. An assortment of rod magnets were simulated where their height and diameter parameters were varied and the resultant force-separation data recorded. Given that the embedded magnet is exposed to a repelling field in normal operation, care must be taken to design with a suitably high permeance coefficient so as to mitigate irreversible damage to the magnet. Assuming the materials of the daughter magnet and embedded magnet are both N40, a permeance coefficient greater than 6 (refer to section 1.1.1.1) is used to limit embedded magnet height for a certain diameter. The height of embedded magnets was found to have little or no effect on the shape of the force response or device controllability when sized with suitably high perme-

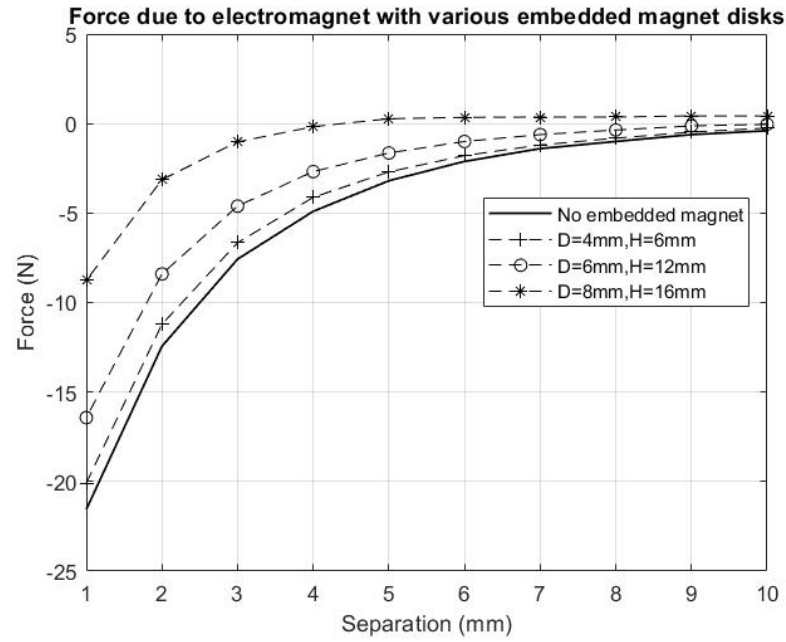


Figure 4.19: Simulated force-separation plot for device with embedded disk magnets of varied dimensions.

ance coefficients. For an embedded magnet of diameter 6 mm there was only a noticeable change in the force response when the magnet had a height of 1 mm. However, the permeance coefficient of that magnet is calculated to be less than 0.4, which is considered unsuitable for operation in repelling fields. Figure 4.19 shows the force response for a range of embedded disk magnets. In each case the slopes at close separations for the resultant force-separation plots are less than the original system. However, the relative slope is greater, meaning the shape of the normalised response is worse with the addition of disk embedded magnets. An additional concern for the design on an embedded disk magnet is the amount of iron displaced which reduces the controllability of the device. This effect is captured in Figure 4.20 whereby the magnitude of force control under steady state current limitations can be reduced from 5.5 N to less than 2 N when an embedded magnet of large diameter is used.

With reference to Figure 4.18, embedded magnets disks (type A) were found to be counter-productive for producing safer magnetic force behaviour and so ring magnets (type B) were next investigated. The lower bound for the permeance coefficient of the embedded magnets was once again set to 6. The lower bound for the inner radius was set to 1 mm and the upper bound for outer radius set to 6 mm. Within these constraints, the thickness of the ring was restricted to no less than 1 mm. From the combinations tested, a promising response was observed

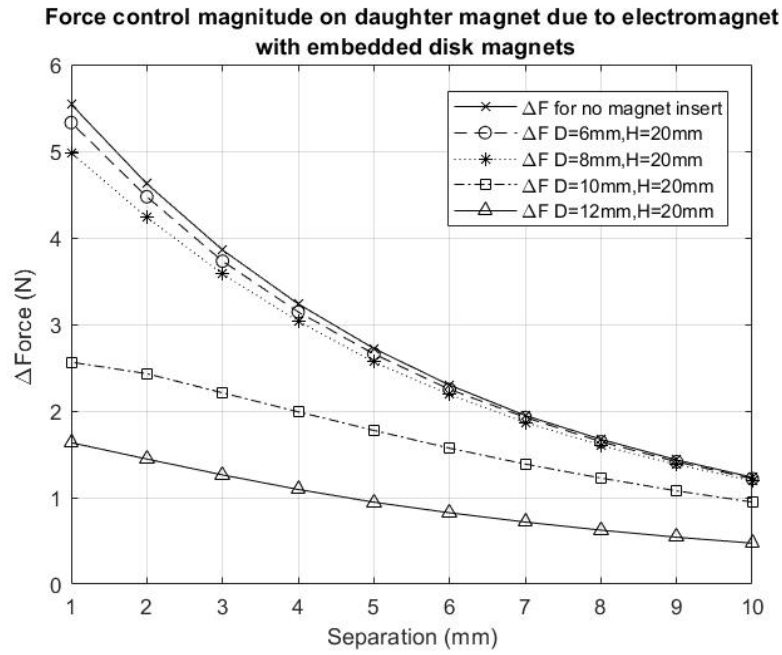


Figure 4.20: Embedded disk magnet diameter effect on the simulated force control magnitude of the device.

for an embedded magnet of inner radius 4 mm, outer radius 6 mm, as shown in Figure 4.21. The degree of control for this embedded magnet was simulated. It was previously noted in the case of embedded disk magnets, a large diameter magnet greatly hampered the magnitude of control of the device but this was found to not always be the case for embedded ring magnets. Figure 4.22 shows the magnitude of force control for this embedded ring design and how it varies with height. Despite its large outer radius, the majority of the force control range is retained. The height of the embedded magnet is observed to have some impact on the magnitude of the force-separation response of the device, where shorter heights result in a similarly shaped but slightly stronger response. When current control is considered there arises the opportunity to introduce a highly desirable force response where the force peaks at a non-zero separation distance, see Figure 4.23. Figure 4.23 also shows how the design with an embedded magnet differs to the original response between the simple electromagnet and daughter magnet.

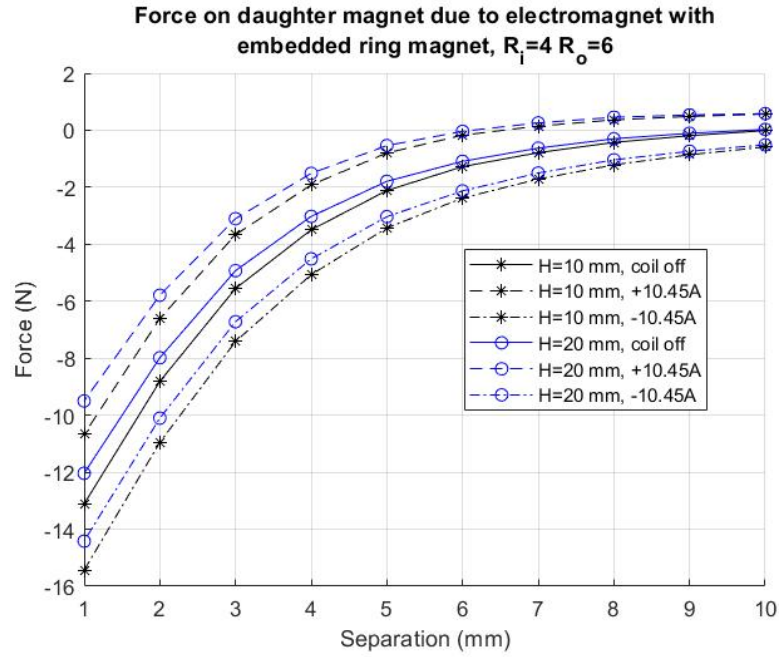


Figure 4.21: Simulated force response variations with height for the promising embedded ring magnet, inner radius 4 mm, outer radius 6 mm and force control range.

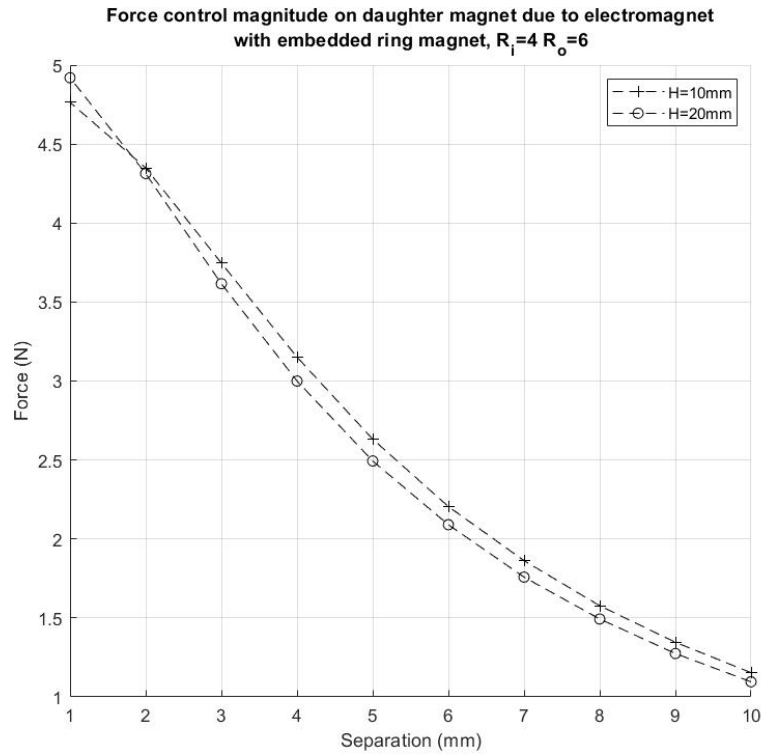


Figure 4.22: Simulated force control magnitude for embedded ring magnet, inner radius 4 mm, outer radius 6 mm for two different heights.

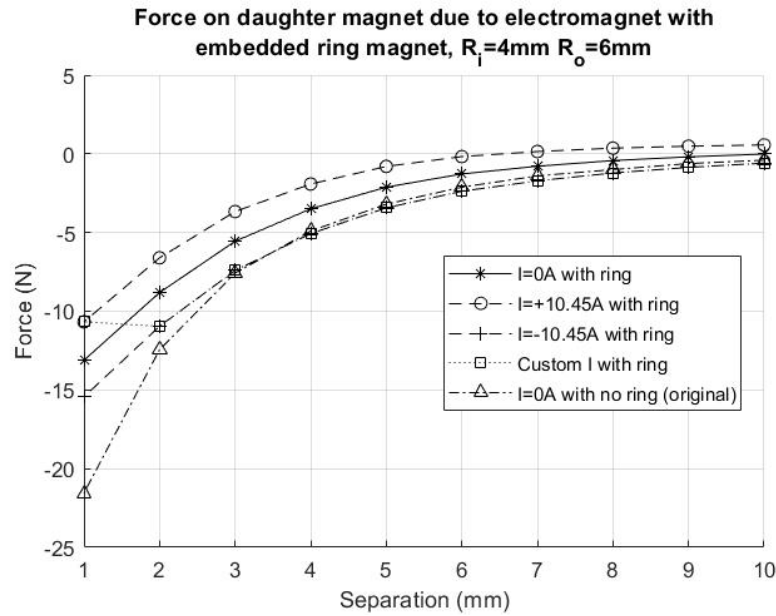


Figure 4.23: Simulated comparison of the original electromagnet device performance to an embedded magnet design with a custom current tuned force response

## 4.5 Advanced Control States

An additional benefit of an electromagnet design, beyond fine tuning of the steady state force response, is that additional states of operation can be reached temporarily using currents beyond the maximum steady state current. There are two main additional states of interest: a strong coupling state used for longer range interactions when compared to normal operation and, a weak interaction state during which there is minimal coupling.

### 4.5.1 Strong Coupling State

When installing the device, a strong coupling state can be used to assist in alignment and to ensure compression is initiated. The maximum steady state current for the device was defined by a temperature increase of  $3^\circ\text{C}$  per minute, leading to a maximum steady state power of around 1.5 watts. When operating over shorter durations, higher powers than the steady state maximum can be used to achieve much stronger coupling forces at relatively large separations. Table 4.4 summarises the powers tested for various rates of temperature increase. The device operation in a strong coupling state using these powers is shown in Figure 4.24. When the coil is off there is almost no compression force generated at 10 mm separation. However, the force at 10 mm can be increased to 1.8 N when the

Table 4.4: Device power consumption for different rates of temperature increase.

Rate of temperature increase	Power consumption (watts)
3°C / min (steady state)	1.55
5°C / 10 s	15.35
3°C / 1 s	92

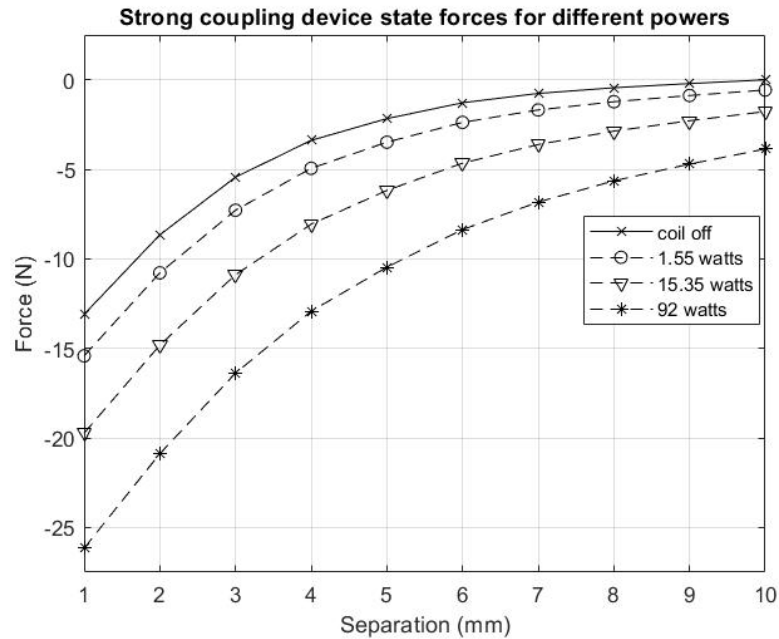


Figure 4.24: Simulated performance of device in the strong coupling state for different powers. The device is observed to exclusively undergo repulsion at higher powers.

coil is powered with 15.35 watts, or 3.9 N if the coil is powered with 92 watts. Coil operation at these high powers is not sustainable but is suitable for transient use to assist in aligning and initiating compression.

### 4.5.2 Weak Interaction State

With all of the colorectal anastomosis devices presented in section 1.4.3, once the anastomosis is initiated, there is no option to stop the device operation in a non-destructive manner. Due to the nature of magnetics, the force between magnets decays exponentially with increased separation distance. Therefore, there exists only small forces between the mother and daughter magnets when they are not aligned and placed closely together. The highly controllable nature of this device allows for the magnets to easily separate even after coupling by powering the electromagnet. Figure 4.25 demonstrates the ability of the device to decouple at all separations if a suitably high power is used.



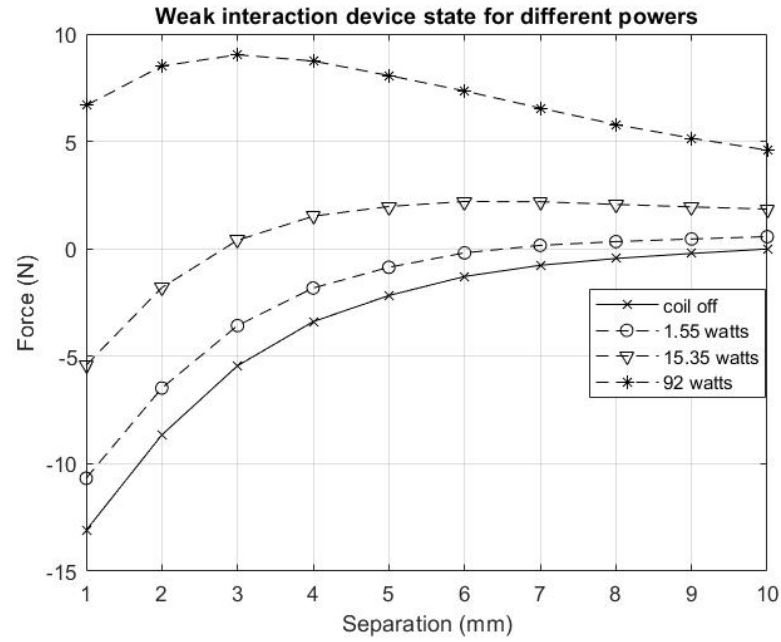


Figure 4.25: Simulated performance of device in the weak interaction state for different powers.

## 4.6 Conclusions

The methods by which an electromagnet device is designed and simulated have been outlined in this chapter. The application of the device for colorectal anastomosis constrains the physical dimensions of the device as well as the amount of heat that it may produce. Within the constraints, the electromagnet design is optimised for achieving the largest degree of pressure control whilst being able to achieve suitable anastomosis pressures. A limitation of the basic electromagnet design was its exponential force response shape. Embedding magnets within the electromagnets iron core allowed for safe magnetic force profiles to be achieved as well as advanced operation states.

# Chapter 5

## Prototype Design Specification

### 5.1 Prototype 1: Using Commercially Available Magnets

To confirm the device behaviour predicted by the embedded magnet simulations, a prototype was constructed. Commercially available components were selected where possible to expedite the prototyping process. The magnets are the key components of the design which, if custom made, can introduce large lead times. All magnets were supplied by HKCM (HKCM Engineering e.K., Eckernförde, Germany) due to their wide range of magnets in stock, short lead/delivery times, and comprehensive datasheets. The material properties of HKCM magnets were added to the simulation database. The majority of permanent magnet materials were suitable for simplified linear demagnetisation curves where the relative permeability was calculated using Equation 5.1. Note the values for  $B_r$  and  $H_{cb}$  are read from experimentally obtained hysteresis loops for a given material (refer to Figure 2.16).

$$\mu_r = \frac{B_r}{\mu_0 H_{cb}} \quad (5.1)$$

Where:

$\mu_r$	Relative permeability
$B_r$	Residual flux density
$\mu_0$	Permeability of free space
$H_{cb}$	Coercivity

Table 5.1: Prototype 1 magnet BOM

Material	Inner diameter (mm)	Outer diameter (mm)	Price (€/piece)	Quantity
N38	na	12	1.35	10
N38	8	12	1.18	10
N45	9	12	1.3	20

Following simulations of various combinations of magnets available from HKCM, the magnets in Table 5.1 were purchased as they demonstrate similar behaviour to that desired albeit at the lower end of acceptable forces. The quoted disk magnets are used for the daughter magnet. There are two options for the embedded magnet, either of which is capable of producing a base working prototype. The simulated performance of both possible designs is shown in Figure 5.1. The use of the N45 embedded magnet is expected to achieve higher overall forces, obtaining a force of 13.5 N at a separation of 1.5 mm compared to only 11 N when the N38 embedded magnet is used. The benefit of the N38 embedded magnet is that it achieves a far more linear force response from 0.5 mm to 2 mm and displays a peak in force at a greater separation.

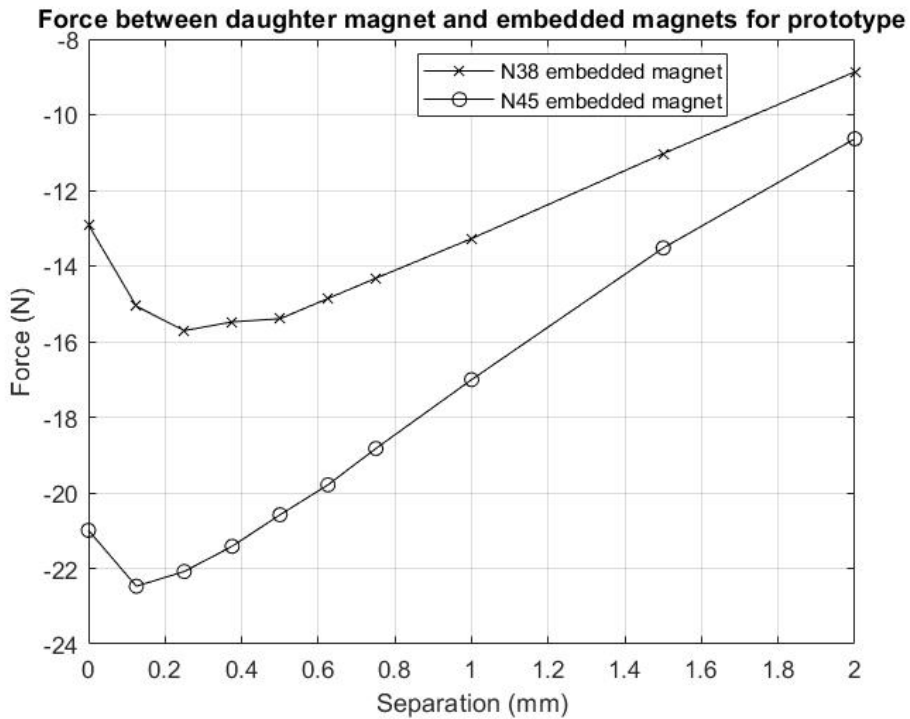


Figure 5.1: Predicted force separation plots for the two different embedded magnets used for first prototypes. N38 ring has an inner diameter of 8 mm compared to 9 mm for the N45 ring.

The first prototype was constructed using the N38 embedded magnets. Figures 5.2 and 5.3 show the tested daughter magnets and electromagnet core respectively. The force response on the device when not powered was to be measured using tensile testing equipment and custom magnet vices to minimise any disturbances from nearby ferromagnetic materials. Due to unforeseeable issues, this testing was not completed, refer to section 1.2.



Figure 5.2: Stack of N38 disk magnets to produce a daughter magnet of diameter 12 mm and height 12 mm.



Figure 5.3: Electromagnet iron core with embedded N38 ring magnet.

To achieve the desired anastomosis sizing, a casing is placed around the daughter magnet which has a thin ring of material protruding at a larger diameter (see Figure 4.7). The ring protrudes forward such that it lies in the same plane as the compression surface of the daughter magnet. The thickness of this ring,  $t$ , contributes to the total compression area of the daughter magnet,  $A_{total}$ , as per Equation 5.2. Note in this case that the outer dimension of the daughter magnet casing is assumed to have a radius of 15 mm. Table 5.2 outlines the forces necessary to achieve desired pressures for a given thickness of this outer ring of material. From the results in this table it is observed that an increase of force of 80% is required if a daughter magnet casing with an outer ring thickness of 1 mm is used. Based on the expected forces from the prototype simulations in Figure 5.1, it is desirable to keep this ring thickness to a minimum in order to achieve the pressures required for successful anastomosis.

$$\begin{aligned} A_{total} &= \pi (0.006^2) + \pi (0.015^2 - (0.015 - t)^2) \text{ m}^2 \\ A_{total} &= \pi (36 + 30t_{mm} - t_{mm}^2) * 10^{-6} \text{ m}^2 \end{aligned} \quad (5.2)$$

Table 5.2: Effect of daughter magnet casing on the forces required to produce suitable anastomosis pressures

Outer ring thickness (mm)	Compression area $A_{total} * 10^{-6} (\text{m}^2)$	Force for 80 kPa (N)	Force for 170 kPa (N)
0	$36\pi$	9.1	19
0.25	$43.5\pi$	10.9	23.2
0.5	$51\pi$	12.8	27.2
1	$65\pi$	16.3	34.7

## 5.2 Prototype 2: Optimised Device Design

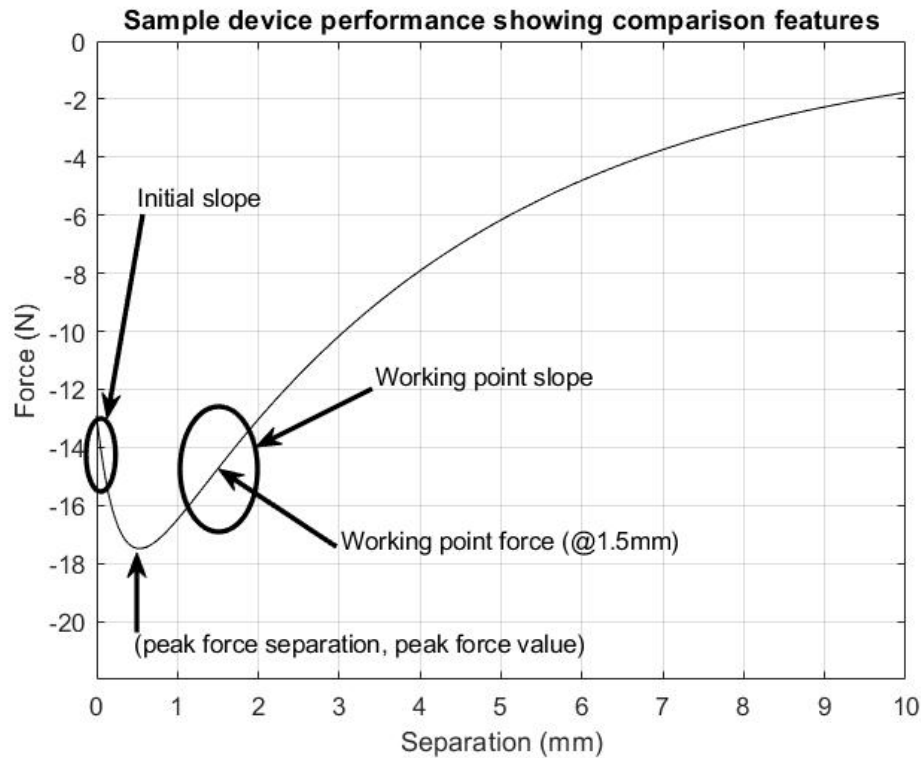


Figure 5.4: A sample force-separation plot for a safe magnetic compression device with key grading features marked.

### 5.2.1 Custom Embedded Magnet Design

The first prototype was designed with a focus on proof of concept and accelerated physical realisation. This was largely achieved by using off the shelf magnets. By specifically designing custom magnet dimensions and materials the device performance can be further improved. The design process for these magnets involved large scale simulations of the interaction between different materials for the embedded magnets and daughter magnet as well as finely tuned dimensions of the embedded magnet. Matlab was used to control the FEMM simulations and collect the resulting data.

The previously added permanent magnet grades from HKCM acted as the set of materials for the simulations. The inner and outer dimensions of the embedded magnet were also varied for each set of interacting daughter magnet and embedded magnet material. The features considered for grading and analysing the different responses are listed next and are shown on an idealised device force-separation plot in Figure 5.4.

Key grading features of device performance:

- Peak force achieved
- Separation at which peak force occurs
- Initial slope of the force response (i.e. around 0 mm)
- Force around the working point (i.e. @ 1.5 mm)
- Slope of the response around working point (i.e. between 1 mm to 2 mm)

The design sequence used for the updated colorectal anastomosis device using the aforementioned features is presented in Figure 5.5. All simulations were run assuming radial air-gaps of thickness of 0.1 mm between the iron core and the embedded magnet. A limitation of the first prototype was that the pressures it could achieve were at the lower limit of that required for successful colorectal anastomosis [54]. Arranging the simulation in order of highest working point force and filtering out cases where the initial slope is very large highlights the strongest force responses that can be expected with linear increases in force as separation reduces. Figure 5.6 is an example of such a response, achieved a working point force of over 17.5 N. There are also configurations in which the force severely drops off at close separations (see Figure 5.7) where the force near 0 mm separation is only 57% of the peak force that occurs around 0.6 mm separation.

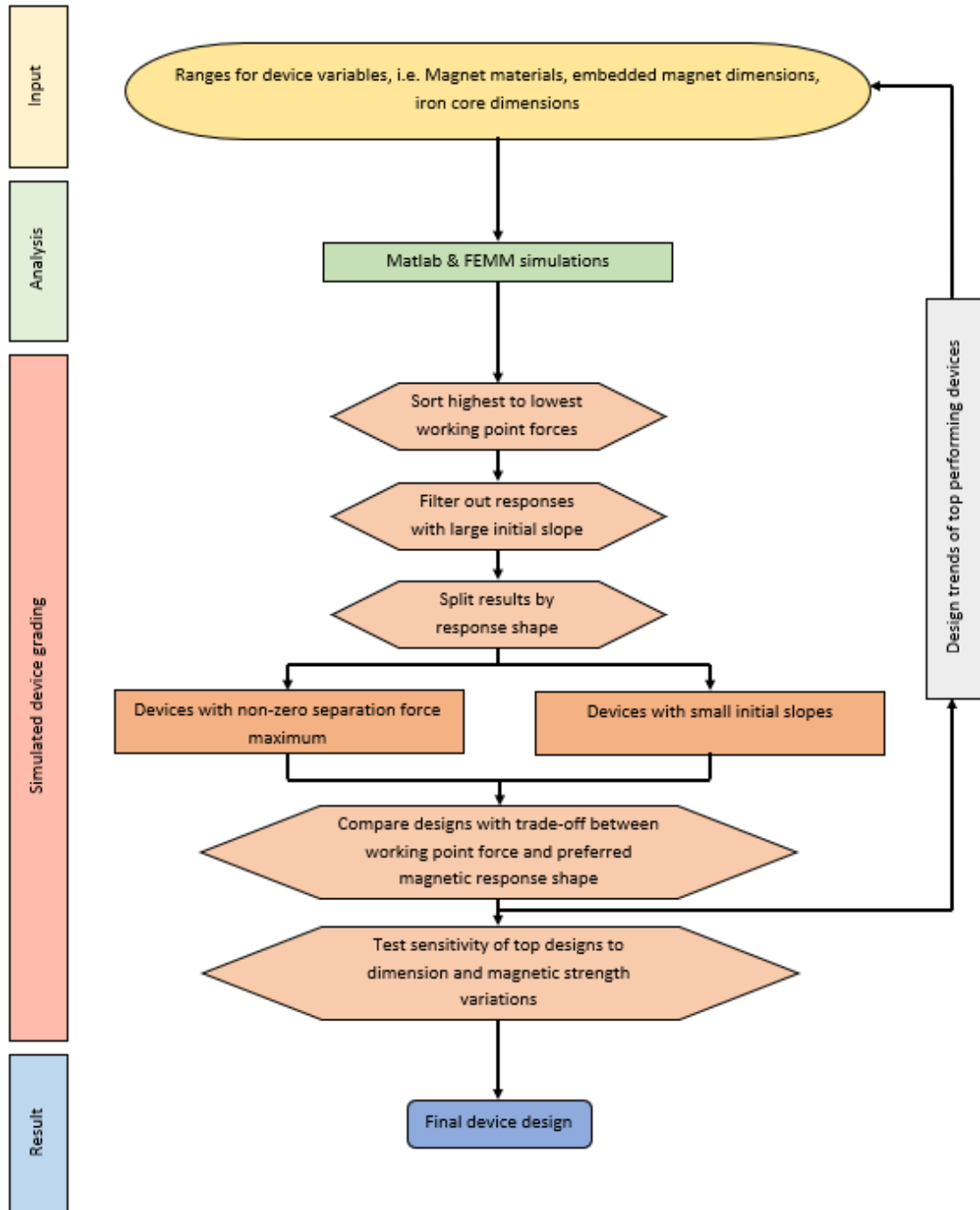


Figure 5.5: Design sequence for selecting the best colorectal anastomosis device given constraints.



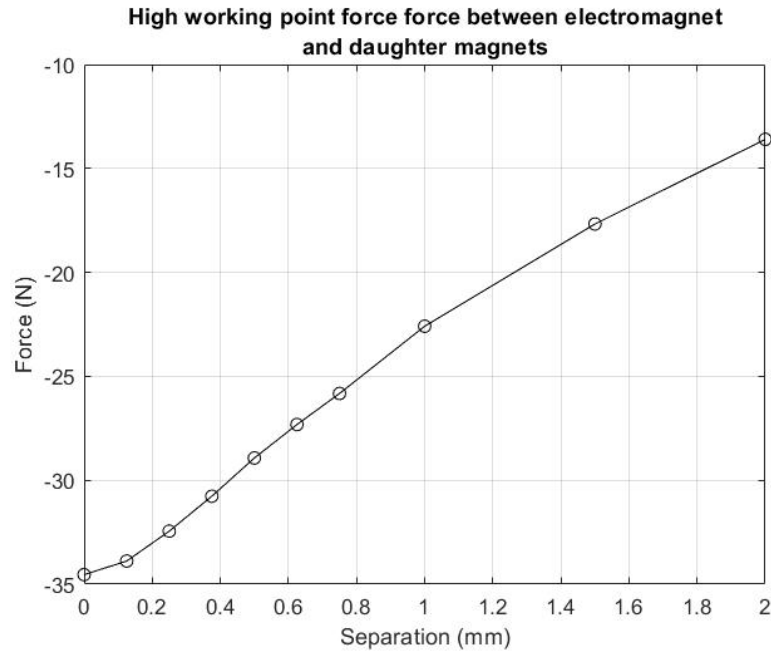


Figure 5.6: Simulated response of a device configuration that produces a strong working point force and a linear response. Daughter magnet material is N48H, Embedded magnet material is N42H with  $R_i = 4.9$  mm and  $R_o = 5.9$  mm.

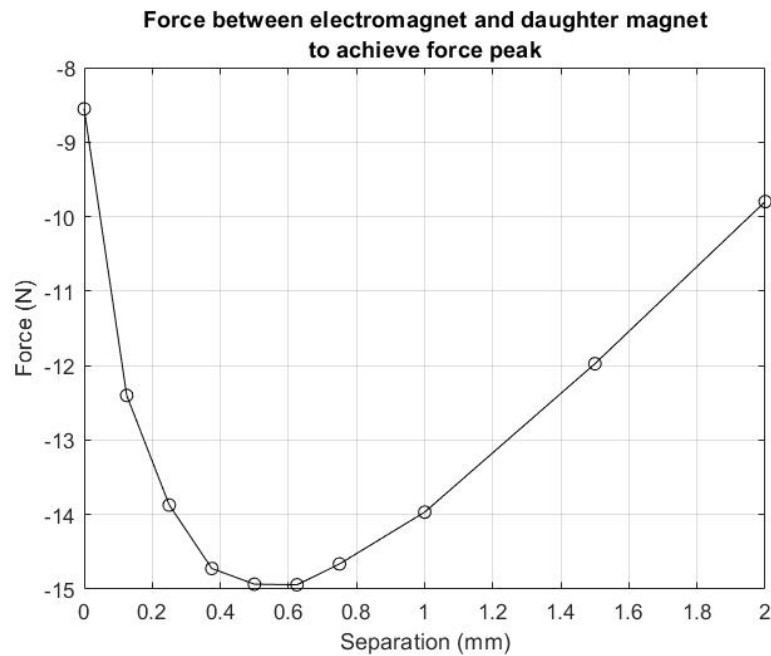


Figure 5.7: Simulated response of a device configuration that produces a strong peak force at a non-zero separation distance. Daughter magnet material is N48H, Embedded magnet material is N42H with  $R_i = 4$  mm and  $R_o = 6$  mm.

### 5.2.2 Further Design Revisions

From the analysis above, the strongest forces achievable at the working point remain near the lower half of the forces required for suitable compression pressures for a daughter magnet case of outer ring thickness 0.5 mm in Table 5.2. The original electromagnet was designed in order to maximise the amount of force control achievable within the steady state current limits. However, as per Figure 4.11, stronger forces between the electromagnet and daughter magnet can be achieved by increasing the diameter of the iron core at the cost of reducing the range of control. The effect of increasing the outer diameter of the iron core is captured in Figure 5.8 for the first prototype. The device retains the shape of the force response and the force at the working point increases by 12% when the core diameter is increased from 13.2 mm to 17.2 mm. The increased core size leads to a reduction in the number of turns on the device, reducing the range of force control. The sharp decrease in this range of control is shown in Figure 5.9 where the degree of force control reduces from 4.3 N to 2.4 N as the core is increased from 13.2 mm diameter to 17.2 mm.

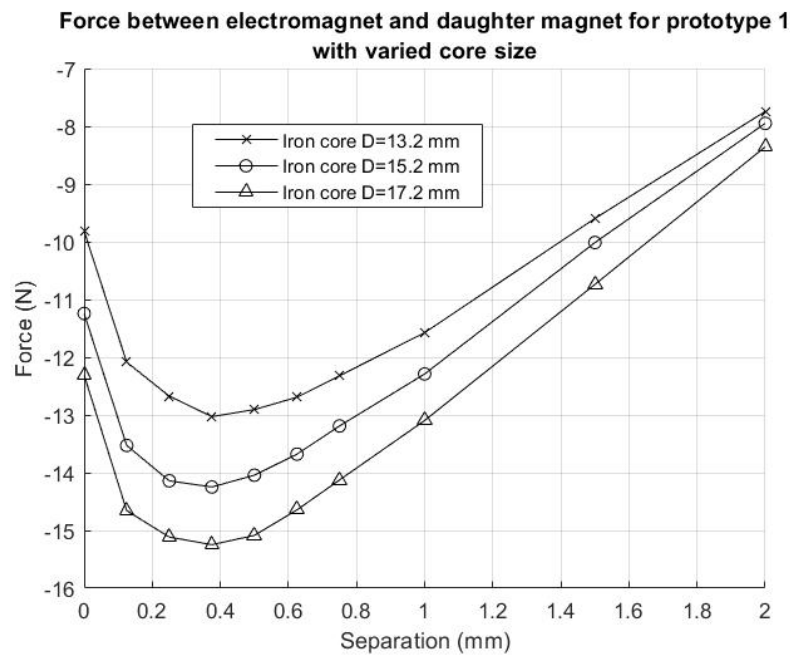


Figure 5.8: Demonstration of how the zero-power force response of the first prototype can be increased by increasing the diameter of the iron core.

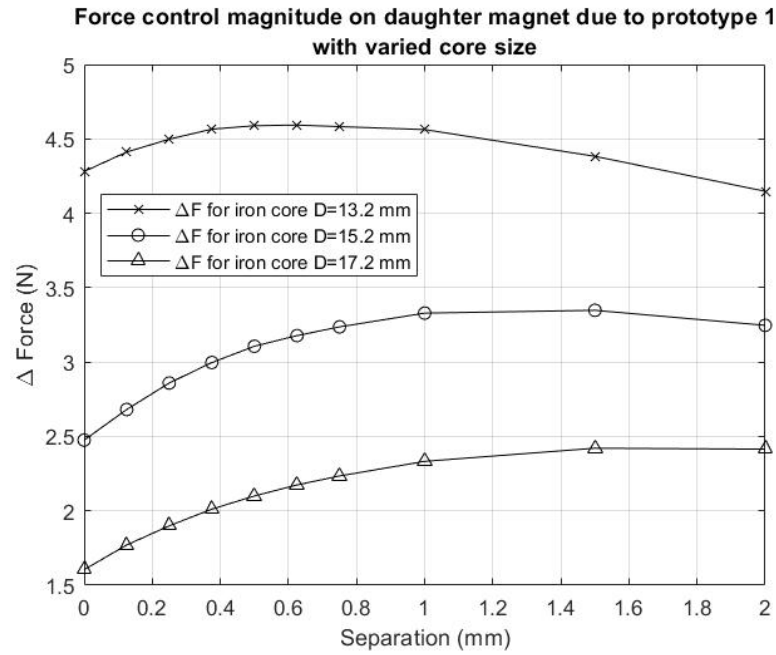


Figure 5.9: Range of force control reducing as the size of the iron core in the first prototype is increased (i.e. reduction in number of turns).

## 5.3 Conclusions

The design methods outlined in the simulations chapter were applied to prototype designs. The first prototype was designed with commercially available magnets, allowing for the device to be constructed and tested quicker than if magnets had to be built to purpose. This prototype focused on acting as a proof of concept for the ability of the device to show safer magnetic behaviour and demonstrate the ability to more finely tune the force response by powering the device. A design process was outlined for how device performance could be improved when the magnets are not limited to those readily available off-the-shelf. This process involved comparing and grading different devices on key force profile features, such as the force around the working point. Modifying the materials and dimensions of the magnets used in the device allowed for prototypes to be specified which achieved stronger initial coupling forces and safer magnetic behaviour.

# Chapter 6

## Clinical Context

### 6.1 Regulatory Overview

The need for regulation of medical devices has been well understood for many years. Earliest implementations of medical device regulation in the United States started in the 1938 when the Federal Food, Drug, and Cosmetic Act was passed. In the 1970s, following large innovations in the medical device industry, the Cooper committee studied the need for more dedicated medical device legislation [56]. They suggested that, due to the different issues posed by medical devices and drugs, there should be more directly targeted legislation for medical devices. This report eventually led to the formation of the Medical Device Regulation Act which was passed in 1976. The concept of ‘substantial equivalence’ was introduced whereby new devices, which are not necessarily truly novel, could progress to market by showing their similarity to existing products. Devices would also now be placed within one of three classes based on their associated risk. Different controls apply to each of the classes, with the strictest controls applying to Class III devices which are subject to pre-market approval. This class based system for control measures is not unique to the US system, but is now a part of major medical device regulation standards world-wide.

During the 1990s in Europe, the Medical Device Directive (MDD) was introduced following a push to harmonise the regulation of medical devices across European countries. Devices adhering to the standards would receive the CE certification marking, allowing the device to be sold across Europe. However, a number of scandals related to devices which made it through MDD regulations, such as the PIP scandal [57], called for a revision of the certification process. In 2017, these

revisions came in the form of Medical Device Regulation (MDR) and in-vitro Diagnostics Regulation (IVDR). The EU regulations came into force in May of that year but a transitional period of three years was given for MDR and five years for IVDR. Whilst MDR should have been in full effect as of May 2020, due to Covid-19, the transitional period has been extended by a year. At nearly three times the total document length, MDR is considered to be more rigorous and robust than its predecessor MDD. MDR is also considered to place more of an emphasis on patient safety, with the word ‘safety’ appearing over seven times more than it did in MDD.

Whilst the implemented regulations are common across many countries, each country has a dedicated body which oversees the implementation of the regulations in their country. The MDR regulations apply directly only to the EU member states however, it was further accepted and incorporated into the European Economic Area (EEA) by the vote of the European Free Trade Association (EFTA) members (i.e. Iceland, Liechtenstein, Norway and Switzerland). Examples of regulatory bodies for a selection of countries are given below.

- Health Products Regulatory Authority (HPRA) - Ireland
- Medicines and Healthcare products Regulatory Agency (MHRA) - United Kingdom
- Food and Drug Administration (FDA) - United States
- Pharmaceuticals and Medical Devices Agency (PMDA) - Japan

## 6.2 Medical Device Classification

Both the United States and European medical device regulation standards organise devices into classes for which there are different control measures. In both cases, it is largely the perceived risk of the device which dictates its classification. In the United States there are three classification groups:

- Class I - devices falling under this class are considered to pose the least risk. As a result, they have the fewest regulatory controls, needing only to complete the General controls. The General controls address things such as misbranding or banned devices. Mechanical wheelchairs and electric toothbrushes are examples of such devices.

- Class II - these devices are considered to pose more possible risk than class I. They are subject to Special controls, which vary depending on the device, in addition to the General controls in order to brought to market. Daily contact lenses and an MRI machines are Class II devices.
- Class III - the most strict control measures are applied to devices of this class. Devices in this classification include life sustaining devices, long term implants, or devices with the potential to cause unreasonable harm. They require Premarket Approval (PMA) in addition to General controls. Pace-makers, prosthetics attached to bone, and cochlear implants are all examples of class III devices.

For Europe, there are four total classification groups for medical devices under MDR. Like with the FDA system, it is not the particular technical characteristics of the device which determines the class but rather, they are organised roughly on their potential risk. More stringent control measures apply to higher class devices. The classifications for medical devices in Europe are listed below with their perceived risk levels.

- Class I - low risk
- Class IIa - low/medium risk
- Class IIb - medium/high risk
- Class III - high risk

Key factors for the classification of devices include:

- whether the device is invasive or non-invasive
- the length of time for which the device will be in use
- whether the device is passive or active

Under the older MDD system, the MEDICAL DEVICES: Guidance document for the Classification of medical device (MEDDEV 2.4/q Rev. 9), as published in June 2010, was a useful resource for determine the class of a medical device. The classification rules for the MDR standard differ slightly to that of MDD but many devices achieve the same classification across both standards. Annex VIII chapter 3 of the European Medical Device Regulation (2017/745) contains the rules for device classification. The following listed considerations are used to determine the class of the proposed controllable magnetic anastomosis device in this thesis.

- the device has short-term use (>60 minutes & <30 days)
- the device is either invasive via body orifices or surgically invasive
- it is an active device (note, device still operates when not powered but sub-optimally)

It is important to consider all MDR classification rules before classifying the device. Depending of the operation of the device, rules 5 ("invasive devices with respect to body orifices"), 7 ("surgically invasive devices intended for short-term"), and 9 ("Active therapeutic devices intended to administer or exchange energy") may all apply. In each case the proposed device obtains the same classification, Class IIa.

### 6.3 Device to Market - United States

In order to determine the regulatory pathway which should be taken for the device being brought to market in the US, it is important to know the class of the device. For nearly all class III devices Pre-market approval (PMA) is required. PMA is the most intensive of all the application processes with the longest expected processing times before a submission will be approved. PMA requires valid scientific evidence that the device is safe and effective, this will normally involve clinical studies for which the device must first obtain an investigational device exemption. In addition to being a lengthy process, PMA submissions have a significantly higher cost associated with them than most other regulatory pathways.

A 510k application is the most common pathway for lower class devices (and a very small number of exempt class III devices) to make it to market. A key component of a 510k submission involves demonstrating that the proposed device is substantially equivalent to an existing device on the market. Substantially equivalent devices will have the same intended use and similar technological characteristics. The goal of this submission type is to demonstrate that the proposed device is just as safe and effective as devices already available. Whilst special controls are required, they are not nearly as involved and costly as a PMA submission. Table 6.1 contains examples of devices approved by the FDA for use in colorectal anastomosis. These devices have the same intended use as the controllable magnetic anastomosis devices presented in this thesis however, there exists too great a difference in the technology characteristics for the approval via a 510(k).

Table 6.1: Devices used for colorectal anastomosis approved for market by FDA.

Device Name	Submission no.	Class
Endopath ILS Endoscopic Circular Stapler	K920752	II
Compression Anastomosis Ring (CAR)	K050356	II

To bring the controllable anastomosis device proposed in this thesis to market the expected regulatory pathway is through that of a De Novo application. Novel devices are classified as Class III when there are exists no currently marketed devices that are substantially equivalent. However, De Novo applications allow for novel devices to be reclassified depending on their risk. This process is both lengthier and more costly than a 510(k) application, but less than that of PMA. The proposed device is likely Class II and therefore, a De Novo application is the preferred route to approval.

De Novo applications must be identified as a "Request for Evaluation of Automatic Class III Designation". A description of the device and its intended use must also be included in the submission. A particularly important component of the De Novo application is that which relates to the classification of the device. This will outline the proposed classification and supporting reasons. A list of possible supporting information is given below.

- Evidence of device performance testing, be it clinical or non-clinical, showing effectiveness.
- Providing relative assurance of safety through testing and control measures.
- Additional information on the safety of the device in relation to the materials used, possible interference with other devices, and electrical components.
- A risk/benefit analysis of device

A full checklist for the acceptance of a De Novo submission is provided in guidance document "Acceptance Review for De Novo Classification Requests" (docket number: FDA-2017-D-6069).

For the proposed device, information supporting its classification as a Class II device could include: bench testing of the device, animal testing results, biocompatibility of materials used, safety measures built into driving electronics, possible benefits of safer force responses compared to existing compression devices.



The final step to legally marketing the medical device in the US involves registering the establishment of the device and listing it with the FDA. Before fully committing to a regulatory pathway, it is recommended to submit a pre-submission to the FDA in order to obtain feedback on how a particular device should navigate regulations.

## 6.4 Device to Market - Ireland

To be sold in Ireland and the rest of the European market, medical devices must first obtain CE certification. MDR is the regulatory pathway through which a device can obtain CE certification. The classification of the medical device dictates the particular regulatory requirements. For the Class IIa device proposed in this thesis, a Quality Management System (QMS) is required. Typically, a QMS in accordance with ISO 13485 is used to achieve compliance. A device of this class will also require a Technical File. This should consist of the required content outlined in Annex's II and III of MDR. A sample of the required content is listed below.

- A description of the device
- Information about previous device versions/ similar devices
- Show the device meets the general safety and performance requirements in Annex I (e.g. choice of materials, packaging, labelling)
- Risk-benefit analysis
- Device testing (pre-clinical/clinical)
- A plan for post-market surveillance

Once completed, for a Class IIa device, the QMS and Technical Files are subject to an audit by a notified body. Finally, a declaration of conformity should be prepared such that the device can be CE certified. It is important to note that post-market surveillance is required in Europe.

## 6.5 Bio-compatibility of Device Materials

To achieve conformity to US and EU standards, the bio-compatibility of the materials used in the device must be tested. ISO 10993 outlines in depth the testing requirements and provides guidelines for achieving bio-compatibility. This process is expected to take number of weeks and should be factored into the plan for any medical device. A brief analysis on the materials selected for the proposed colorectal anastomosis follows.

- Enamelled copper wire for electromagnet coil:
  - Concerns: Copper ions pose a risk of irritation as well as possible organ damage if at a high level. The enamel on the prototype wire was not designed for medical applications.
  - Solutions: Medical grade wire is widely available and could be easily substituted for the device. The coil should also be enclosed and sealed.
- Pure iron electromagnet core:
  - Concerns: Possible bio-degrading
  - Solutions: Investigate the rate of possible bio-degrading. If necessary, apply bio-compatible coatings.
- NdFeB used for the embedded and daughter magnets:
  - Concerns: NdFeB oxidises simply due to the moisture in the air therefore, coatings are applied to the magnets. The coating material may be of concern.
  - Solutions: A Parylene coating applied to a NdFeB magnet protects from oxidation and is FDA approved. The coating has the added benefit of being very thin.
- Daughter Magnet casing:
  - Concerns: The 3D printed daughter magnet casing is made of PLA, a biodegradable polymer. The rate of bio-degradation may affect device performance.
  - Solutions: Bio-compatible PLA is widely available. Test the significance of bio-degradation over the use time of the device. If necessary, other bio-compatible plastics are widely available.

## 6.6 Risk Analysis and Electrical Safety

As an electrical medical device, the device proposed in this thesis should conform with IEC 60601/EN 60601 (Note both IEC and EN standards are identical but refer to the US and EU versions respectively). IEC 60601 is composed of a large number of technical standards aimed at ensuring basic safety and essential performance of medical electrical equipment. Evidence of conformity to these standards form an important section of the accompanying documentation for both EU and US applications for medical device approval. A risk management process (conforming with ISO 149710) should be implemented to assist in identifying the tests and acceptable limits. IEC 60601 consists of a general standard, IEC 60601-1, collateral standards, IEC 60601-1-X, and particular standards, IEC 60601-2-X. For a particular device, parts of the the general standard can be overridden by the collateral or particular standards.

IEC 60601 is generally accepted as being a complex standard and it is recommended that one should work with an experienced body when seeking conformity. Some of the electrical considerations made when seeking conformity with IEC 60601 for the device proposed in this thesis are as follows:

- Many concerns relating to the driving voltage/current of the device can be addressed by using a power supply which is already IEC 60601 compliant.
- The handheld controller for the device does not have any high power requirements and can make use of acceptably low voltages.
- There may be concerns about the electromagnetic compatibility (EMC) due to the non-contained magnetic fields produced by the electromagnet and permanent magnets. EMC testing should be done to confirm that the fields produced will not negatively interact with any other medical equipment that may be in proximity to the device.

## 6.7 Patent Protection

When commercialising a product, where possible, measures should be take to protect any related intellectual property (IP). Patents can allow the holder to legally exclude others from producing and selling a certain invention. Many countries have there own patent offices but there also exists larger IP offices such as the European Patent Office. Patent protection in the US is organised through the United States Patent and Trademark Office (USPTO). The USPTO offers

three different types of patents: Design, Utility, and Plant. A Utility patent is best suited to protecting the IP of a novel medical device like that presented in this thesis. Elements typically in a Utility patent application include:

- Background information relating to the device being patented.
- Device specification with at least one claim. For the proposed device, a suitable claim may be "A controllable magnetic compression anastomosis device where the compression pressures are produced between: (a) an iron core electromagnet with an embedded permanent magnet, (b) a permanent magnet with a cylindrical outer casing of which the outer diameter dictates the anastomosis size."
- Drawings of the device with descriptions. This might include figures showing the operation of the device in different operating states.
- Related patents.

When preparing the application for submission, it is worth consulting with legal experts to give the highest chance of a successful application. The patent application is not guaranteed to be granted but rather, if the examiner determines it unsatisfactory, feedback will be given as why the application was unsuccessful and an opportunity will be provided to amend the application. Once a patent is granted, maintenance fees at scheduled intervals are required.

## 6.8 Summary

Device classification for the US and EU markets was examined and suggests that the proposed device is of class II/IIa. A De Novo application and Technical files should be prepared in order to legally market the device. As part of these submissions, the device must be tested for safety (e.g. electrical, bio-compatibility, bench testing) and effectiveness (e.g. bench testing, animal trials). To protect the IP relating to the device, patents should be filed outlining the claims of the device and its design. It is generally recommended that much of this work should be carried out whilst communicating with companies specialising in the regulatory testing and laws.

## Chapter 7

# Future Work and Closing Comments

The work covered in this thesis highlighted the different types of safer magnetic coupling and how these safer responses can be obtained by combining magnets. The design considerations for magnets working in different operating conditions are presented, with particular attention paid to magnets operating in demagnetising fields. The simulation and development stages are given for designing a controllable device capable of achieving safer force responses. A controllable magnetic colorectal anastomosis compression device was designed using off-the-shelf magnets. A prototype was built using these off-the-shelf magnets which, according to simulations, can produce forces adequate for successful anastomosis, albeit at the lower end of the acceptable range. The device was optimised through larger scale incremental simulations making use of specifically designed magnets. Finally, the steps to bring a medical device to market were investigated, with a focus on the particular regulatory processes to bring the proposed device into key markets.

With the aim of bringing the proposed safer magnetic medical device to market, there remains quite a body of work to be done. Of key importance is the experimental work on the first prototype, confirming that the device behaves as expected during pull tests, and taking note of any differences between the expected and observed results. This will lead to the production of a second prototype using the custom designed magnets. Regulatory guidelines, outlined in chapter 5, should be applied to this prototype where possible. Once the second prototype has been produced and bench tested, the device can be put through

animal testing to gain evidence of the effectiveness of the device.

There remains modifications that could be made to the device to improve its functionality. Real-time measuring of the forces between the magnets and the compressed tissue thickness would not only allow for the device to perform better, but would also contribute to a better understanding of the compression anastomosis process. Better performance could be expected in this case by adjusting the force contribution from the electromagnet on the fly, allowing the device to react to biological variations between patients. As the force-separation profile of the device will be known, knowing the either value will allow for both to be interpreted. Compression sensors and hall effect sensors should be investigated for achieving the desired measurements. The force may be directly interpreted from the compression sensor however the effect of the sensor on device performance may be of concern. Alternatively, the Hall effect sensor could be attached to the electromagnet away from direct contact with the anastomosis site, where the measured field variation due to the mother and daughter magnets coupling could be related to their separation distance.

There is still room for the improvement for medical devices purposed for colorectal anastomosis. The body of work presented in this thesis looked to highlight some of the limitations of current devices and proposed a new medical device design to achieve magnetic compression in a safer and more versatile manner. Whilst the proposed device has been specifically designed to address colorectal anastomosis, the design principles of producing a controllable safer magnetic device can be carried across to many other applications both in and out of the medical field.

## 7.1 Lessons Learned

Various difficulties and road bumps encountered over the course of this project meant far more than just the related technical knowledge was acquired. A great number of lessons have been learned, from the simple best practices of recording and reporting information, to how to learn from and deal with a failed design concept, and even how to adapt a projects development to a global pandemic. I have also picked up innumerable skills since the outset of the project, 3D design, electromagnetic simulation, and 3D printing are to name but a few. Overall, the project has led to immense academic and personal growth for which I could not have asked for better peers and supervision along the way.

# References

- [1] M. S. Thomas and D. A. Margolin, “Management of Colorectal Anastomotic Leak,” *Clinics in Colon and Rectal Surgery*, vol. 29, pp. 138–144, jun 2016.
- [2] G. Branagan and D. Finnis, “Prognosis after anastomotic leakage in colorectal surgery,” *Diseases of the Colon and Rectum*, vol. 48, pp. 1021–1026, may 2005.
- [3] M. E. Pezim, “Gastrointestinal tract: anatomy.”
- [4] NCRI, “National Cancer Registry Ireland.”
- [5] Blausen.com Staff, “Medical gallery of Blausen Medical 2014,” *WikiJournal of Medicine*, vol. 1, no. 2, 2014.
- [6] S. R. Hunt and M. L. Silveira, “Anastomotic Construction,” in *The ASCRS Textbook of Colon and Rectal Surgery*, pp. 141–160, Cham: Springer International Publishing, 2016.
- [7] J. W. Bosmans, A. C. Jongen, N. D. Bouvy, and J. P. Derikx, “Colorectal anastomotic healing: Why the biological processes that lead to anastomotic leakage should be revealed prior to conducting intervention studies,” *BMC Gastroenterology*, vol. 15, p. 180, dec 2015.
- [8] W. G. Everett, “A comparison of one layer and two layer techniques for colorectal anastomosis,” *British Journal of Surgery*, vol. 62, no. 2, pp. 135–140, 1975.
- [9] G. Pye and R. Steele, “Anastomoses Involving the Colon and Rectum: An 8-year Experience,” *Journal of the Royal College of Surgeons of Edinburgh*, vol. 41, no. 2, pp. 95–96, 1996.
- [10] G. Luglio and F. Corcione, “Stapled versus handsewn methods for ileocolic anastomoses,” *Techniques in Coloproctology*, vol. 23, pp. 1093–1095, nov 2019.

- [11] A. Nordholm-Carstensen, M. S. Rasmussen, and P. M. Krarup, “Increased leak rates following stapled versus handsewn ileocolic anastomosis in patients with right-sided colon cancer: A nationwide cohort study,” *Diseases of the Colon and Rectum*, vol. 62, pp. 542–548, may 2019.
- [12] C. B. Neutzling, S. A. Lustosa, I. M. Proenca, E. M. da Silva, and D. Matos, “Stapled versus handsewn methods for colorectal anastomosis surgery,” *Cochrane Database of Systematic Reviews*, feb 2012.
- [13] J. Murphy, “Cholecysto-intestinal, gastro-intestinal, entero-intestinal anastomosis, and approximation without sutures,” *Medical Record*, vol. 42, pp. 665–676, 1892.
- [14] K. A. Forde, K. H. Goodell, and M. DellaBadia, “A 10-year single-institutional study of the biofragmentable anastomosis ring,” *American Journal of Surgery*, vol. 191, pp. 483–487, apr 2006.
- [15] Y. Khromov, I. Pliakos, M. Ibrahim, A. P. Zbar, J. Sayfan, and T. S. Papavramidis, “A prospective multi-institutional study assessing clinical outcome with the NiTi compression anastomosis ring (biodynamix colon-ring™) in elective colorectal anastomoses,” *Hepato-Gastroenterology*, vol. 60, pp. 522–527, may 2013.
- [16] C. E. Graves, C. Co, R. S. Hsi, D. Kwiat, J. Imamura-Ching, M. R. Harrison, and M. L. Stoller, “Magnetic Compression Anastomosis (Magnamosis): First-In-Human Trial,” *Journal of the American College of Surgeons*, vol. 225, pp. 676–681.e1, nov 2017.
- [17] R. Jamshidi, J. T. Stephenson, J. G. Clay, K. O. Pichakron, and M. R. Harrison, “Magnamosis: magnetic compression anastomosis with comparison to suture and staple techniques,” *Journal of Pediatric Surgery*, vol. 44, pp. 222–228, jan 2009.
- [18] D. J. Coleman, B. C. Lucas, M. J. Rondeau, and S. Chang, “Management of Intraocular Foreign Bodies,” *Ophthalmology*, vol. 94, pp. 1647–1653, dec 1987.
- [19] M. Sendoh, K. Ishiyama, and K. I. Arai, “Fabrication of Magnetic Actuator for Use in a Capsule Endoscope,” in *IEEE Transactions on Magnetics*, vol. 39, pp. 3232–3234, sep 2003.



- [20] I. S. Zeltser and J. A. Cadeddu, “A novel magnetic anchoring and guidance system to facilitate single trocar laparoscopic nephrectomy,” *Current Urology Reports*, vol. 9, pp. 62–64, jan 2008.
- [21] M. R. Mourino, “From thales to lauterbur, or from the lodestone to MR imaging: Magnetism and medicine,” *Radiology*, vol. 180, pp. 593–612, sep 1991.
- [22] G. L. Verschuur, *Hidden attraction: the history and mystery of magnetism*. Oxford University Press on Demand, 1996.
- [23] S. Chikazumi, S. Chikazumi, and S. H. Charap, *Physics of Magnetism*. Wiley Series on the Science and Technology of Materials, Wiley, 1964.
- [24] E. P. Furlani, *Permanent Magnet and Electromechanical Devices*. Academic Press, 2001.
- [25] J. M. Coey, “Rare-earth magnets,” *Endeavour*, vol. 19, pp. 146–151, jan 1995.
- [26] G. N. Levesque, “Releasable permanent magnet holding device,” US2280437A, 1939.
- [27] K. Yanagisawa, M. Uchikune, M. Tagami, T. Shimizu, K. Horiuchi, and H. Sakaguchi, “Magnetic base,” US4251791A, aug 1979.
- [28] M. Baermann, “Switchable permanent magnetic holding devices,” US4055824A, apr 1976.
- [29] P. J. Underwood and F. Kocijan, “Switchable permanent magnetic device,” US6707360B2, 2004.
- [30] A. Israelson, “Turn-off permanent magnet,” US3452310A, nov 1969.
- [31] A. K. Bey, “Magnetic holding device,” US3184654A, jun 1962.
- [32] J. M. Coey, “Permanent magnet applications,” *Journal of Magnetism and Magnetic Materials*, vol. 248, pp. 441–456, aug 2002.
- [33] M. Tavakoli, C. Viegas, J. C. Romao, P. Neto, and A. T. De Almeida, “Switchable magnets for robotics applications,” in *IEEE International Conference on Intelligent Robots and Systems*, vol. 2015-Decem, (Hamburg), pp. 4325–4330, IEEE, sep 2015.
- [34] T. Ito, T. Okura, and T. Takami, “Device for electromagnetically controlling the position off an armature,” US3514674A, may 1967.

- [35] H. J. Shin, J. Y. Choi, K. H. Jung, J. M. Lee, and C. H. Kim, “Influence of Lateral-Impact Force on Electropermanent Magnet Suspension Conveyor with Inherent Guidance Force,” *IEEE Transactions on Magnetics*, vol. 52, pp. 1–4, jul 2016.
- [36] N. A. Shirazee and A. Basak, “Electropermanent Suspension System for Acquiring Large Air-gaps to Suspend Loads,” *IEEE Transactions on Magnetics*, vol. 31, no. 6, pp. 4193–4195, 1995.
- [37] I. El-Amri, A. S. Iquebal, A. Srinivasa, and S. Bukkapatnam, “Localized magnetic fluid finishing of freeform surfaces using electropermanent magnets and magnetic concentration,” *Journal of Manufacturing Processes*, vol. 34, pp. 802–808, aug 2018.
- [38] A. Knaian, *Electropermanent magnetic connectors and actuators : devices and their application in programmable matter*. PhD thesis, Massachusetts Institute of Technology, 2010.
- [39] J. I. Padovani, S. S. Jeffrey, and R. T. Howe, “Electropermanent magnet actuation for droplet ferromicrofluidics,” *Technology*, vol. 04, pp. 110–119, jun 2016.
- [40] P. Ward and D. Liu, “Design of a high capacity Electro Permanent Magnetic adhesion for climbing robots,” in *2012 IEEE International Conference on Robotics and Biomimetics, ROBIO 2012 - Conference Digest*, (Guangzhou), pp. 217–222, IEEE, dec 2012.
- [41] P. Kriengkamol, K. Kamiyama, M. Kojima, M. Horade, Y. Mae, and T. Arai, “A New Close-Loop Control Method for an Inspection Robot Equipped with Electropermanent-Magnets,” *Journal of Robotics and Mechatronics*, vol. 28, pp. 185–193, apr 2016.
- [42] F. Ochoa-Cardenas and T. J. Dodd, “Design of a Continuously Varying Electro-Permanent Magnet Adhesion Mechanism for Climbing Robots,” in *Lecture Notes in Computer Science (including subseries Lecture Notes in Artificial Intelligence and Lecture Notes in Bioinformatics)*, vol. 9287, pp. 192–197, 2015.
- [43] W. Cassing, T. Pohl, and F. Steger, “Using electro-permanent magnets to lift loads in modern logistics networks,” Tech. Rep. 1, 2008.

- [44] J. Bydžovský, M. Kollár, K. Ondreička, and J. Pal'a, "Design and experimental examination of new type of electro-permanent magnetic chuck," *Journal of Electrical Engineering*, vol. 61, no. 7 SUPPL, pp. 152–155, 2013.
- [45] A. Gawel, M. Kamel, T. Novkovic, J. Widauer, D. Schindler, B. P. von Altshofen, R. Siegwart, and J. Nieto, "Aerial picking and delivery of magnetic objects with MAVs," in *2017 IEEE International Conference on Robotics and Automation (ICRA)*, (Singapore), pp. 5746–5752, IEEE, may 2017.
- [46] A. D. Marchese, C. D. Onal, and D. Rus, "Soft robot actuators using energy-efficient valves controlled by electropermanent magnets," in *2011 IEEE/RSJ International Conference on Intelligent Robots and Systems*, (San Francisco), pp. 756–761, IEEE, sep 2011.
- [47] B. Van Ninhuijs, T. E. Motoasca, B. L. Gysen, and E. A. Lomonova, "Modeling of spherical magnet arrays using the magnetic charge model," *IEEE Transactions on Magnetics*, vol. 49, pp. 4109–4112, jul 2013.
- [48] J. M. Rovers, J. W. Jansen, and E. A. Lomonova, "Modeling of relative permeability of permanent magnet material using magnetic surface charges," *IEEE Transactions on Magnetics*, vol. 49, pp. 2913–2919, jun 2013.
- [49] M. F. Kremers, J. J. Paulides, E. Ilhan, J. L. Janssen, and E. A. Lomonova, "Relative permeability in a 3D analytical surface charge model of permanent magnets," *IEEE Transactions on Magnetics*, vol. 49, pp. 2299–2302, may 2013.
- [50] O. Craiu, N. Dan, and E. A. Badea, "Numerical Analysis of Permanent Magnet DC Motor Performances," *IEEE Transactions on Magnetics*, vol. 31, no. 6, pp. 3500–3502, 1995.
- [51] O. Chubar, C. Benabderrahmane, O. Marcouille, F. Marteau, J. Chavanne, and P. Elleaume, "Application of Finite Volume Integral Approach to Computing of 3D Magnetic Fields Created by Distributed Iron-dominated Electromagnet Structures," *Proceedings of EPAC*, vol. I, pp. 1675–1677, 2004.
- [52] C. Abert, C. Huber, F. Bruckner, C. Vogler, G. Wautischer, and D. Suess, "A fast finite-difference algorithm for topology optimization of permanent magnets," *Journal of Applied Physics*, vol. 122, p. 113904, sep 2017.
- [53] G. Dominguez, L. Durand, J. De Rosa, E. Danguise, C. Arozamena, and P. A. Ferraina, "Retraction and triangulation with neodymium magnetic

- forceps for single-port laparoscopic cholecystectomy,” *Surgical Endoscopy*, vol. 23, no. 7, pp. 1660–1666, 2009.
- [54] G. Zhao, J. Ma, X. Yan, J. Li, F. Ma, H. Wang, Y. Liu, and Y. Lv, “Optimized force range of magnetic compression anastomosis in dog intestinal tissue,” *Journal of Pediatric Surgery*, vol. 54, pp. 2166–2171, oct 2019.
- [55] J. G. Kassakian, M. F. Schlecht, and G. C. Verghese, *Principles of Power Electronics*. Addison-Wesley series in electrical engineering, Addison-Wesley, 1991.
- [56] Department of Health Education and Welfare (U.S.), *Medical Devices: A Legislative Plan*. U.S. Department of Health, Education and Welfare, 1970.
- [57] V. Martindale and A. Menache, “The PIP scandal: An analysis of the process of quality control that failed to safeguard women from the health risks,” *Journal of the Royal Society of Medicine*, vol. 106, pp. 173–177, aug 2013.